University of Alberta

PERFORMANCE OF MULTILEVEL ASK SIGNALS IN A HYBRID AM/VSB-MULTILEVEL ASK SUBCARRIER MULTIPLEXED OPTICAL FIBER TRANSMISSION SYSTEM

by

DAVID J. S. MOORE

A thesis submitted to the Faculty of Graduate Studies and Research in partial fulfillment of the requirements for the degree of **Master of Science**.

Department of Electrical Engineering

Edmonton, Alberta
FALL, 1996

National Library of Canada

Acquisitions and Bibliographic Services Branch

395 Wellington Street
Ottawa, Ontario
K1A 0N4

Bibliothèque nationale du Canada

Direction des acquisitions et des services bibliographiques

395, rue Wellington
Ottawa (Ontario)
K1A 0N4

Your file *Votre référence*

Our file *Notre référence*

The author has granted an irrevocable non-exclusive licence allowing the National Library of Canada to reproduce, loan, distribute or sell copies of his/her thesis by any means and in any form or format, making this thesis available to interested persons.

L'auteur a accordé une licence irrévocable et non exclusive permettant à la Bibliothèque nationale du Canada de reproduire, prêter, distribuer ou vendre des copies de sa thèse de quelque manière et sous quelque forme que ce soit pour mettre des exemplaires de cette thèse à la disposition des personnes intéressées.

The author retains ownership of the copyright in his/her thesis. Neither the thesis nor substantial extracts from it may be printed or otherwise reproduced without his/her permission.

L'auteur conserve la propriété du droit d'auteur qui protège sa thèse. Ni la thèse ni des extraits substantiels de celle-ci ne doivent être imprimés ou autrement reproduits sans son autorisation.

ISBN 0-612-18301-7

Canada

University of Alberta

Library Release Form

Name of Author: David J. S. Moore

Title of Thesis: Performance of Multilevel ASK Signals in a Hybrid AM/VSB-Multilevel ASK Subcarrier Multiplexed Optical Fiber Transmission System

Degree: Master of Science

Year this Degree Granted: 1996

Permission is hereby granted to the University of Alberta Library to reproduce single copies of this thesis and to lend or sell such copies for private, scholarly, or scientific research purposes only.

The author reserves all other publication and other rights in association with the copyright in the thesis, and except as hereinbefore provided, neither the thesis nor any substantial portion thereof may be printed or otherwise reproduced in any material form whatever without the author's prior written permission.

David Moore

8655-77 Street
Edmonton, Alberta, Canada
T6C 2L9

DATE: September 26, 1996

University of Alberta

Faculty of Graduate Studies and Research

The undersigned certify that they have read, and recommend to the Faculty of Graduate Studies and Research for acceptance, a thesis entitled **PERFORMANCE OF MULTILEVEL ASK SIGNALS IN A HYBRID AM/VSB-MULTILEVEL ASK SUBCARRIER MULTIPLEXED OPTICAL FIBER TRANSMISSION SYSTEM** submitted by **DAVID J. S. MOORE** in partial fulfillment of the requirements for the degree of **MASTER OF SCIENCE**.

Dr. J. Conradi, Supervisor

Dr. W. Krzymien, Internal

Prof. U. Maydell, External

DATE: September 26/96

Dedication

To my parents, John and Marlene Moore,
for their unconditional love, encouragement and support.

To my brother, Dean Moore,
for teaching me the true meaning of perseverance.

Abstract

In the near future, analog CATV signals and digital High Def[illegible]ion Television (HDTV) signals will be broadcast side-by-side in North America. The HDTV format adopted by the Federal Communications Commission in the United States is known as N-VSB. This modulation format involves the use of a vestigial-filtered multilevel ASK carrier with a number of forward error correction coding algorithms. In this thesis, the performance of a multilevel ASK signal is studied when transmitted alongside 42 analog AM/VSB carriers in an optical fiber transmission system.

Both Gaussian noise and nonlinear distortion have an impact on the bit error ratio performance of a multilevel ASK signal transmitted in a hybrid AM/VSB-multilevel ASK transmission system. When the transmission medium consists of optical fiber, nonlinear distortion resulting from threshold clipping of the laser diode and from the combination of laser diode chirp and fiber dispersion are the two greatest sources of system nonlinear distortion. This thesis theoretically and experimentally examines the manner in which both sources of nonlinear distortion contribute to performance degradation of a multilevel ASK signal.

Acknowledgments

I would like to begin by thanking my supervisor, Dr. Jan Conradi, for the opportunity to study in an environment that is conducive to research. I appreciate the technical guidance and support offered by Dr. Conradi during my days as an undergraduate student and as a graduate student.

I wish to acknowledge my colleagues and friends, Tom Young, Ping Wan, Steve Lai, Mike Sieben and Sheldon Walklin for the many interesting discussions and good times we enjoyed together.

I would like to thank Dave Clegg, Jason Lamont and Tim Friesen for assisting me during the design and construction of the digital encoder and decoder used during the experimental stage of this work. Your suggestions and expertise are both greatly appreciated.

This work was made possible by the Natural Sciences and Engineering Research Council of Canada (NSERC), Bell-Northern Research, and TRLabs through the NSERC/BNR/TRLabs Industrial Research Chair in Fiber Optic Communications at the University of Alberta. I wish to recognize NSERC, TRLabs and the University of Alberta for the generous financial support received during the course of my graduate studies.

Finally, I want to say a special thank you to my family and friends for their never-ending support over the years. I particularly wish to thank my best friend, Nicola, for her words of wisdom and encouragement.

Table of Contents

1.0 Introduction 1

1.1 Current Analog CATV Transmission System 2
1.2 CATV Distribution of Digital Television 2
1.2.1 Hybrid Fiber Coaxial Network Architecture 3
1.2.2 Subcarrier Multiplexing 5
1.2.3 Overview of N-VSB 6
1.3 Research Objectives and Thesis Organization 10

2.0 Optical Fiber Transmission of Analog and Digital Video Signals 12

2.1 Modulation Formats 12
2.1.1 Vestigial Sideband Amplitude Modulation (AM/VSB) 13
2.1.2 Quadrature Amplitude Modulation (QAM) 14
2.1.3 Multilevel Amplitude Shift Keying (ASK) 15
2.2 Sources of Degradation in a Lightwave SCM System 16
2.2.1 Gaussian Noise 16
2.2.2 Nonlinear Distortion due to Laser Diode Clipping 17
2.2.3 Nonlinear Distortion due to the Combination of Laser Diode Chirp and Nonlinear Optics 21
2.3 Results of Nonlinear Distortion in a Multichannel SCM System 22

3.0 Theoretical Error Performance of Multilevel ASK in a Hybrid AM/VSB - Multilevel ASK Subcarrier Multiplexed Lightwave Transmission System 24

3.1 System Parameters of an AM/VSB Signal 24
3.1.1 AM/VSB Modulation Index 24
3.1.2 Carrier-to-Noise Ratio for an AM/VSB Channel 26
3.2 BER Analysis of a Multilevel ASK Signal in the Presence of Gaussian Noise 27
3.2.1 Matched Filter Demodulation Analysis 28
3.2.2 Alternative Analysis for Determining the BER of Multilevel ASK in Gaussian Noise 31

3.3 BER Analysis of a Multilevel ASK Signal in the Presence of Gaussian Noise and Non-Gaussian Impulsive Noise 34
3.3.1 SNR and SNLD for an M-ary ASK Signal 34
3.3.2 Derivation of the BER for Multilevel ASK in Combined Gaussian and Non-Gaussian Impulsive Noise using Middleton's Class A Noise Model 35
3.4 Transmission System Simulations 41
3.5 Impact of Vestigial Sideband Filtering on the Error Performance of Multilevel ASK in Gaussian and Non-Gaussian Impulsive Noise 46

4.0 Design and Characterization of a Fiber Optic Multichannel AM/VSB-Multilevel ASK Transmission System 54

4.1 Optical Transmission Components 55
4.1.1 Analog Optical Transmitter 55
4.1.2 Analog Optical Receiver 57
4.2 Optical Link Characterization 57
4.2.1 Nonlinear Distortion Performance of the Laser Diode 58
4.2.2 Receiver Frequency Response 59
4.3 Analog Channel Modulators 60
4.4 8-Level ASK Encoder 61
4.5 8-Level ASK Decoder 67
4.6 Optical Modulation Index (OMI) Calibration 69
4.6.1 OMI of the Analog CATV Carriers 69
4.6.2 OMI of the Multilevel ASK Signal 72
4.7 Multilevel ASK Back-to-Back Calibrations 73
4.7.1 Electrical Back-to-Back 74
4.7.2 Optical Back-to-Back 76

5.0 Experimental Performance of a Fiber Optic Multichannel AM/VSB-Multilevel ASK Transmission System 81

5.1 Carrier-to-Noise Ratio Performance of an AM/VSB Carrier 81
5.2 Nonlinear Distortion in a High Frequency Digital Channel 85
5.2.1 Nonlinear Distortion in the Absence of Fiber Optics 85

5.2.2 Nonlinear Distortion due to the Combination of Laser Chirp and Fiber Dispersion 90
5.3 Performance of 8-Level ASK in a Hybrid SCM Optical Transmission System Dominated by Nonlinear Distortion due to Laser Clipping 93
5.3.1 Error Performance as a Function of ASK Modulation Index 95
5.3.2 Error Performance as a Function of Signal-to-Noise Ratio and Signal-to-Nonlinear Distortion Ratio 97
5.3.3 Error Performance as a Function of Received Optical Power and ASK Modulation Index 99
5.3.4 Alternative Analysis of Clipping-Induced Impulse Noise 101
5.4 Performance of 8-Level ASK in a Hybrid SCM Optical Transmission System with Nonlinear Distortion due to Laser Clipping and the Combination of Laser Chirp and Fiber Dispersion 103
5.4.1 Error Performance as a Function of ASK Modulation Index 103
5.4.2 Error Performance as a Function of AM/VSB Modulation Index 105

6.0 Conclusions 107

6.1 Summary of Conclusions 107
6.2 Recommendations for Further Research 110

REFERENCES 111

Appendix A: Computer Program Listings 116

Appendix B: Encoder/Decoder Circuit Diagrams 135

List of Figures

Figure 1.1: Typical CATV Network Architecture 3
Figure 1.2: Advanced Hybrid Fiber Coaxial Architecture 4
Figure 1.3: Block Diagram of a Subcarrier Multiplexed System 6
Figure 1.4: Block Diagram of an 8-VSB Transmitter and Receiver 8
Figure 2.1: NTSC Analog Television Spectrum 13
Figure 2.2: Constellation Diagram for 16-QAM 14
Figure 2.3: Constellation (or Space State) Diagram for Multilevel ASK 16
Figure 2.4: Laser Diode Threshold Clipping 18
Figure 3.1: Modulation Index from Laser Power-Current Curve 26
Figure 3.2: Signal Space Diagram for 8-level ASK 31
Figure 3.3: Bit Error Ratio as a Function of SNR for an 8-Level ASK Signal 39
Figure 3.4: Bit Error Ratio as a Function of SNR for a 16-Level ASK Signal 39
Figure 3.5: Bit Error Ratio as a Function of SNLD for an 8-Level ASK Signal 40
Figure 3.6: Bit Error Ratio as a Function of SNLD for a 16-Level ASK Signal 40
Figure 3.7: Transmission System Simulation Model 42
Figure 3.8: Simluated Eye Diagram after Transmitter Baseband Filter and Receiver Baseband Filter with 2nd order Butterworth Filters (fc = 7 MHz) 44
Figure 3.9: Simulated Eye Diagram after Transmitter Baseband Filter and Receiver Baseband Filter with 3rd order Butterworth Filters (fc = 7 MHz) 45
Figure 3.10: 16-level Eye Diagram after Transmitter Baseband Filter 46
Figure 3.11: CSO Product Count for a 42-Channel CATV System 51
Figure 3.12: CTB Product Count for a 42-Channel CATV System 52
Figure 3.13: CSO and CTB Power for a 42-Channel CATV System 52
Figure 3.14: Nonlinear Distortion Power of a VSB System Versus that of a DSB System at a Carrier Frequency of 420 MHz 53
Figure 4.1: Block Diagram of Multichannel AM/VSB-Multilevel ASK Transmission System Experimental Setup 54
Figure 4.2: Output Optical Power as a Function of Bias Current for Fujitsu Laser 56
Figure 4.3: Block Diagram Representation of the Analog Optical Transmitter 57
Figure 4.4: Experimental Setup for Measuring Laser Linearity 58
Figure 4.5: Nonlinear Distortion Performance of Laser Diode versus Bias Current 59
Figure 4.6: Experimental Setup for Measuring Receiver Frequency Response 60
Figure 4.7: Frequency Response of the Ortel Receiver 60

Figure 4.8: Block Diagram of the 8-Level Encoder 61
Figure 4.9: Output of 8-Level Encoder with 5 Mbps Binary Input 63
Figure 4.10: Output of 8-Level Encoder with 50 Mbps Binary Input 64
Figure 4.11: Eye Diagram for a Single Eye with a 30 Mbps Binary Input 64
Figure 4.12: Power Spectral Density of 8-Level Signal Before Baseband Filter 65
Figure 4.13: Power Spectral Density of 8-Level Signal After Baseband Filter 66
Figure 4.14: Eye Diagram of 8-Level Signal After Baseband Filter 66
Figure 4.15: Eye Diagram of 8-Level Signal at Input of Decoder Board 67
Figure 4.16: Block Diagram Representation of 8-Level ASK Decoder 68
Figure 4.17: Modulation Index Calibration Experimental Setup 70
Figure 4.18: Carrier Power of Channel 21 versus Laser Bias Current 71
Figure 4.19: Frequency Response of the Optical Receiver and Frequency Response of Each CATV Carrier through the Optical Transmitter and Receiver 72
Figure 4.20: Electrical Back-to-Back Experimental Setup 74
Figure 4.21: Electrical Back-to-Back Performance for Three Bit Rates 75
Figure 4.22: Binary Signal at Input to Encoder 76
Figure 4.23: Binary Signal at Output of Decoder 76
Figure 4.24: Block Diagram of Optical Back-to-Back Experimental Setup 77
Figure 4.25: BER of 28 Mbps Digital Signal in Back-to-Back Configuration 78
Figure 4.26: Bit Error Ratio as a Function of Prx for an ASK Mod. Index of 0.48% 79
Figure 4.27: BER versus ASK Modulation Index 80
Figure 5.1: Experimental Setup for Measuring Analog CNR 82
Figure 5.2: CNR versus Received Optical Power for Modulation Index of 4.1% 84
Figure 5.3: CNR versus Received Optical Power for Modulation Index of 5.8% 85
Figure 5.4: Experimental Setup for Viewing Intermodulation Distortion Products 86
Figure 5.5: Distortion Products near 450 MHz with a Modulation Index of 4.1% 87
Figure 5.6: Distortion Products near 450 with a Modulation Index of 5.8% 88
Figure 5.7: Distortion Products near 450 MHz with a Modulation Index of 6.5% 88
Figure 5.8: CSO and CTB Power near 450 MHz as a Function of μ 90
Figure 5.9: CSO Distortion versus μ for Various Fiber Lengths 92
Figure 5.10: CTB Distortion versus μ for Various Fiber Lengths 93
Figure 5.11: Experimental Setup for Measuring BER Performance of an 8-Level ASK Signal in an Optical Fiber Hybrid SCM Transmission System 95

Figure 5.12: BER versus ASK Modulation Index for AM/VSB Modulation Indices of 0%, 3.85%, 4.80%, 6.00% 96
Figure 5.13: BER versus SNR for SNLD's of 31.3 dB, 39.6 dB and Infinity 98
Figure 5.14: BER vs. ASK Modulation Index with no AM/VSB Carriers and with Received Optical Powers of -1.0 dBm and -6.0 dBm..... 99
Figure 5.15: BER vs. ASK Modulation Index for an AM/VSB Modulation Index of 4.80% and Received Optical Powers of -1.0 dBm and -6.0 dBm..... 100
Figure 5.16: BER vs. ASK Modulation Index for an AM/VSB Modulation Index of 6.0% and Received Optical Powers of -1.0 dBm and -6.0 dBm 100
Figure 5.17: BER versus ASK Modulation Index with Comparison to Simulations using Lai's and Middleton's models for Clipping-Induced Impulse Noise..... 102
Figure 5.18: BER versus ASK Modulation Index with and without 10 km Fiber 104
Figure 5.19: BER versus Per Channel AM/VSB Modulation Index for Various Lengths of Optical Fiber 105

List of Symbols

A	impulsive index
A_m	amplitude of level m for a multilevel ASK signal
d_{min}	minimum distance between signaling points of a space state diagram
B	channel bandwidth
$\mathcal{E}$	energy of the pulse $p(t)$
$E(x)$	expected or mean value of x
$erfc(x)$	complementary error function of a variable x
F	amplifier noise figure
f_c	RF subcarrier frequency
f_i	carrier frequency for channel i
f_o	frequency of the center channel of a multichannel system
G	current gain of the transformer
Γ'	mean power ratio of the Gaussian noise component (σ_g^2) to the non-Gaussian noise component (σ_I^2)
$h_{o,k}$	coefficient used to define the autocorrelation function of the laser output
$\lvert H(\omega) \rvert$	filter magnitude response
ΔI	peak amplitude of the modulating current
$\left\langle i_{AM/VSB}{}^2 \right\rangle$	mean square AM/VSB signal noise current
I_{bias}	laser bias current
I_c	bias current for a modulation depth of 100%
I_{th}	laser threshold current
$\left\langle i_{RIN}^2 \right\rangle$	mean square RIN noise current
$\left\langle i_{sh}^2 \right\rangle$	mean square shot noise current

$\langle i_t^2 \rangle$	mean square thermal noise current
k	Boltzmann's constant (1.38054×10^{-23} J/K)
K_{nv}	power product count of the n^{th} order nonlinear distortion at frequency v
m	per channel peak modulation index
M	number of signaling levels in a multilevel ASK signal
m_{ask}	multilevel ASK modulation index
m_i	peak modulation index for channel i
m_{rms}	per channel rms modulation index
$m(t)$	time-varying modulation signal
μ	total rms modulation index
N	total number of AM/VSB channels
$\langle N \rangle$	noise power spectral density in dBm/Hz
N_p	nonlinear distortion in channel p
N_{tot}	total Gaussian and impulsive noise power ($\sigma_g^2 + \sigma_I^2$)
P_{ave}	average transmitted signal power
P_b	probability of a bit error
P_{bias}	optical power for bias current I_{bias}
P_e	probability of error for binary ASK
PF	peak power factor
$p_{I+G}(n)$	amplitude probability distribution function for combined Gaussian noise and non-Gaussian impulsive noise
$\langle (\Delta P_L)^2 \rangle$	mean square intensity fluctuation of the laser output
$\langle P_L \rangle$	average laser light output power
P_M	average probability of a symbol error

$p_n(n)$	probability density function of a Gaussian noise variable
P_o	average received optical power
$p(t)$	baseband pulse shape
$P(t)$	time-varying transmitted optical power waveform
q	electronic charge (1.602×10^{-19} C)
$\Re$	photodetector responsivity in A/W
R_{eq}	receiver equivalent load resistance
$Re[x]$	real portion of a complex variable x
${}_nR_o(\tau)$	autocorrelation function of the laser noise output
${}_sR_o(\tau)$	autocorrelation function of the laser signal output
S	peak signal envelope
$s_m(t)$	transmitted waveform for multilevel ASK
$S(\omega)$	signal power spectral density
σ^2	variance of the received photocurrent
σ_g^2	Gaussian noise variance
σ_f^2	non-Gaussian noise variance
σ_v^2	noise variance
T	absolute temperature (in Kelvin) or symbol period
θ_i	carrier phase for channel i
$V_{in(p\text{-}p)}$	peak-to-peak input voltage
${}_nW_o\left(f_p\right)$	clipping-induced nonlinear distortion power spectral density

List of Abbreviations and Acronyms

ACATS	Advisory Committee on Advanced Television Service
A/D	Analog-to-Digital Converter
AM/VSB	Vestigial Sideband Amplitude Modulation
ASK	Amplitude Shift Keying
BER	Bit Error Ratio
CATV	Community Antenna Television
CNR	Carrier-to-Noise Ratio
CSO	Composite Second Order
CTB	Composite Triple Beat
D/A	Digital-to-Analog Converter
dB	Decibel
DFB	Distributed Feedback
DSB	Double Sideband
DSP	Digital Signal Processing
EDFA	Erbium Doped Fiber Amplifier
FEC	Forward Error Correction
FCC	Federal Communications Commission
FDM	Frequency Division Multiplexing
FTTC	Fiber-to-the-Curb
FTTH	Fiber-to-the-Home
HDTV	High Definition Television
HFC	Hybrid Fiber Coaxial
IC	Integrated Circuit
IMD	Intermodulation Distortion
ISI	Intersymbol Interference
L-I	Light power versus Current
LO	Local Oscillator
LPF	Low Pass Filter
N-VSB	N-Level Vestigial Sideband Digital Modulation
NCTA	National Cable Television Association
NLD	Nonlinear Distortion
NTSC	National Television System Committee
PLL	Phase Lock Loop

PRBS	Pseudorandom Bit Stream
PSD	Power Spectral Density
QAM	Quadrature Amplitude Modulation
RF	Radio Frequency
RIN	Relative Intensity Noise
rms	Root-Mean-Square
SCM	Subcarrier Multiplexed
SNR	Signal-to-Noise Ratio
SNLD	Signal-to-Nonlinear Distortion Ratio
SONET	Synchronous Optical Network
SSB	Single Sideband
TCM	Trellis Coded Modulation
TDM	Time Division Multiplexed
TV	Television
VOA	Variable Optical Attenuator

1.0 Introduction

Fiber optics has revolutionized the world of communications in the past several years. The traditional copper plant used for data, voice and video transmission is quickly being replaced with optical fiber. The advantages of optical fiber communications are many, including higher capacity, low signal loss, immunity to crosstalk and electromagnetic interference, and reduced physical size. In addition, there have been numerous breakthroughs in the development of lightwave technology, allowing the design of faster and more reliable semiconductor lasers and photodiodes. The deployment of optical communication links has been underway for two decades in the telephone industry for trunking of voice and high-speed data. Recently, there has been a great deal of interest in the use of fiber optics for the delivery of broadcast video in the Community Antenna Television (CATV) industry. This stems from developments in broadcast architectures, such as Hybrid Fiber Coaxial (HFC), as well as advances in the development of digital television.

High-Definition Television (HDTV) is expected to replace the present National Television System Committee (NTSC) analog color television system that has been in place for more than forty years. The present CATV system in North America uses an analog modulation technique known as vestigial sideband amplitude modulation (AM/VSB). However, recent advances in the development of digital video compression algorithms have spearheaded the drive to define a digital modulation format for the delivery of broadcast digital video. In the United States, the Federal Communications Commission (FCC) has chosen to adopt an HDTV format known as N-VSB. This transmission system combines the use of a vestigial-filtered multilevel amplitude shift keyed (ASK) carrier with a number of forward-error correction coding techniques including Trellis-coded modulation and Reed-Solomon coding. The FCC has ruled that over the next several years, broadcasters are required to transmit both analog AM/VSB signals and HDTV signals side-by-side. Therefore, it is necessary to examine the performance of the digital HDTV signal when transmitted alongside a large number of analog television signals.

In this introductory chapter, an overview of the current CATV system will be given. Following that, some key aspects of the future hybrid CATV system will be discussed, including a description of HFC and N-VSB. Finally, an overview of the content and organization of this thesis will be presented.

1.1 Current Analog CATV Transmission System

Historically, CATV systems were designed to distribute television signals within rural communities. That is, an antenna would receive off-the-air broadcasts and then distribute these television signals to the community via a coaxial cable distribution network. The capability of carrying numerous signals with fairly high signal quality over a coaxial network resulted in coaxial CATV systems becoming commonplace in large urban markets as well. Hence, the majority of today's cable companies have a vast investment in coaxial cable networks.

Figure 1.1 shows a typical cable TV network that exists today [1], [2]. This is known as a tree-and-branch architecture, since all the signals that reach each subscriber originate at a central head end. The modulation and multiplexing functions inherent to NTSC video are undertaken at the head end. The signals are picked up through satellite receivers and off-air antennas. They are then brought down to baseband, amplitude modulated and vestigial filtered at an Intermediate Frequency. Each of the video channels is modulated by a unique RF carrier and the composite frequency division multiplexed signal is transmitted via supertrunking to local distribution sites known as hubs. The broadcast video is distributed to the subscribers via amplified trunks, splitters, taps and subscriber drops. The amplifiers are designed to compensate for propagation and splitting losses.

Today's coaxial CATV systems are cost-effective for the delivery of analog video, but have performance problems and limitations due to the large number of repeatered amplifiers. Current coaxial trunks may contain up to 30 electronic amplifiers which contribute unacceptable levels of nonlinear distortion and noise [1] according to recommended cable television standards [3]. In addition, these amplifiers contain active components that must be able to withstand the harsh environment of the outside plant and must be provided with electrical power. Both of these factors affect the reliability of the transmission system. On the other hand, low loss optical fiber systems can provide repeaterless transmission, which results in improved system reliability, increased transmission capacity and higher picture quality.

1.2 CATV Distribution of Digital Television

Since the FCC has indicated that broadcasters will have to deliver both analog and digital television signals simultaneously, an architecture is required that can maintain a high signal quality for both the analog and digital television signals. One possibility is the use of subcarrier multiplexing over a hybrid fiber coaxial network. In subcarrier multiplexing, the analog and digital signals are frequency division multiplexed into a composite signal which

then modulates an optical transmitter. The optical signal is distributed over an HFC network as a means of meeting the performance objectives for all channels across a much wider bandwidth than is possible with an all-coaxial network.

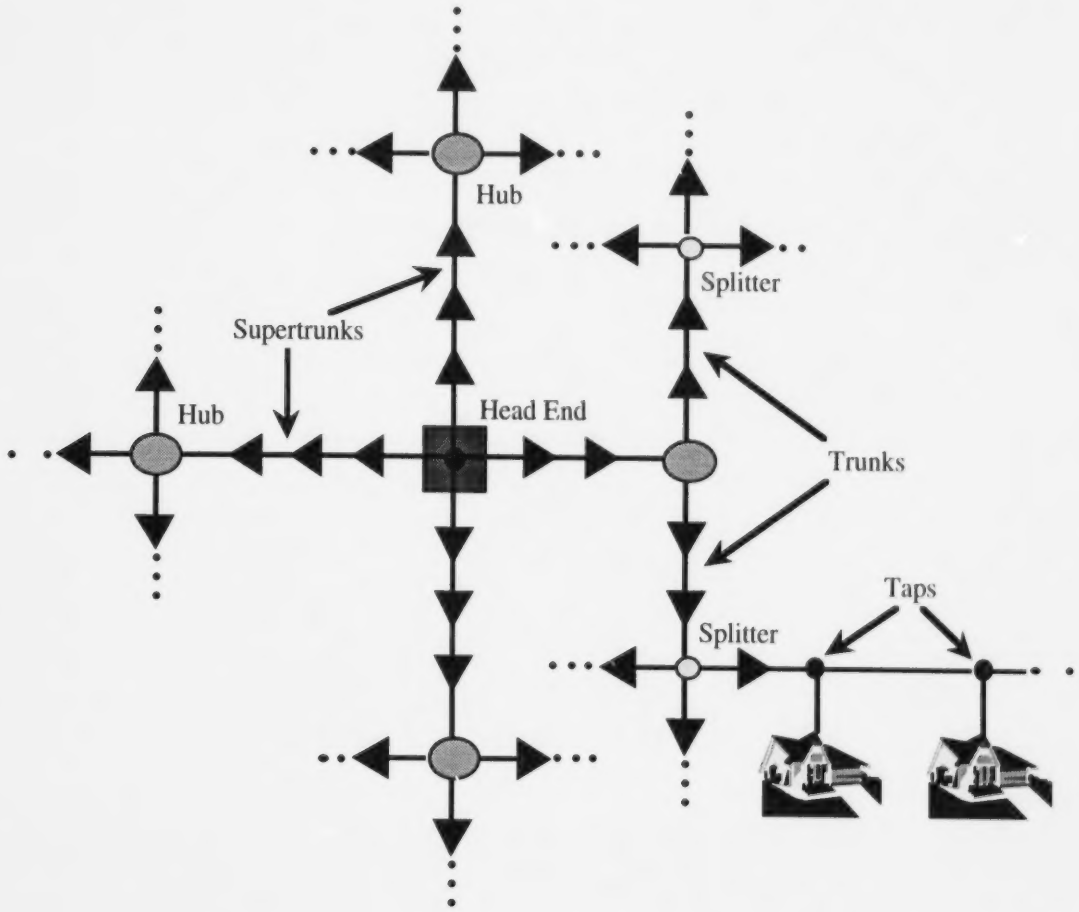

Figure 1.1: Typical CATV Network Architecture

1.2.1 Hybrid Fiber Coaxial Network Architecture

HFC is proving to be the architecture of choice for providing broadband services including hybrid analog/digital video [4]-[8]. One of the first hybrid fiber coax techniques involved the use of a 'fiber backbone' to replace the supertrunking portion of the traditional coaxial CATV network shown in Figure 1.1. In this configuration, all amplifiers between the head end and the hubs are removed. In addition, the hubs become 'conversion nodes' in which the optical signal is converted to an equivalent electrical signal for distribution to

the subscriber's home. Hybrid fiber coaxial networks based on the use of a fiber backbone have found favor with a number of service providers for a few main reasons. First of all, this architecture is quite cost effective since it utilizes much of the existing electrical equipment between the conversion nodes and the home. The capital investment in buried coaxial cable within each community is very high, and therefore, any architecture that reuses this investment has an inherent advantage. In addition, HFC upgrades offer improved broadcast quality and higher channel capacity, while laying the groundwork for interactive video and data services [8].

An increasingly more popular architecture for hybrid fiber coaxial networks is the one shown in Figure 1.2 [6]. In this setup, the fiber portion of the network is no longer a single-fiber link but rather based on fiber rings connecting the distribution centers. Synchronous Optical Network (SONET) rings are used for the transmission of digital information since SONET offers improved survivability and provisioning capabilities. This HFC architecture is useful for a full service network in which all types of services are offered, including broadcast video, video-on-demand and multimedia digital services. In this configuration, separate fibers are used to transport the broadcast video and the digital data from the headend to the distribution centers.

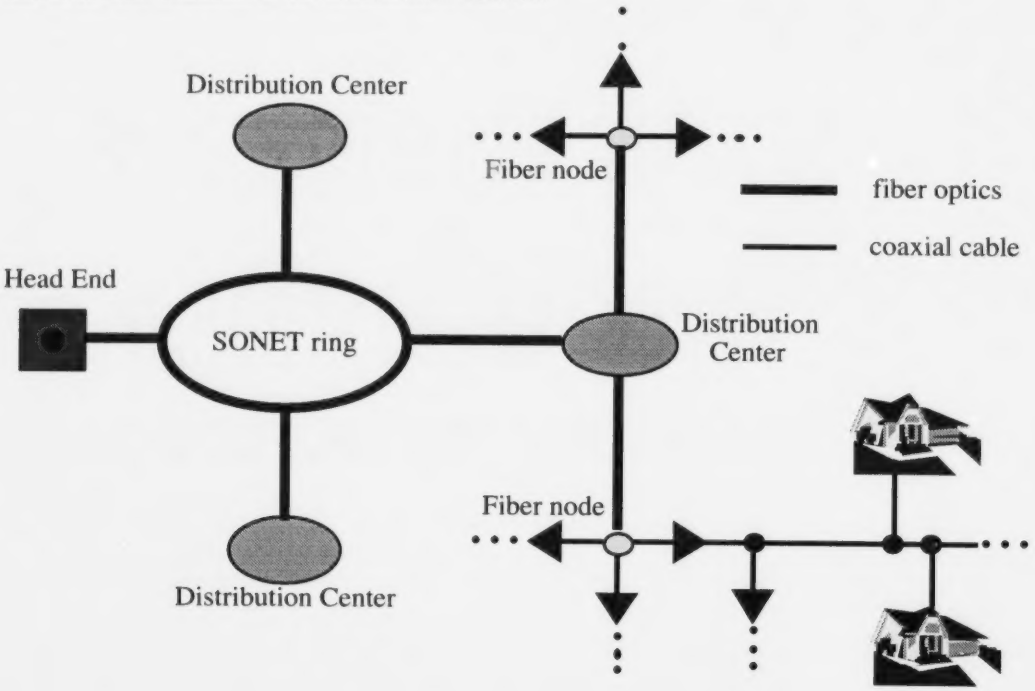

Figure 1.2: Advanced Hybrid Fiber Coaxial Architecture

Other architectures utilizing fiber optics have been proposed for the delivery of analog and digital signals, including Fiber-to-the-Curb (FTTC) and Fiber-to-the-Home (FTTH). The difference between these architectures generally lies in how far the fiber is pushed out into the distribution plant. In an HFC system, the fiber nodes or hubs generally serve 500-2000 homes [6], while a typical FTTC system is configured such that each optical network interface serves approximately 20 homes. To date, all-fiber systems are not cost effective due to the high cost of laying fiber to each home. It is for this reason that hybrid fiber coaxial designs have moved to the forefront as the most economically-feasible means of delivering combined analog and digital video to the home.

1.2.2 Subcarrier Multiplexing

Subcarrier multiplexing (SCM) is considered to be the most promising multiplexing technique for fiber optic multichannel video systems [1]. SCM provides a versatile platform for delivering a wide range of broadband services, including both analog and digital video. In an SCM system, each baseband analog and digital signal modulates a particular RF carrier. The set of modulated carriers are then frequency division multiplexed [9] into a single RF signal. Guard bands are placed between adjacent channels in order to limit the amount of interference from neighboring channels. The combined signal modulates the intensity of a laser diode. Since the optical frequency is the actual carrier, the RF carrier frequencies of the video signals are known as the subcarriers. The output of the laser diode is coupled into an optical fiber for transmission. After being converted back to an electrical signal through a photodetector, any one of the multiplexed signals can be received by tuning a local oscillator to the appropriate frequency. The individual channel can then be downconverted to baseband and demodulated. Figure 1.3 shows a block diagram of a typical SCM lightwave system.

There are a number of reasons for using SCM techniques for delivering combined analog and digital television signals. First of all, subcarrier multiplexing is a simple and low cost method of transmitting multichannel video through fiber optics. SCM networks take advantage of the full range of existing electronic techniques, including presently-used analog and digital modulation formats [10]. The NTSC AM/VSB signal directly modulates a laser without the need for signal conversion to a digital format. Secondly, subcarrier multiplexing takes advantage of the large modulation bandwidth of semiconductor lasers [11]. Finally, SCM offers greater flexibility in allocating bandwidth since the individual channels are independent [10]. In time division multiplexed (TDM) systems, synchronization is required, therefore services carried by different subcarriers become

interdependent [9]. Based on the above advantages, SCM networks are considered to be the most practical alternative for the delivery of analog and digital television signals in a fiber optic transmission system.

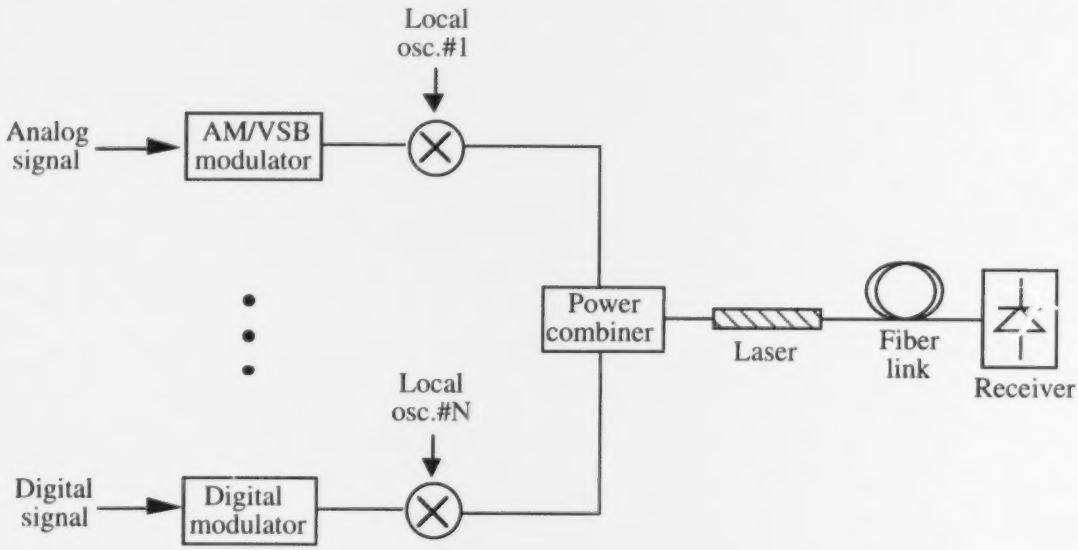

Figure 1.3: Block Diagram of a Subcarrier Multiplexed System

1.2.3 Overview of N-VSB

There are a number of advantages to using a digital television format rather than analog [12]. Digital transmission is more robust and flexible than its analog counterpart. Digital transmission allows error-free regeneration of relayed television pictures, lower transmitter power is required due to lower signal-to-noise ratio objectives, multipath images can be canceled through the use of digital signal processing, multiple sound channels of CD quality can be included with the video transmission and co-channel digital signals interfere less with each other than do co-channel NTSC analog signals. For these reasons, most of the technically-advanced countries in the world are working towards implementation of a high-definition television system.

In the United States, the Federal Communications Commission (FCC) has been working quite closely with the Digital HDTV Grand Alliance in the selection and implementation of a digital television standard. The Grand Alliance is a consortium of technical experts from AT&T, General Instrument, MIT, Philips, David Sarnoff Research

Center, Thomson and Zenith. The Grand Alliance was formed in 1993 in an effort to evaluate technologies and HDTV proposals, reporting directly to the FCC's Advisory Committee on Advanced Television Service (ACATS). The FCC has already declared that any broadcast transmission scheme must be compatible with the current 6 MHz NTSC standard, while maintaining the current frequency spectrum allocation given to VHF/UHF NTSC broadcasts [13], [14].

There have been four main proposals for digital HDTV systems received by the FCC [15]-[17]. Three of the proposals, originating from General Instrument, the Advanced Television Research Consortium (ATRC) and MIT, are based on the use of quadrature amplitude modulation (QAM) techniques. The remaining system uses a vestigial sideband (VSB) modulation technique proposed by Zenith. During 1993, all four of these systems were tested by the Grand Alliance in cooperation with the FCC. In February of 1994, the Grand Alliance selected Zenith's N-VSB proposal as its recommendation to the FCC's Advisory Committee on Advanced Television Service [12]. After conducting their own series of laboratory and field tests, ACATS released a press release on Nov.28, 1995, urging the FCC to adopt the Digital HDTV Grand Alliance system, which is based on the N-VSB modulation format, as the new digital television broadcast standard in the United States.

The N-VSB digital television transmission system has been well-documented and analyzed [18]-[22], and a high-level description of the system will be given in the following paragraphs. An N-VSB modulator converts a binary stream of data to an N-level amplitude shift keyed (ASK) signal. Before the binary-to-multilevel conversion, the data stream goes through a number of forward error correction (FEC) modules, in an effort to overcome the effects of Gaussian noise and impulsive noise. The multilevel signal is then upconverted to an IF frequency, at which point vestigial sideband (VSB) filtering is applied. The symbol rate is 10.76 Msymbols/sec, which is transmitted in a vestigial sideband bandwidth of 6.0 MHz. The 3-dB bandwidth of the VSB filter is 5.38 MHz, with 620 kHz rolloff regions at each end of the vestigial sideband filter, resulting in a root-raised cosine filter transfer function.

There are two different modes of N-VSB, depending on the transmission environment. For terrestrial broadcasts, 8-level signaling is used, which is referred to as 8-VSB. The other mode, 16-VSB, is a high data rate cable standard that uses 16-level signaling. While 16-VSB can achieve a higher throughput, 43 Mbits/sec as compared to 32 Mbits/sec, it requires a much higher signal-to-noise ratio, and is therefore less robust than 8-VSB.

Figure 1.4 gives a block diagram description of the main components of an 8-VSB transmitter and receiver. The 16-VSB cable mode is identical except that Trellis-coded modulation is not used and the receiver does not include an NTSC interference rejection filter.

8-VSB Transmitter:

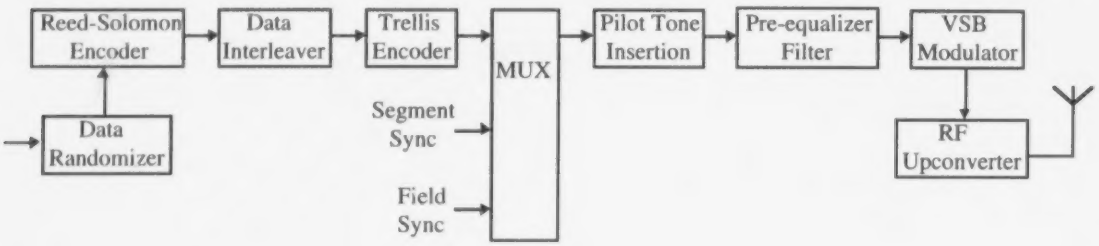

8-VSB Receiver:

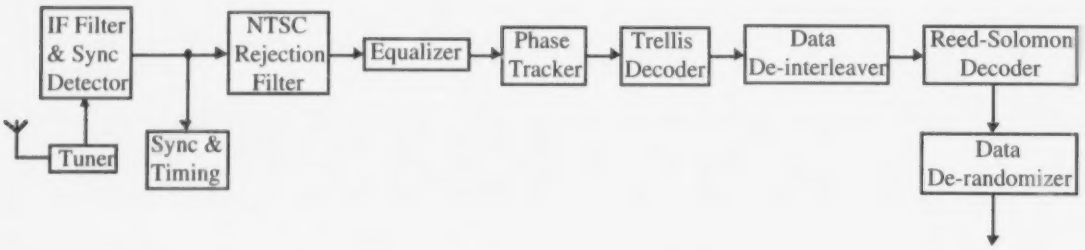

Figure 1.4: Block Diagram of an 8-VSB Transmitter and Receiver

The 8-VSB transmitter is composed of 9 elements. The data randomizer randomizes the data packets before Reed-Solomon encoding. This is achieved by combining the incoming data with a pseudorandom sequence through an XOR (exclusive OR) gate. Reed-Solomon encoding is used because of its capability to correct errors due to burst noise. Each 208-byte block consists of 188 bytes of data and 20 Reed-Solomon parity bytes. Up to 10 byte errors can be corrected within each block. The goal of the data interleaver is to spread the data bytes from the same Reed-Solomon block over time, such that a long burst of noise or interference is required to use up all 10 data bytes of Reed-Solomon error correction capability. The next module within the 8-VSB transmitter is a Trellis encoder. Trellis encoding is quite powerful at enhancing the system white noise performance, but

not that useful at combating the effects of impulse or burst noise. A 2/3 Trellis code is used, in which for every two input bits, the first input bit is encoded into two output bits while the other bit is left unencoded. Trellis coded modulation (TCM) combines multilevel modulation and coding to achieve coding gain without bandwidth expansion [12]. With TCM, movement from one symbol to another is constrained by the coding scheme [23]. If a received symbol sequence could not have been transmitted, error correction is possible. The next stage of the transmitter multiplexes the 8-level Trellis encoded signal with the segment and field synchronization signals. Each segment contains 4 segment synchronization symbols and 832 data symbols. Each field consists of 313 segments, of which one is strictly for field synchronization. Both the segment and field synchronization symbols are binary rather than 8-level symbols. Segment synchronization is required to make clock recovery rugged, while field synchronization indicates whether 8 or 16-level signaling is used, frames the data and is used to train the equalizer.

A key component of the 8-VSB system is the use of a pilot tone for carrier recovery. Since suppressed carrier modulation is used, the pilot tone is placed at the suppressed carrier frequency. Pilot insertion is achieved at baseband through the addition of a DC level to the 8-level baseband signal. The increase in transmitted power due to the use of a pilot tone is only 0.3 dB, resulting in a very efficient means of aiding the carrier recovery at the receiver. A pre-equalizer filter follows the pilot insertion unit in the 8-VSB transmitter. This equalizer is only used in over-the-air broadcasts where the high power transmitter may have significant in-band ripple or roll-off at the band edges. The final stage before upconversion to RF is the VSB modulator. The IF frequency is 46.69 MHz. The input to the VSB modulator is a 10.76 Msymbols/sec 8-level composite signal that includes the data, synchronization signals and pilot tone. Vestigial sideband filtering is accomplished through the use of linear-phase square root-raised cosine filters. Identical VSB filters are placed in both the transmitter and receiver. The final stage of the 8-VSB transmitter is the RF upconverter. A two-step modulation process is used, with a resulting average signal power that is 12 dB lower than the NTSC peak signal power.

The 8-VSB receiver also consists of 9 stages, 5 of which provide reverse functions of their counterpart in the transmitter. The tuner consists of two stages of filtering and mixing, using standard consumer electronic components. After passing through a VSB filter at the IF frequency, a frequency and phase lock loop (FPLL) provides synchronous detection of the pilot tone. An additional phase lock loop (PLL) derives a clean 10.76 MHz clock tone from the received signal, to be used for timing purposes throughout the receiver. In the 8-VSB receiver (but not the 16-VSB receiver), an NTSC rejection filter follows the

synchronous detector. The rejection filter uses a baseband comb filter with periodic nulls corresponding to the locations of the video, color and audio subcarriers of an NTSC signal. In reducing NTSC interference, the rejection filter modifies the data slightly and degrades the white noise performance slightly, and is therefore not used in the 16-VSB system in which NTSC interference is less prevalent. The next stage is a channel equalizer which compensates for linear channel distortions, and converges on a known tap training sequence embedded within the data signal. Following the equalizer is a phase tracker, which is used to remove phase noise missed by the IF PLL operating on the pilot tone. The final four stages of the 8-VSB receiver are the Trellis decoder, data de-interleaver, Reed-Solomon decoder and data de-randomizer. These stages perform the decoding and error correction associated with their respective counterparts in the transmitter. Note that the data de-interleaver can handle noise bursts of up to 170 μsec in total duration.

1.3 Research Objectives and Thesis Organization

Much work has gone into the design of an HDTV format that is compatible with the existing NTSC television system, while very little work has been done on analyzing how this system would perform in the noise and nonlinear distortion environment of an actual fiber optic system. Consequently, there is a need to study and characterize the system performance of a hybrid SCM fiber optic analog/digital transmission system. The performance of hybrid AM/QAM systems have been investigated, but to date no one has examined how a multilevel ASK system (with or without VSB filtering) would perform in such an environment. Hence, the main research objectives of this work can be defined as:

(i) Theoretically and experimentally study the impact of noise and nonlinear distortion of a lightwave SCM system on the error performance of a multilevel ASK signal transmitted in such a noise environment.

(ii) Determine the manner in which nonlinear distortion due to threshold clipping and nonlinear distortion due to the combination of laser chirp and fiber dispersion individually and collectively impact the error performance of a multilevel ASK signal in a lightwave SCM transmission system.

This thesis consists of 6 chapters, the organization of which is described as follows. Chapter 2 gives an overview of transmitting analog and digital signals over fiber optics, including common modulation formats and the main sources of signal degradation

in a lightwave SCM system. Chapter 3 presents a theoretical analysis of the performance of a multilevel ASK signal transmitted in a hybrid subcarrier multiplexed AM/VSB-multilevel ASK transmission system. In chapter 4, the design and characterization of a multichannel fiber optic transmission system is outlined. Chapter 5 gives an experimental study of the error performance of a single 8-level ASK signal transmitted in a hybrid multichannel AM/VSB-multilevel ASK television system. The theoretical results obtained in chapter 3 are also compared to the experimental results in chapter 5. Finally, concluding remarks relating to the theoretical and experimental study are presented in chapter 6.

2.0 Optical Fiber Transmission of Analog and Digital Video Signals

In the introductory chapter, a migration path from broadcast analog video to broadcast digital video was outlined. With advances in both video compression and digital modulation techniques, it is feasible that broadcast CATV will be in the form of digital HDTV by the early part of the 21st century. However, in the interim, it is quite likely that both analog and digital techniques will be used for delivery of video to the home. Subcarrier multiplexing, as described in the previous chapter, is the most efficient means of multiplexing the video signals, while a hybrid fiber/coaxial (HFC) network is often considered the infrastructure of choice [5], [7], [8]. Therefore, it is necessary to understand the implications of transmitting combined analog and digital video over an optical fiber system.

In the first section of the current chapter, modulation formats used for transmission of analog and digital video will be presented. This includes the NTSC format used for broadcast of analog video, AM/VSB, as well as two possibilities for transmission of digital video: multilevel amplitude shift keying (ASK) and quadrature amplitude modulation (QAM). Following that, the system impairments associated with an SCM optical fiber system will be discussed. This includes Gaussian noise, nonlinear distortion due to laser clipping, and nonlinear distortion resulting from the combined effects of laser chirp and fiber dispersion. Special attention will be given to explaining the manner in which nonlinear distortion affects analog and digital signals in an SCM system.

2.1 Modulation Formats

Currently, analog video is broadcast in North America using vestigial sideband amplitude modulation (AM/VSB). In keeping with the Federal Communications Commission (FCC) rulings in the United States, CATV broadcasters who begin transmitting HDTV signals must continue transmitting analog television channels for close to a decade [12]. The FCC will be assigning a new UHF TV channel for digital transmission of each existing analog NTSC TV station [12], with the digital signals limited to the present 6 MHz channel bandwidth. Consequently, there is a need for the use of spectrally-efficient digital modulation formats. The proposals that have risen to the top are either based on QAM modulation techniques or multilevel ASK, combined with vestigial sideband filtering.

2.1.1 Vestigial Sideband Amplitude Modulation (AM/VSB)

Current transmission of CATV signals in North America is accomplished through vestigial sideband amplitude modulation (AM/VSB). In order to convert a baseband signal into an AM/VSB signal, the amplitude of a sinusoidal carrier is varied in proportion to the input information signal, resulting in a double-sideband spectrum at a higher frequency. The modulated carrier enters a vestigial sideband filter, which passes the entire upper sideband and a portion of the lower sideband. Vestigial sideband filtering is used because it is more spectrally efficient than double sideband techniques and easier to implement than single sideband filtering.

For NTSC broadcast of analog television, 525 lines of video information are transmitted every 1/30 of a second. In actuality, the frame rate is 60 frames/sec; however, interlaced scanning is used to half the line rate to 15.75 klines/sec [23]. This results in a baseband bandwidth of 4 MHz, which would require 8 MHz per channel if double sideband modulation is used. Vestigial sideband filtering removes a portion of the signal spectrum since each channel is allotted only 6 MHz of the RF frequency band. A typical AM/VSB channel spectrum is displayed in Figure 2.1. In addition to the video information signal, the three major frequency components are the video carrier, sound carrier, and color subcarrier, of which the video carrier is the most dominant.

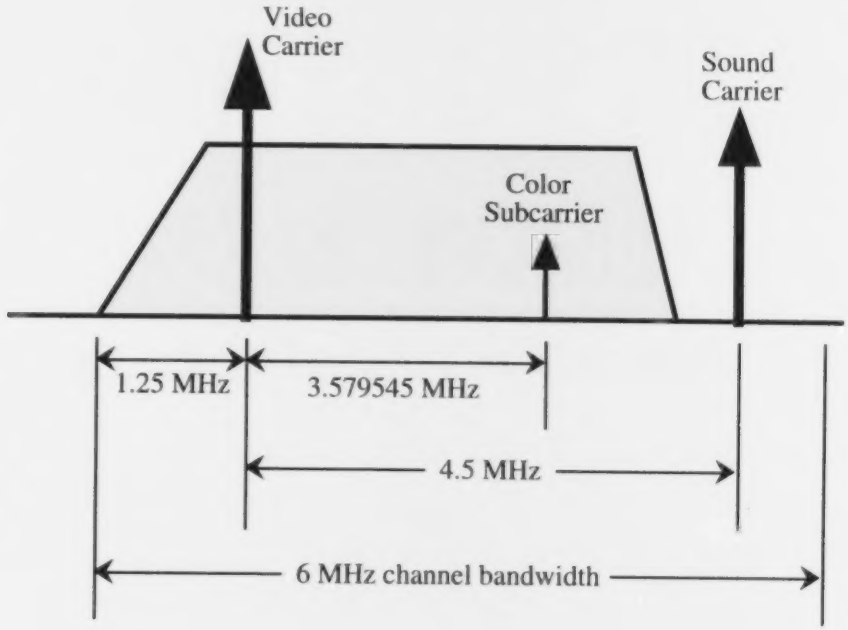

Figure 2.1: NTSC Analog Television Spectrum

2.1.2 Quadrature Amplitude Modulation (QAM)

Quadrature amplitude modulation is the most widely-studied format for the delivery of digital television signals [24]-[31]. The reason for the popularity of QAM transmission is its spectral efficiency. For a single-carrier modulation technique, the amplitude, phase or frequency of the carrier can be varied in proportion to the modulating signal. For QAM transmission, both the carrier amplitude and phase are modulated. This is accomplished by controlling the amplitude of two separate quadrature carriers (i.e. 90° out-of-phase) which are located at the same frequency. The constellation diagram for a 16-QAM signal is shown in Figure 2.2. The I-Q plane represents the In-phase and Quadrature components of the modulated carrier. Each discrete point in the constellation diagram represents a vector sum of the magnitude of the in-phase carrier and the magnitude of the out-of-phase or quadrature carrier. For M^2-QAM, there are M possible levels for each of the two carrier components. Therefore, the bit efficiency is twice that of a double sideband M-level ASK system. Every symbol in an M^2-QAM signal is generated from two binary input sequences, each with a bit length of $\log_2 M$. Therefore, each symbol for 16-QAM represents one of 16 four-bit words and every symbol for 64-QAM represents one of 64 six-bit words. Consequently, the symbol rate is much lower than the bit rate, reducing the bandwidth required to transmit the modulated signal. However, as the number of states increases, the distance between these states is reduced, resulting in lower immunity to noise and intersymbol interference.

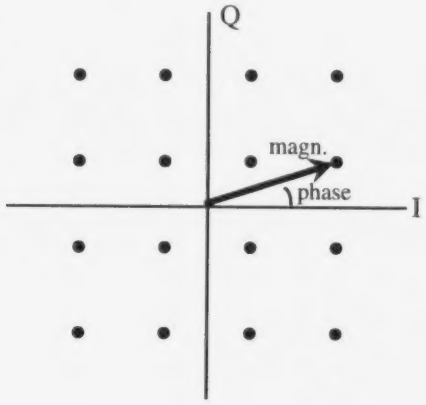

Figure 2.2: Constellation Diagram for 16-QAM

Much of the research into the effects of noise and nonlinear distortion on SCM optical fiber transmission has been directed towards the performance of an AM/VSB - QAM transmission system. However, it will be shown that the same analyses apply to a multichannel AM/VSB-multilevel ASK system due to the close similarities between QAM and multilevel ASK.

2.1.3 Multilevel Amplitude Shift Keying (ASK)

Binary ASK (often referred to as 'on-off keying') is a modulation technique whereby the amplitude of a carrier can take on one of two values, depending on whether the input to the modulator is a 0 or a 1. Multilevel ASK is a digital signaling technique in which the input binary stream is first converted to a multilevel signal through a pulse-coded modulation (PCM) algorithm. The encoded multilevel signal is then used to modulate the amplitude of a carrier; therefore, the carrier frequency and phase remain fixed while the carrier amplitude can take on one of M distinct values.

The transmitted waveform for an M-ary ASK signal can be given as:

$$s_m(t) = A_m \cdot Re\left[p(t) \cdot e^{j2\pi f_c t}\right] \tag{2.1}$$

where: A_m = 2m-1-M, m = 1, 2, ..., M

$Re[x]$ is the real part of x

$p(t)$ is the baseband pulse shape

Examination of equation (2.1) reveals that multilevel ASK is a one-dimensional modulation technique. Since only the amplitude of a fixed carrier is modulated, all the symbol points are located on the real axis of the constellation diagram, as shown in Figure 2.3. Notice that multilevel ASK is equivalent to one dimension of a QAM-modulated signal. Each symbol in M-ary ASK is defined by $\log_2 M$ bits from an input binary stream. Therefore, the use of multilevel ASK reduces the bandwidth required to transmit a signal, but has half the spectral efficiency of 2-dimensional QAM. However, since the spectral components on either side of the carrier for an ASK signal are equivalent, single sideband (SSB) or vestigial sideband (VSB) filtering can be utilized. Consequently, M-ary ASK-SSB and M^2-QAM have the same bit efficiency.

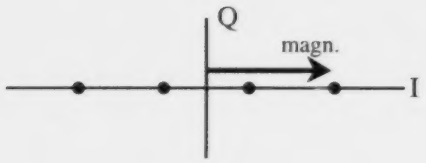

Figure 2.3: Constellation (or Space State) Diagram for Multilevel ASK

2.2 Sources of Degradation in a Lightwave SCM System

There are two main sources of degradation in a subcarrier multiplexed optical fiber transmission system. These system impairments are Gaussian noise and nonlinear distortion. Gaussian noise is considered to have a white power spectral density across the bandwidth of any CATV channel. However, nonlinear distortion results in a number of distortion products existing at discrete frequencies, which are defined by the subcarrier frequencies of the analog signals. As will be demonstrated later, Gaussian noise and nonlinear distortion affect the performance of a multilevel ASK signal in differing manners.

2.2.1 Gaussian Noise

The three main types of Gaussian noise in a fiber optic transmission system are thermal noise, shot noise, and laser relative intensity noise (RIN) [11]. Thermal noise is a result of thermally-excited random motion of free electrons in a conducting medium, such as a resistor [32]. Shot noise is generated when current flows in a circuit [1] and, in the case of photocurrent, is due to the statistical nature of the production and collection of photoelectrons when an optical signal is incident upon a photodetector [33]. Laser RIN noise is generally defined as the ratio of the mean square of laser intensity fluctuation to the mean square of the laser output intensity [10]. The RIN noise spectral density at the output of the photodetector is proportional to the square of the output DC photocurrent. With increasing received optical power, three distinct regimes exist in which each noise term is the dominant source of Gaussian noise. That is, for low received optical power levels, thermal noise dominates over the other two noise sources. As the received optical power increases, a point is reached whereby the shot noise current becomes larger than the thermal noise current. Eventually, RIN noise will become the dominant source of Gaussian noise as the received optical power reaches a certain value. The three main sources of Gaussian noise currents in an optical fiber system can be described by the following equations [33]:

$$\text{Thermal noise: } \left\langle i_t^2 \right\rangle = \frac{4kTF}{R_{eq}} \cdot B \tag{2.2}$$

where k is Boltzmann's constant (1.38054×10^{-23} J/K), T is the absolute temperature (in Kelvin), R_{eq} is the receiver equivalent load resistance, F is the noise factor of the preamplifier, and B is the single-sided noise bandwidth of the receiver.

$$\text{Shot noise: } \left\langle i_{sh}^2 \right\rangle = 2q\Re P_o \cdot B \tag{2.3}$$

where q is the electronic charge (1.602×10^{-19} C), $\Re$ is the photodetector responsivity (in A/W), and P_o is the average received optical power.

$$\text{RIN noise: } \left\langle i_{RIN}^2 \right\rangle = RIN \left(\Re P_o\right)^2 \cdot B \tag{2.4}$$

where $RIN = \dfrac{\left\langle \left(\Delta P_L\right)^2 \right\rangle}{\left\langle P_L \right\rangle^2}$

and $\left\langle \left(\Delta P_L\right)^2 \right\rangle$ is the mean square intensity fluctuation of the laser output with $\left\langle P_L \right\rangle$ as the average laser light output power.

2.2.2 Nonlinear Distortion due to Laser Diode Clipping

Numerous types of nonlinear distortion exist in an optical subcarrier multiplexed transmission system. Nonlinear distortion is created through optical reflections in the transmission medium, resonance distortion resulting from intrinsic nonlinearities described by the laser rate equations [11], [34], distortion produced by the combined effects of laser diode chirp and fiber dispersion [11], [31], and distortion caused by nonlinearities in the laser power-current (L-I) characteristic. A dominant form of nonlinear distortion (NLD) in a lightwave SCM system is clipping-induced NLD, which is often considered to be the most severe type of distortion created in an SCM system [11], [24], [28], [34]-[39].

A typical laser power-current curve exhibits a threshold level below which the output optical power is negligible. If intensity modulation of the laser causes the input current to fall below the threshold level, the output power is nearly clamped at a low level, as shown in Figure 2.4. Since the output is no longer a linear function of the input, higher

order harmonics of the frequency components contained within the input signal are created. In a multichannel frequency-division multiplexed system, the variance of the composite signal is a function of both the number of channels and the modulation index of each channel. Therefore, the maximum number of channels and the maximum per channel modulation index are both limited by the distortion created through clipping of the laser diode output power [35].

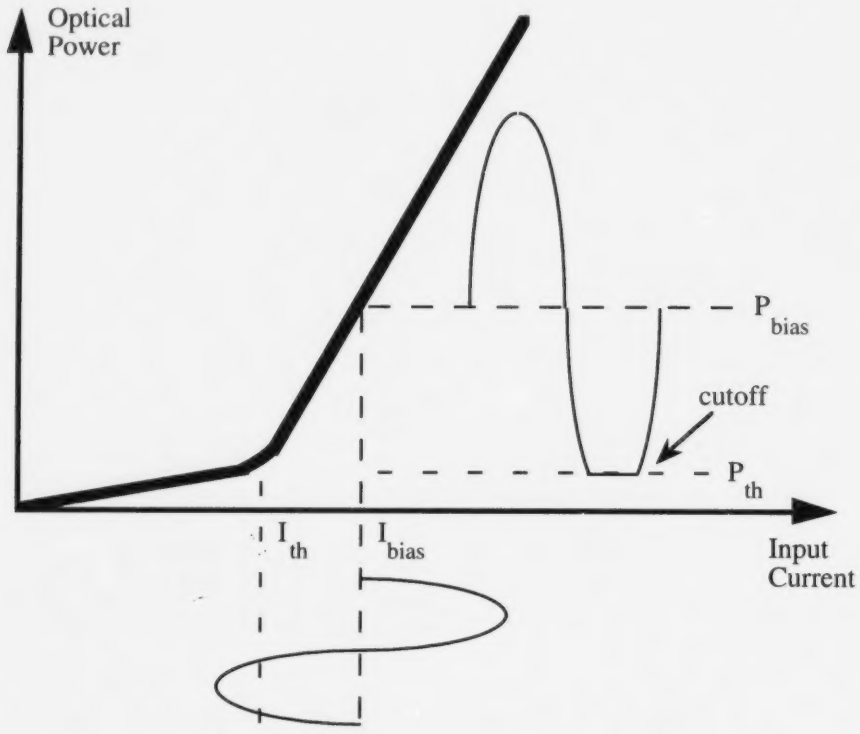

Figure 2.4: Laser Diode Threshold Clipping

Much effort has recently been directed towards understanding the effect of clipping distortion in CATV systems. A simple model of clipping-induced nonlinear distortion was presented by Saleh [35], where the clipping process is considered to be the superposition of an ideal modulation and a noise process in which the added power is equal to the power that was originally clipped [38]. Saleh interpreted the total photocurrent due to the signal as a Gaussian random process with the constraint that the number of subcarriers be greater than 10. The Gaussian approximation follows from application of the Central Limit

Theorem with the assumption that the individual subcarriers are statistically-independent zero-mean random processes. Since the total photocurrent is the summation of the photocurrent generated from each subcarrier, the Central Limit Theorem can be accurately applied. Finally, Saleh proposed that all of the nonlinear distortion power created through clipping is uniformly distributed over the CATV band. Based on his model, Saleh was able to determine an equation for the carrier-to-nonlinear distortion ratio (C/NLD) due to clipping.

Saleh's work on clipping-induced distortion was taken one step further by Alameh and Minasian [36], who recognized that the majority of the distortion spectral density falls outside the transmission band and therefore has no effect on the C/NLD. Alameh and Minasian used a transform method to determine the distortion power within a single channel band. Their analysis begins by defining the autocorrelation function of the laser output, which consists of a signal term ${}_sR_o(\tau)$ and a noise term ${}_nR_o(\tau)$:

$$ {}_sR_o(\tau) = \frac{(m\Re P_o)^2}{2} \cdot {h_{o,1}}^2 \cdot \sum_{n=1}^{N} \cos(2\pi f_n \tau) \tag{2.5} $$

$$ {}_nR_o(\tau) = \sum_{k=2}^{\infty} \frac{{h_{o,k}}^2}{k!} \cdot \sigma^{2k} \cdot sinc^k(\pi NB\tau) \cdot \cos^k(2\pi f_o \tau) \tag{2.6} $$

where m is the per channel modulation index, $\Re$ is the detector responsivity, P_o is the average received optical power, N is the total number of channels, B is the channel bandwidth, f_o is the frequency of the center channel, $h_{o,k}$ is a function that depends on the laser transfer characteristic, and σ^2 is the variance of the received photocurrent.

If $N > 10$, the received photocurrent is modeled as a Gaussian random process in which the variance is given as $\sigma^2 = \mu^2 \cdot (\Re P_o)^2$, where μ is the 'total rms modulation index' as defined by Saleh [35]:

$$ \mu = \sqrt{\frac{N \cdot m^2}{2}} \tag{2.7} $$

If we are concerned only with threshold clipping and not with saturation at high input current levels, $h_{o,k}$ can be defined as:

$$h_{o,k} = \frac{1}{2\pi} \cdot (-1)^{\frac{k-2}{2}} \cdot \left[\frac{\sqrt{2}}{\sigma}\right]^{k-1} \cdot exp\left(-\frac{1}{2\mu^2}\right) \cdot G_{k-2}\left[\frac{-\sqrt{2}}{\mu}\right] \qquad (2.8)$$

where [2]:

$$G_{k-2}\left[\frac{-\sqrt{2}}{\mu}\right] = \sum_{i=0}^{k-2} \frac{(k-2)!}{(i)! \cdot (k-2-i)!} \cdot \left[\frac{\sqrt{-1}}{\sqrt{2} \cdot \mu}\right]^{i} \cdot \int_{-\infty}^{\infty} \left(y^{k-2-i} \cdot e^{-y^2}\right) dy \qquad (2.9)$$

The power spectral density of the nonlinear distortion term is assumed to be constant over a small bandwidth and is found by taking the Fourier transform of the autocorrelation function given in (2.6). The total nonlinear distortion power in the pth channel is determined through multiplication of the double-sided power spectral density by twice the channel bandwidth. Using this technique, Alameh and Minasian give the clipping-induced nonlinear distortion power spectral density in the following form:

$${}_nW_o(f_p) = \sum_{k=2}^{\infty} \frac{{h_{o,k}}^2}{k!} \cdot \sigma^{2k} \cdot \int_{-\infty}^{\infty} sinc^k(\pi NB\tau) \cdot cos^k(2\pi f_o \tau) \cdot cos(2\pi f_p \tau)\, d\tau \qquad (2.10)$$

and therefore the nonlinear distortion power in the pth channel is:

$$N_p = {}_nW_o(f_p) \cdot 2B \qquad (2.11)$$

Numerous other models and modifications have been proposed for relating threshold clipping of an SCM signal to nonlinear distortion created in the CATV band. Modification to Saleh's equation was made by Mazo [39] who indicated that for large values of the total rms modulation index, approximately half of the distortion power appears outside of the CATV band. Mazo then proceeds to derive a model of the threshold crossing behavior of a Gaussian random process, whereby the clipping events are considered to be a Poisson random process, the probability density of the time between any upcrossing and subsequent downcrossing follows a Rayleigh distribution, and the shape of each clipped pulse is modeled as a parabola. Mazo's progress in understanding the statistical nature of threshold clipping has led to a number of follow-up analyses that predict the effect of clipping on the performance of digital signals transmitted in the CATV band

[24], [26], [30], [40], [41]. One of these analyses [40] will be used for comparison to experimental results in a later chapter of this thesis.

In an analysis by Shi *et. al.* [42], the power spectral density of second and third order distortion created by laser clipping within the bandwidth of a given channel is determined. The autocorrelation function of the laser output is written in a Taylor series, so that the C/NLD can be expressed as a function of frequency and order of distortion. Another model of interest is presented by Frigo *et. al.* [37], [38], who determine the clipping distortion at intermodulation frequencies, allowing for easier comparison between theoretical results and standard CATV experimental measurements. The authors use the model of clipped Gaussian noise to define a new 'effective' transfer function for the laser power-current (L-I) curve. Later work by Ho and Kahn demonstrated that the model presented by Frigo et. al. [37], [38] is identical to the series model presented by Shi *et. al.* [42].

2.2.3 Nonlinear Distortion due to the Combination of Laser Diode Chirp and Nonlinear Optics

In a subcarrier multiplexed optical fiber transmission system operating at a wavelength of 1550 nm, nonlinear distortion is also created through the combination of laser chirp and fiber dispersion as well as the combination of laser chirp and the non-flat gain spectrum of an erbium-doped fiber amplifier (EDFA). In chapter 5, the impact of chirp and dispersion is experimentally investigated for a multichannel SCM transmission system. The impact of placing an EDFA in the optical link will be briefly discussed in this section, but was not examined further in this work.

Laser diode chirp is a phenomenon in which the output optical frequency (or wavelength) of a laser is inadvertently modulated as a result of directly modulating the laser diode. As the drive current is modulated, the carrier density is varied, which results in modulation of the refractive index of the laser's active layer. The output wavelength is a function of the laser's refractive index, and therefore direct modulation causes variations in the output wavelength of the laser.

Light at different wavelengths travels through optical fibers at different group velocities due to intramodal fiber dispersion. A common form of intramodal dispersion is chromatic dispersion [33], which arises from the fact that the refractive index of optical fiber core material varies with wavelength. Consequently, laser diode chirp causes modulation of the source wavelength, which, when combined with fiber dispersion, results

in modulation of the transmission delay. Variations in the transmission delay give rise to second order distortion in the system.

If operating at a wavelength of 1550 nm, it is desirable to include Erbium-doped fiber amplifiers in the setup as a means of increasing the link power budget or the total number of subscribers. However, the addition of an EDFA introduces extra noise terms and extra nonlinear distortion due to the combination of laser diode chirp and the non-flat gain spectrum of an EDFA. Since laser chirp results in modulation of the optical wavelength, the non-flat gain characteristic of an EDFA combined with chirp results in variation of the signal gain, thus causing nonlinear distortion [43]. In earlier experimental work at TR*Labs* [2], it was found that chirp/dispersion-induced nonlinear distortion has a much more severe impact on the performance of a digital signal transmitted in a multichannel system than does distortion arising from the combination of laser chirp and the non-flat gain spectrum of an Erbium-doped fiber amplifier.

2.3 Results of Nonlinear Distortion in a Multichannel SCM system

Multichannel nonlinear distortion arises from the mixing of microwave subcarriers within a nonlinear device such as a laser cavity. The three main types of nonlinear distortion are cross-modulation, harmonic distortion, and intermodulation distortion [9]. Of the three, intermodulation distortion tends to dominate in CATV systems, and is used to characterize the distortion performance of a given channel.

Cross-modulation involves the transfer of modulation from one or more subcarriers to another subcarrier. It occurs as a result of nonlinear gain in the system [2]. Modulation in one channel varies the gain of the laser which in turn causes modulation of other subcarriers. Harmonic distortion causes harmonics of a subcarrier frequency to exist in the bandwidth of another channel due to a nonlinearity in the system. Harmonic distortion products would exist at frequencies of $2f_1$, $3f_1$, etc. for a subcarrier at a frequency of f_1.

Intermodulation distortion occurs in multichannel systems due to the interaction of two or more subcarrier frequencies. The resulting distortion products are located at discrete frequencies, many of which appear in the passband of other CATV channels. Interaction between two frequencies, f_1 and f_2, may result in second-order distortion products at $|f_1 \pm f_2|$. Third-order distortion can take the form of either two-tone intermodulation distortion at $|2f_1 \pm f_2|$ and $|2f_2 \pm f_1|$ or triple beat distortion at $|f_1 \pm f_2 \pm f_3|$ resulting from the interaction of three discrete subcarriers. For a large number of channels, triple beat distortion is the dominant form of third-order distortion [9].

In measuring the performance of a CATV system, generally only the second-order and third-order distortion products are considered, since the distortion power decreases significantly as the order of distortion increases. Third-order intermodulation distortion is highest in the central channels of a multichannel system, while second-order distortion products are most prevalent at the low and high edges of the CATV band. Nonlinear distortion performance of a CATV system is specified by two parameters known as composite second order (CSO) distortion and composite triple beat (CTB) distortion. In a multichannel transmission system, many of the numerous second-order and third-order intermodulation distortion products will be located at or near the same frequency. The result is known as beat stacking [33]. The CSO and CTB terms are the ratios of the accumulated power of second-order and third-order intermodulation products, respectively, located within a 6 MHz channel bandwidth to the carrier power.

Typical distortion specifications at the subscriber's television set for a fiber-based system are a CSO of -50 dBc and a CTB of -55 dBc [11]. Cross-modulation distortion, harmonic distortion, and other forms of intermodulation distortion will exist in a multichannel SCM system. However, these others forms of distortion are relatively small in comparison to CSO and CTB, and are therefore not considered when determining system performance.

3.0 Theoretical Error Performance of Multilevel ASK in a Hybrid AM/VSB - Multilevel ASK Subcarrier Multiplexed Lightwave Transmission System

Subcarrier multiplexing is an efficient method for distributing multichannel video signals on lightwave CATV networks. In the near future, it is likely that cable companies will transmit both analog AM/VSB signals and HDTV signals side-by-side using SCM techniques. Therefore, it is necessary to examine the performance of the digital HDTV signal when transmitted alongside a large number of analog television signals.

In a multichannel SCM system, Gaussian noise and nonlinear distortion are the two main sources of signal degradation. For a transmission system that involves short fiber lengths, such as a metropolitan CATV network, threshold clipping of the headend laser diode is the dominant source of nonlinear distortion. This theoretical analysis will examine the effects of Gaussian noise and clipping-induced nonlinear distortion on the bit error ratio (BER) performance of a multilevel ASK digital signal in a hybrid AM/VSB - multilevel ASK subcarrier multiplexed lightwave CATV transmission system.

3.1 System Parameters of an AM/VSB Signal

The noise performance of an analog CATV signal is determined through measurement of the analog carrier-to-noise ratio (CNR). The carrier power is a function of the optical modulation index, while the noise power is the summation of the three Gaussian noise terms defined in section 2.2.1. The distortion performance of an analog signal is given by the composite second order (CSO) and composite triple beat (CTB) distortion terms within the 6 MHz channel of interest. CSO and CTB result from the accumulation of second-order and third-order intermodulation products, respectively, as a result of nonlinearities in a subcarrier multiplexed system. In this section, equations for the modulation index and corresponding carrier-to-noise ratio of an AM/VSB signal are derived. Experimental CSO and CTB performance is presented in a later chapter.

3.1.1 AM/VSB Modulation Index

The transmitted optical power for a directly-modulated lightwave transmission system can be written as:

$$P(t) = P_{bias}\left(1 + m(t)\right) \tag{3.1}$$

where P_{bias} is the average output optical power for a given bias current I_{bias}, and $m(t)$ is the time-varying modulation signal. If N subcarriers are transmitted via SCM direct modulation of the laser diode, the optical power can be rewritten in the following form:

$$P(t) = P_{bias}\left[1 + \sum_{i=1}^{N} m_i \cdot cos(2\pi f_i t + \theta_i)\right] \tag{3.2}$$

where f_i, θ_i and m_i are the carrier frequency, carrier phase and peak modulation index for channel i, respectively. The modulation index for each channel m_i is determined from analysis of the laser power-current curve as shown in Figure 3.1. The peak modulation index can be represented mathematically as

$$m = \frac{P_{peak}}{P_{bias}} = \frac{\Delta I}{I_{bias} - I_{th}} \tag{3.3}$$

where ΔI is the peak amplitude of the modulating current and I_{th} is the threshold current. If all the analog channels have the same modulation index, m is referred to as the 'peak modulation index per channel'. The rationale for including the threshold current term in equation (3.3) is that the laser has a very sharp threshold turn-on characteristic and therefore generates a negligible amount of optical power when the driving current is lower than the threshold value.

Since system performance for analog CATV is determined using unmodulated sinusoidal carriers, the peak modulation index m, as defined in equation (3.3), relates to the time-varying modulation signal $m(t)$ used in equation (3.1) in the following manner:

$$m(t) = m \cdot cos(2\pi f t) \tag{3.4}$$

where only a single carrier is being transmitted.

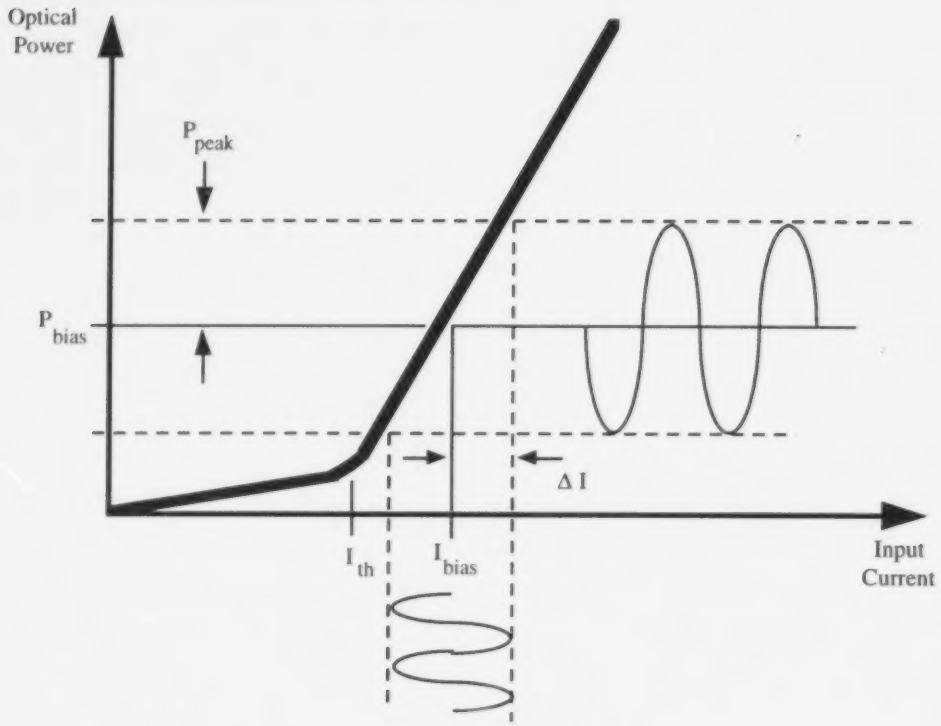

Figure 3.1: Modulation Index from Laser Power-Current Curve

3.1.2 Carrier-to-Noise Ratio for an AM/VSB Channel

For a single AM/VSB channel with a peak modulation index m, the mean square carrier current at the output of the photodiode is [33]

$$\left\langle i_{AM/VSB}{}^2 \right\rangle = \frac{I}{2}\left(m\Re P_o\right)^2 \tag{3.5}$$

where $\Re$ is the photodiode responsivity and P_o is the average received optical power. If the rms modulation index is used rather than the peak modulation index, the mean square carrier current has the following form:

$$\left\langle i_{AM/VSB}{}^2 \right\rangle = \left(m_{rms}\Re P_o\right)^2 \tag{3.6}$$

where m_{rms} is the per channel rms modulation index. For the remainder of this work, the peak modulation index is used for all theoretical and experimental results.

As mentioned earlier, the noise performance of an analog CATV signal is determined through measurement of the carrier-to-noise ratio, which is given as

$$CNR = \frac{Carrier\ Power}{Thermal\ noise + Shot\ noise + RIN\ noise} \tag{3.7}$$

Substituting the carrier power as defined in equation (3.5) and the three Gaussian noise terms as given in equations (2.2), (2.3) and (2.4), the CNR for a single analog channel can be written in the following form:

$$CNR = \frac{\frac{1}{2}(m\Re P_o)^2}{\frac{4kTF}{R_{eq}} \cdot B + 2q\Re P_o \cdot B + RIN\,(\Re P_o)^2 \cdot B} \tag{3.8}$$

3.2 BER Analysis of a Multilevel ASK Signal in the Presence of Gaussian Noise

For multilevel ASK signaling, an input binary stream is converted to a multilevel baseband signal according to a pulse code modulation (PCM) algorithm. The multilevel signal amplitude modulates a subcarrier at a given frequency; therefore, the signal amplitude can take on one of M levels while maintaining a constant frequency and phase. Traditional error analysis for multilevel signaling [44], [45] assumes that a matched filter demodulator is used in the receiver, and develops an equation for the bit error ratio accordingly. Although this analysis is valid, it can not be easily expanded to include the effects of non-Gaussian impulsive noise. A second method for determining the bit error ratio of a multilevel ASK signal in the presence of Gaussian noise will be introduced in this section. This technique stems from analysis of an M-ary ASK constellation diagram, in which the 'minimum distance between signaling points' d_{min} and the peak signal envelope S are defined graphically. These parameters are then related to the 'peak power factor' PF, and the error performance is determined through integration of the tails of a Gaussian noise pdf for each signaling point. This techique can be easily modified to include the effects of impulsive noise, as will be demonstrated in a subsequent section of this chapter. Since this second analysis method is not commonly used to determine the BER of a multilevel ASK signal, the equivalence between this technique and a matched filter analysis will be shown.

3.2.1 Matched Filter Demodulation Analysis

Before determining the probability of error for M-ary ASK, it is necessary to obtain an equation for the average transmitted power of a multilevel ASK signal. The transmitted waveform for multilevel ASK can be written as

$$s_m(t) = A_m \cdot Re\left[p(t) \cdot e^{j2\pi f_c t}\right] \tag{3.9}$$

as previously defined in section 2.1.3. For most error analyses, the baseband pulse is assumed to have a rectangular shape, which results in a power spectral density that follows a $\text{sinc}^2(x)$ function. However, pulse shaping can be used at baseband in an effort to reduce the spectral content of the bandpass signal. This is useful in situations whereby the bandpass filtering of the modulated signal would result in intersymbol interference (ISI) in the absence of baseband filtering. At this point in the analysis, it is assumed that ISI is not a major factor in the error performance of the transmitted signal and therefore pulse shaping will not be taken into account.

The energy for each level of a modulated multilevel ASK signal can be given as [44]:

$$\mathcal{E}_m = \int_0^T s_m^2(t) \cdot dt = A_m^2 \cdot \mathcal{E} \tag{3.10}$$

where $\mathcal{E}$ is the energy of the pulse $p(t)$. The average transmitted signal power is calculated by determining the mean value of the signal power over all M symbols:

$$P_{ave} = \frac{1}{T}\int_0^T E\left[s_m^2(t)\right]dt = \frac{E\left(A_m^2\right)}{T} \cdot \mathcal{E} \tag{3.11}$$

where $E(x)$ is the expected or mean value of x, and T is the period of the baseband pulse or the symbol period. From [44], the expected value of A_m^2, assuming that each of the signaling levels are equi-probable, can be given as

$$E\left(A_m^2\right) = \frac{M^2 - 1}{3} \tag{3.12}$$

and therefore the average transmitted power can be found through substitution of equation (3.12) into equation (3.11) to obtain the following result:

$$P_{ave} = \frac{M^2 - 1}{3} \cdot \frac{\mathcal{E}}{T} \tag{3.13}$$

The average probability of error for a multiamplitude ASK signal is equal to the probability that the noise variable *n* is greater in magnitude than 1/2 the distance between signaling levels. The probability of error for the two most outer symbols is similar to the binary case since there is only one direction in which an error can be made. For the remaining M-2 amplitudes, each symbol has two neighboring symbols, and therefore the probability of error given that an inner symbol is transmitted is twice as much as that for one of the two outer signaling levels.

The error ratio when an outer symbol is transmitted is equivalent to the error ratio for bipolar binary signaling [45] and can be determined in the following manner. Assume that the pulse amplitudes for a binary ASK system are A_p and $-A_p$. If the probability of transmitting a 0 or a 1 is the same, the average probability of error is equal to the probability of error when either a 0 or a 1 is transmitted. If a 0 is transmitted, an error occurs if the noise variable *n* is greater than the pulse amplitude A_p. If the noise source consists of additive white Gaussian noise, the probability density function of the noise has the following form:

$$p_n(n) = \frac{1}{\sqrt{2\pi} \cdot \sigma_n} \cdot e^{-n^2/2\sigma_n^2} \tag{3.14}$$

where σ_n^2 is the noise variance. The probability of error for binary ASK is calculated by integrating the tail of the Gaussian noise term to give

$$P_e = \frac{1}{\sqrt{2\pi} \cdot \sigma_n} \cdot \int_{A_p}^{\infty} e^{-n^2/2\sigma_n^2} \cdot dn \tag{3.15}$$

This result can be written in terms of the 'complementary error function', erfc(x), in the following manner:

$$P_e = \frac{1}{2} \cdot erfc\left(\frac{A_p}{\sqrt{2} \cdot \sigma_n}\right) \tag{3.16}$$

where: $erfc(x) = \frac{2}{\sqrt{\pi}} \int_x^{\infty} e^{-y^2} \cdot dy$ (3.17)

Equation (3.16) gives the probability of error if one of the two outer symbols is transmitted. For a multilevel ASK signal in which each signal is equi-probable, the average probability of error is equal to [45]:

$$P_M = \frac{2(M-1)}{M} \cdot P_e \tag{3.18}$$

where M is the total number of symbols and P_M is the average probability of a symbol error. Substitution of equation (3.16) into equation (3.18) gives the following result:

$$P_M = \frac{M-1}{M} \cdot erfc\left(\frac{A_p}{\sqrt{2} \cdot \sigma_n}\right) \tag{3.19}$$

If the filter in the receiver is matched to the received pulse in such a way that the signal-to-noise amplitude ratio is maximized at the decision-making instant, it can be shown [45] that the noise variance and signal amplitude can be rewritten in terms of the pulse energy $\mathcal{E}$ to give an average symbol error probability equal to

$$P_M = \frac{M-1}{M} \cdot erfc\left(\sqrt{\frac{\mathcal{E}}{\eta}}\right) \tag{3.20}$$

where $\eta/2$ is the two-sided power spectral density of the additive Gaussian noise. Derivation of equation (3.20) from equation (3.19) is given in [45] and follows from utilization of a matched filter demodulator in a multilevel ASK system. By manipulating equation (3.13) in terms of $\mathcal{E}$ and applying the definition of *SNR* as given in [44], the probability of a symbol error for multilevel ASK in a Gaussian noise environment can be written in the following form:

$$P_M = \frac{M-1}{M} \cdot erfc\left(\sqrt{\frac{3}{M^2-1} \cdot SNR}\right) \tag{3.21}$$

Equation (3.21) defines the symbol error ratio for a multilevel ASK system. If an equation for the bit error ratio is desired, the relation between a symbol error and a bit error must be known. For all experimental measurements, Gray coding is used to convert the input binary stream to a multilevel signal before upconversion. If a Gray code is used, an error in detecting a symbol will cause only one error in the k bits transmitted for that symbol. Therefore, the bit error ratio is equal to the symbol error ratio divided by k, where k is equal to $\log_2 M$. Consequently, the bit error ratio for a Gray-encoded multilevel ASK signal determined using a matched filter analysis can be written as:

$$P_b = \frac{M-1}{M \cdot \log_2 M} \cdot erfc\left(\sqrt{\frac{3}{M^2-1} \cdot SNR}\right) \tag{3.22}$$

3.2.2 Alternative Analysis for Determining the BER of Multilevel ASK in Gaussian Noise

Although the derivation of equation (3.22) in the previous section is mathematically sound, it does not lend itself to extension into a system in which other forms of non-Gaussian noise are present. Consequently, an alternative method for determining the error performance of multilevel ASK is presented in this section, and the equivalence between the results of this analysis and equation (3.22) will be shown.

The analysis in this section relates the error performance to the 'minimum distance between signaling points' d_{min}, since this allows easy extension to any noise probability density function, not just Gaussian. Figure 3.2 shows a signal space diagram for an 8-level ASK signal, in which d_{min} and the 'peak signal envelope' S are defined graphically.

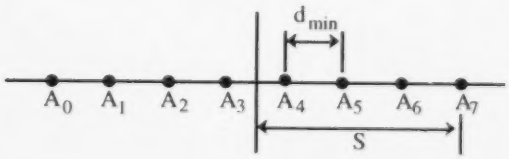

Figure 3.2: Signal Space Diagram for 8-level ASK

If a given symbol, such as A_4, is transmitted, an error will occur if the magnitude of the noise variable n centered at A_4 is greater than $d_{min}/2$. Therefore, the probability of error in a single direction for one symbol can be found by integrating the noise pdf from $d_{min}/2$ to ∞. Since it is preferable to relate the bit error ratio to the received signal-to-noise ratio, it is useful to define d_{min} in terms of SNR. The peak signal envelope S for an M-ary ASK signal can be given as

$$S = \frac{M-1}{2} \cdot d_{min} \tag{3.23}$$

The peak power factor PF_M is defined as the ratio of the signal peak power to the average transmitted signal power. Therefore, the peak signal envelope can be written in terms of PF_M in the following manner:

$$S = \sqrt{2 \cdot P_{ave} \cdot PF_M} \tag{3.24}$$

Finally, the minimum signaling distance can be written in terms of the average transmitted power by combining equations (3.23) and (3.24) to give

$$d_{min} = \frac{2\sqrt{2} \cdot \sqrt{P_{ave} \cdot PF_M}}{M-1} \tag{3.25}$$

The peak power factor PF_M is a constant whose value depends on the number of signaling levels. PF_M is equal to 2.333 for 8-level ASK and 2.647 for 16-level ASK. With the average signal power as given in equation (3.13), it is possible to express the peak power factor in terms of the number of levels M in the following manner:

$$PF_M = \frac{(M-1)^2 \cdot \dfrac{\varepsilon}{T}}{\dfrac{M^2-1}{3} \cdot \dfrac{\varepsilon}{T}} = \frac{3(M-1)}{M+1} \tag{3.26}$$

As previously explained, the error probability in a single direction can be determined by integrating the noise probability density function from $d_{min}/2$ to ∞. With white Gaussian noise as defined in equation (3.14), the symbol error probability in a single direction for one symbol can be written as:

$$
\begin{aligned}
P_e &= \int_{d_{min}/2}^{\infty} p_n(n) \cdot dn \\
&= \frac{1}{\sqrt{2\pi} \cdot \sigma_n} \cdot \int_{d_{min}/2}^{\infty} exp\left(\frac{-n^2}{2 \cdot {\sigma_n}^2}\right) \cdot dn \\
&= \frac{1}{2} \cdot erfc\left(\frac{d_{min}}{2\sqrt{2} \cdot \sigma_n}\right)
\end{aligned}
\tag{3.27}
$$

Applying the derivation of d_{min} given in equation (3.25) and using equation (3.18) to relate the average probability of a symbol error P_M to the error probability in a single direction, the following result for the symbol error rate is obtained:

$$
P_M = \frac{M-1}{M} \cdot erfc\left(\frac{\sqrt{P_{ave} \cdot PF_M}}{(M-1) \cdot \sigma_n}\right) \tag{3.28}
$$

With the average signal-to-noise ratio defined as

$$
SNR = \frac{P_{ave}}{{\sigma_n}^2} \tag{3.29}
$$

and substituting equation (3.26) for PF_M and employing Gray-encoding as part of the PCM algorithm, the bit error ratio of an M-ary ASK signal transmitted in a Gaussian noise environment can be written in the following form:

$$
P_b = \frac{M-1}{M \cdot log_2 M} \cdot erfc\left(\sqrt{\frac{3 \cdot SNR}{M^2 - 1}}\right) \tag{3.30}
$$

which is identical to equation (3.22) obtained through a matched filter demodulator analysis in section 3.2.1. This demonstrates that the alternative error analysis used in this section is legitimate and can be extended to include the effects of non-Gaussian impulsive noise.

3.3 BER Analysis of a Multilevel ASK Signal in the Presence of Gaussian Noise and Non-Gaussian Impulsive Noise

In section 3.2, the bit error ratio performance of the multilevel ASK signal was determined in the presence of Gaussian noise alone. However, in an optical SCM system, a second form of performance degradation also exists. Since a large number of subcarriers are combined together to modulate the laser, any form of nonlinearity in the optical transmission system will cause nonlinear distortion as a result of subcarriers beating together. This type of noise does not have a white power spectral density and actually falls at discrete frequencies that depend on the frequencies of the subcarriers that are beating together. If nonlinear distortion is caused by threshold clipping of the laser diode, it has been shown that the resulting nonlinear distortion is actually impulsive in nature. Consequently, the probability density function of combined Gaussian and non-Gaussian impulsive noise must be determined before the performance of the multilevel ASK signal can be analyzed.

In chapter 2, recent work involving the impact of nonlinear distortion due to laser diode clipping was examined, with a resulting equation presented (i.e. equation 2.11) for calculating the amount of nonlinear distortion that exists in a given CATV channel. In this section, a noise model for combined Gaussian and non-Gaussian impulsive noise will be introduced. This model will be used to determine the bit error ratio of a multilevel ASK signal in such a noise environment following the analysis presented in section 3.2.2.

3.3.1 SNR and SNLD for an M-ary ASK Signal

In the analysis of the error performance of the digital ASK signal, both the signal-to-noise ratio and the signal-to-nonlinear distortion ratio of the multilevel signal are required parameters. With an M-ary ASK modulation index of m_{ask}, the signal-to-noise ratio will be

$$SNR = \frac{\frac{1}{2}\cdot\left(m_{ask}\Re P_o\right)^2}{\left\langle i_{th}^2\right\rangle + \left\langle i_{sh}^2\right\rangle + \left\langle i_{RIN}^2\right\rangle} \tag{3.31}$$

where the three noise terms in the denominator are thermal noise, shot noise and RIN noise, respectively, which are defined in equations (2.2) - (2.4). In section 2.2.2, the amount of nonlinear distortion in the p^{th} channel due to threshold clipping of the laser diode was given as ${}_nW_o(f_p)\cdot 2B$, and therefore the signal-to-nonlinear distortion ratio for a multilevel ASK signal is equal to

$$SNLD = \frac{\frac{1}{2} \cdot \left(m_{ask} \Re P_o\right)^2}{{}_nW_o\left(f_p\right) \cdot 2B} \tag{3.32}$$

where ${}_nW_o(f_p)$ is the clipping-induced nonlinear distortion power spectral density as derived by Alameh and Minasian [36].

3.3.2 Derivation of the BER for Multilevel ASK in Combined Gaussian and Non-Gaussian Impulsive Noise using Middleton's Class A Noise Model

Nonlinear distortion resulting from threshold clipping is known to have impulsive characteristics in the time domain. Impulsive noise has a highly structured form that can drastically degrade the performance of systems designed to handle the deleterious effects of Gaussian noise only. Therefore, in order to study the error performance of a digital signal transmitted in such an environment, it is necessary to use a noise model that includes both Gaussian noise and non-Gaussian impulsive noise. One such model is Middleton's class A noise model [46], [47], which can be used when the frequency components of the impulsive noise are limited to within the bandwidth of the receiver bandpass filter. Middleton's model has been successfully employed to evaluate the performance of quadrature amplitude modulated (QAM) signals transmitted in hybrid AM/QAM optical SCM transmission systems [27], [48], [49]. With Middleton's model for combined Gaussian and non-Gaussian impulsive noise, the signal amplitude probability distribution function for the combined noise has the following form:

$$p_{I+G}(n) = e^{-A} \cdot \sum_{j=0}^{\infty} \frac{A^j}{j!} \cdot \frac{1}{\sqrt{2\pi N_{tot} {\sigma_j}^2}} \cdot exp\left(\frac{-n^2}{2N_{tot} {\sigma_j}^2}\right) \tag{3.33}$$

$$\text{where } {\sigma_j}^2 = \frac{\frac{j}{A} + \Gamma'}{1 + \Gamma'} \tag{3.34}$$

and N_{tot} is the total noise power ($\sigma_g^2 + \sigma_I^2$), Γ' is the mean power ratio of the Gaussian noise component (σ_g^2) to the non-Gaussian noise component (σ_I^2), and A is the impulsive index, which is the product of the average number of received impulses in a second and the duration of an impulse.

Using a similar line of reasoning as that given in section 3.2.2, the probability of error in a single direction for one symbol in the presence of both Gaussian and impulsive noise is equal to

$$P_e = \int_{d_{min}/2}^{\infty} p_{I+G}(n) \cdot dn \tag{3.35}$$

Therefore, substituting (3.33) into the above equation and recalling the definition of erfc(x) from equation (3.17), the following is obtained for the error probability in a single direction:

$$P_e = \frac{e^{-A}}{2} \cdot \sum_{j=0}^{\infty} \frac{A^j}{j!} \cdot erfc\left(\frac{d_{min}}{2\sqrt{2N_{tot} \cdot \sigma_j}} \right) \tag{3.36}$$

For M-ary amplitude shift keying, the minimum distance between signaling points was previously determined in section 3.2.2 to be:

$$d_{min} = \frac{2\sqrt{2} \cdot \sqrt{P_{ave} \cdot PF_M}}{M-1} \tag{3.37}$$

Through substitution of equation (3.37) into equation (3.36), and making the assumption that each symbol is equi-probable and that Gray-encoding is used, the bit error ratio for a multilevel ASK signal in the presence of Gaussian and non-Gaussian impulsive noise can be expressed in the following form:

$$P_b = \frac{M-1}{M \cdot log_2 M} \cdot e^{-A} \cdot \sum_{j=0}^{\infty} \frac{A^j}{j!} \cdot erfc\left(\frac{\sqrt{P_{ave} \cdot PF_M}}{(M-1)\sqrt{N_{tot} \cdot \sigma_j}} \right) \tag{3.38}$$

Since N_{tot} is the total noise power, equation (3.38) can be described in terms of the signal-to-noise ratio providing that SNR is the ratio of the average ASK signal power to the total noise power (i.e. Gaussian noise power + impulsive noise power). Therefore, SNR for such a noise environment is equal to

$$SNR = \frac{P_{ave}}{N_{tot}} = \frac{1}{SNR_G^{-1} + SNLD^{-1}} \tag{3.39}$$

Consequently, the bit error ratio can be expressed as:

$$P_b = \frac{M-1}{M \cdot log_2 M} \cdot e^{-A} \cdot \sum_{j=0}^{\infty} \frac{A^j}{j!} \cdot erfc\left(\frac{\sqrt{SNR \cdot PF_M}}{(M-1) \cdot \sigma_j} \right) \tag{3.40}$$

Since Γ' is the mean power ratio of Gaussian noise to impulsive noise, this parameter can be written in the following form:

$$\Gamma' = \frac{\sigma_g^{\,2}}{\sigma_I^{\,2}} = \frac{SNLD}{SNR_G} \tag{3.41}$$

Therefore, through substitution of equations (3.34), (3.39) and (3.41) into equation (3.40), the bit error ratio of Gray-encoded multilevel ASK in a noise environment that includes both Gaussian noise and non-Gaussian impulsive noise is equal to

$$P_b = \frac{M-1}{M \cdot log_2 M} \cdot e^{-A} \cdot \sum_{j=0}^{\infty} \frac{A^j}{j!} \cdot erfc\left(\frac{\sqrt{\left(SNR_G^{-1} + SNLD^{-1}\right)^{-1} \cdot PF_M}}{(M-1) \cdot \sqrt{\dfrac{\dfrac{j}{A} + \dfrac{SNLD}{SNR_G}}{1 + \dfrac{SNLD}{SNR_G}}}} \right) \tag{3.42}$$

Figures 3.3 through 3.6 show theoretical results obtained using equation (3.42) to model the bit error ratio of an M-ary ASK signal in the presence of Gaussian noise and nonlinear distortion caused by laser diode clipping. In Figures 3.3 and 3.4, the BER is determined as a function of Gaussian SNR while the signal-to-nonlinear distortion ratio remains constant. For Figures 3.5 and 3.6, the Gaussian SNR is maintained at a certain value and the bit error ratio is measured as a function of SNLD. For both scenarios, the BER is determined for 8-level ASK and 16-level ASK. These two values correspond to the number of levels used in the N-VSB system for terrestial and cable broadcasting,

respectively. For all simulations, the impulsive index A is given a value of 0.022, which corresponds to a per channel modulation index of ~ 6% as previously measured at TR*Labs* [27]. The operating parameters for the optical transmitter and receiver correspond to those of the actual transmitter and receiver that will be used for obtaining experimental results. Finally, simulations are based on the transmission of one multilevel ASK channel alongside 42 analog carriers.

Three main observations can be made from analysis of the simulation results shown in Figures 3.3 and 3.4. First, it is apparent that a bit error ratio floor exists if the signal-to-nonlinear distortion ratio is below a certain value. Once this value of SNLD is reached, an increase in SNR has no impact on the bit error ratio. For example, in Figure 3.3 it is observed that for an SNLD of 40 dB, increasing the SNR above 30 dB has negligible impact on the BER. This indicates that the error performance of the digital signal is more dependant on SNLD than it is on SNR. Secondly, there is a threshold point at which a slight decrease in the SNLD causes a large degradation in the BER performance. For 8-level ASK, decreasing the SNLD from 45 dB to 40 dB causes the BER floor to increase from 10^{-12} to 10^{-7}. Finally, it is apparent that 16-level ASK is much more susceptible to the effects of nonlinear distortion than is 8-level ASK. Not only is there an SNR penalty for 16-level signaling (Figure 3.4) over 8-level signaling (Figure 3.3), but also the BER floors for a given SNLD are much worse for 16-ASK than they are for 8-ASK. Although higher level signaling increases the spectral efficiency of the transmitted signal, there are penalties to be paid due to both Gaussian noise and nonlinear distortion.

In Figures 3.5 and 3.6, it is obvious that as long as the Gaussian SNR is above a certain value, the bit error ratio is mainly dictated by the signal-to-nonlinear distortion ratio. In Figure 3.5, an increase in SNLD results in a corresponding increase in the BER performance for the three curves with signal-to-noise ratios of 30, 35 and 40 dB. When the SNR is lowered to 25 dB, the impact of Gaussian noise on error performance becomes evident. Figures 3.5 and 3.6 demonstrate that the BER performance of a digital signal transmitted in a hybrid SCM system is more strongly dependent on nonlinear distortion than on Gaussian noise. For a 16-level ASK signal (Figure 3.6), the impact of noise is more severe, seen by the fact that a sharp BER degradation occurs at an SNR of 30 dB. The same level of degradation is not seen for an 8-level ASK signal (Figure 3.5) until the SNR is lowered to 25 dB. This is due to the fact that the signaling levels are closer together for 16-level ASK than they are for 8-level ASK with the same average power, and therefore the error performance is more dependent on the signal-to-noise ratio.

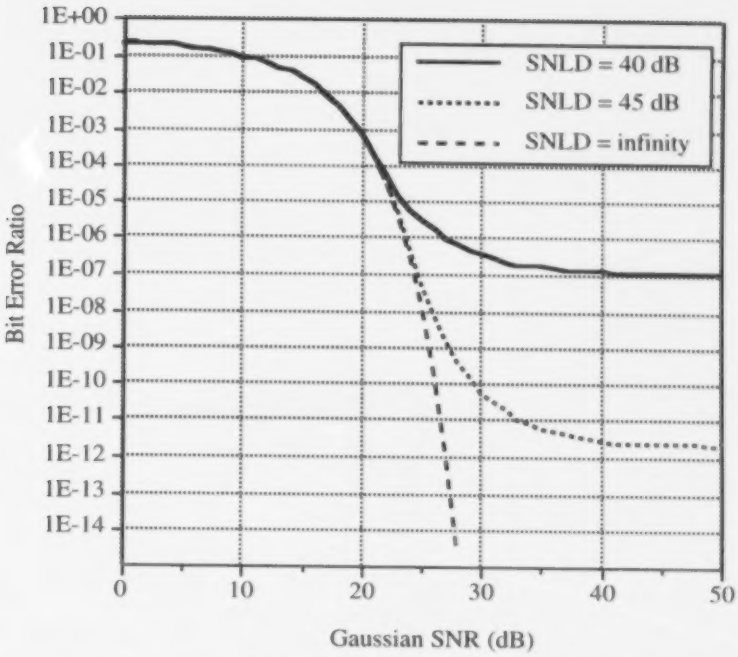

Figure 3.3: Bit Error Ratio as a Function of SNR for an 8-Level ASK Signal

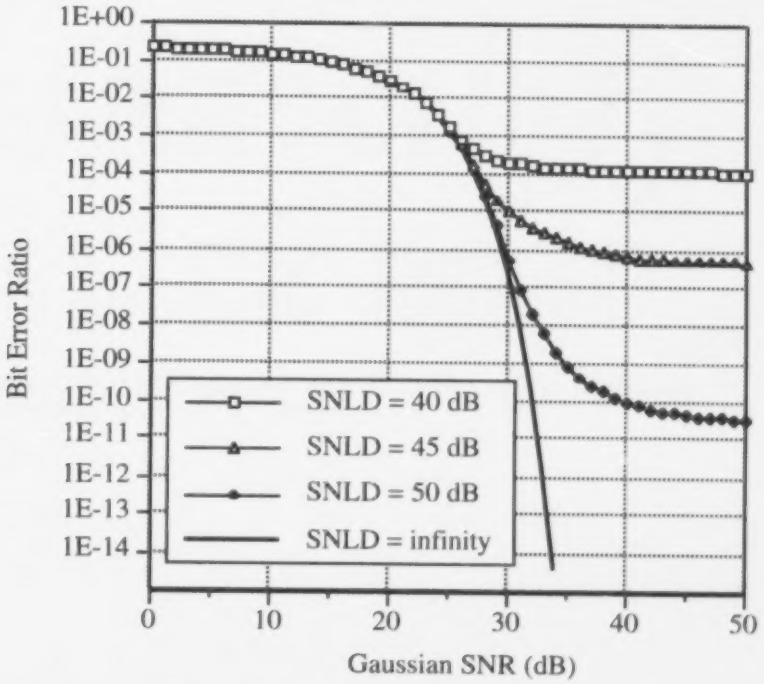

Figure 3.4: Bit Error Ratio as a Function of SNR for a 16-Level ASK Signal

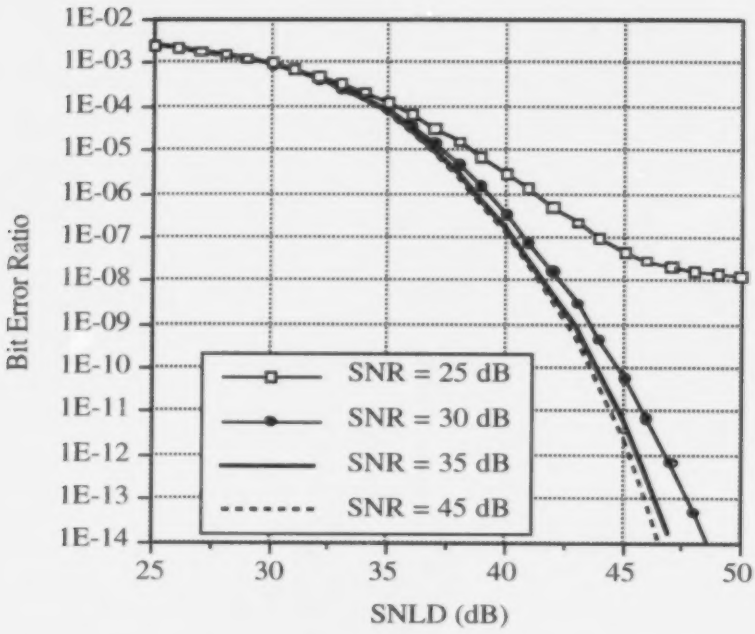

Figure 3.5: Bit Error Ratio as a Function of SNLD for an 8-Level ASK Signal

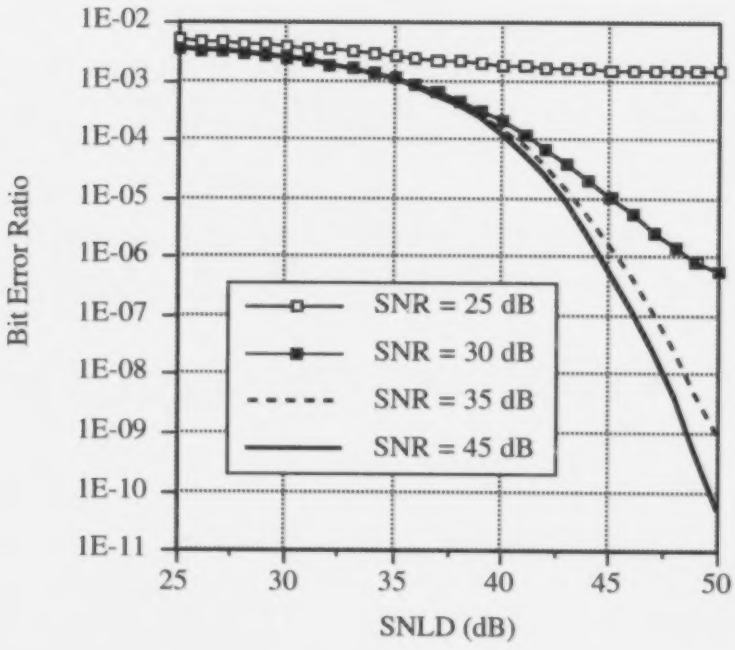

Figure 3.6: Bit Error Ratio as a Function of SNLD for a 16-Level ASK Signal

3.4 Transmission System Simulations

Since this work involved an experimental component, it was necessary to model the digital transmission link before designing the circuitry for the ASK modulator, demodulator and baseband filters. All system simulations were performed using MATLAB on a UNIX workstation. System modeling was used to select appropriate baseband filters in the transmitter and receiver and to compare the transmission of 8-level ASK with 16-level ASK. The simulation model utilized is shown in Figure 3.7. Each block is a module in the simulation code, and italics denote either a user input or output. The first module is a pseudorandom bit stream (PRBS) generator, derived from a maximal-length shift register technique described in [44]. The PRBS binary data is converted to a multilevel signal where the number of signaling levels is defined by the user. The multilevel signal is scaled so that a linear swing across the output of the D/A converter is achieved. A time record is then created with a sampling rate given by the user. The power spectral density of the signal can be determined by taking the Fourier transform of the time record and squaring the absolute value of this result. At this point, a pilot tone may be added to the multilevel signal. A pilot tone was used in Zenith's N-VSB system for aiding in the detection process, but was not used for the experimental results obtained in this work.

The final stage before upconversion of the multilevel signal is baseband filtering. Baseband filters are often located in the transmitter for pulse shaping purposes and also as a means of limiting the high frequency information incident on the first mixer, thereby reducing the amount of frequency overlap. Raised-cosine filtering is often used to eliminate intersymbol interference (ISI) at the receiver [12]. To eliminate ISI, the impulse response of the system must equal zero at all multiples of the bit rate. In the N-VSB system, this filtering is achieved through the use of identical square root-raised-cosine filters in the transmitter and receiver. In practice, a raised-cosine response is difficult to achieve [50] and "most distorted pulses can be matched relatively closely by a low-order classical filter like a 2-pole or 3-pole Butterworth or Chebyshev filter set at an appropriate bandwidth" [51]. Since these filters are easy to implement in hardware, simulations were used to choose a low-order analog filter for baseband filtering in both the transmitter and receiver.

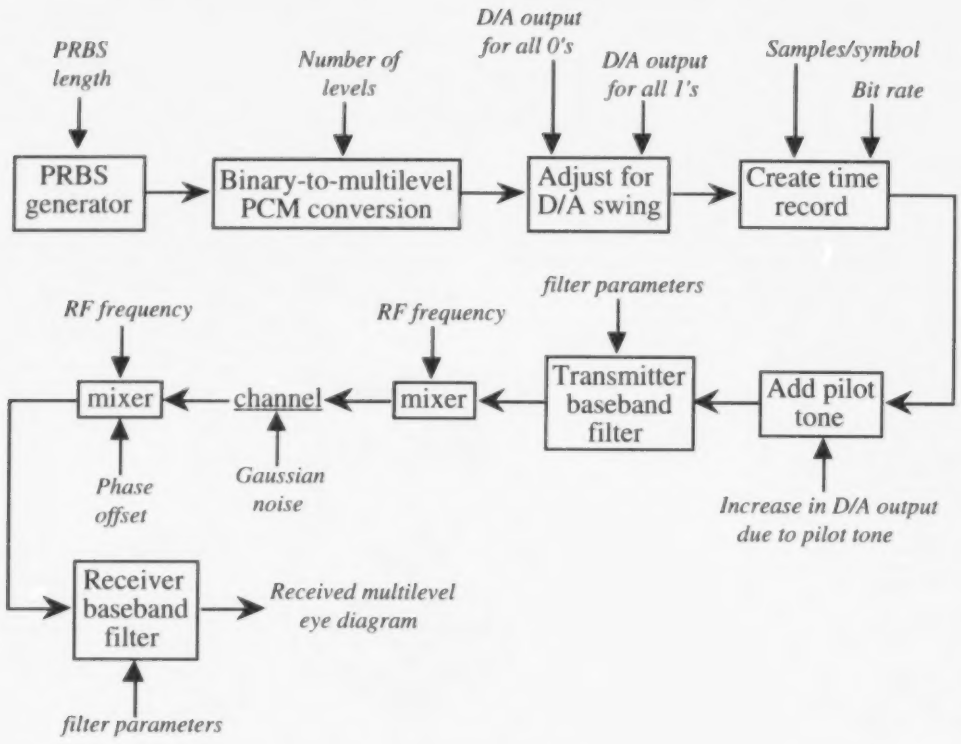

Figure 3.7: Transmission System Simulation Model

After baseband filtering in the transmitter, the multilevel signal is upconverted to an RF frequency. Variations of the simulation program allow the use of an IF modulator and IF filtering as well. For accurate modeling of the transmission link, noise is added to the signal before baseband filtering is introduced in the receiver. A Gaussian random variable is used to simulate additive noise. With the signal power as calculated by the program and for a user-defined signal-to-noise ratio, the noise power and corresponding noise variance that should be added to the time record of the signal can be determined. The noisy signal is downconverted to baseband, with the capability of adding a phase offset between the oscillator sinusoid in the upconverter and the oscillator sinusoid in the downconverter. Finally, the received signal is passed through a receiver baseband filter and the multilevel eye diagram is displayed.

In order to determine the optimal combination of baseband filters in the transmitter and receiver, trial-and-error was used to select the proper filter parameters. Early simulations demonstrated that it would be very difficult to maintain an open eye for a 16-

level signal using classical filters, and therefore emphasis was placed on designing an 8-level ASK system. For the 16-level ASK signal, there was extreme eye closure in the time domain, which makes it quite difficult to choose an optimal decision point for the decoder. An RF carrier frequency of 450 MHz was used for all simulations and the input bit rate was set at 32 Mbps. For later experimental work, it was found that a slightly lower bit rate gave much better back-to-back results.

The Signal Processing Toolbox contained within MATLAB allows analysis of both Butterworth and Chebyshev filter designs. Both of these filter types were simulated in combination with varying filter orders and lowpass cutoff frequencies. After numerous combinations were analyzed, hardware implementations utilized 2nd order Butterworth low pass filters with a cutoff frequency f_c of 7 MHz in both the transmitter and receiver. Figure 3.8 displays the eye diagram of a received 8-level ASK signal using 2nd order Butterworth filters, with f_c approximately equal to 7 MHz, in the transmitter and receiver. This choice of baseband filter results in a useable eye opening of approximately 18 ns for a signal transmitted at a rate of 10. 75 Msymbols/sec. Also, the signal peak power is down by 45 dB at a frequency of 40 MHz. Consequently, when the signal is upconverted to 450 MHz, there would be very little interference with the 42 analog carriers whose carrier frequencies range from 55.25 MHz to 337.25 MHz. Note that in a multichannel hybrid system, the amount of adjacent channel interference must be maintained below a specific level. Consequently, low-order classical filters would no longer be appropriate. In such systems, raised cosine filters are used, often generated through the use of digital signal processing (DSP) techniques.

The rationale for choosing second order Butterworth filters is seen by examining eye diagrams based on the use of other filter designs. Figure 3.9 shows eye diagrams for an 8-level ASK system with 3rd order Butterworth filters in the transmitter and receiver. Note that the optimal decision interval is quite a bit smaller than that of Figure 3.8. A 16-level eye at the output of a single 2nd order Butterworth filter in the transmitter is shown in Figure 3.10. Each eye in Figure 3.10 has closed quite substantially in comparison to the upper eye diagram shown in Figure 3.8. Consequently, hardware implementations focused on 8-level ASK rather than 16-level ASK.

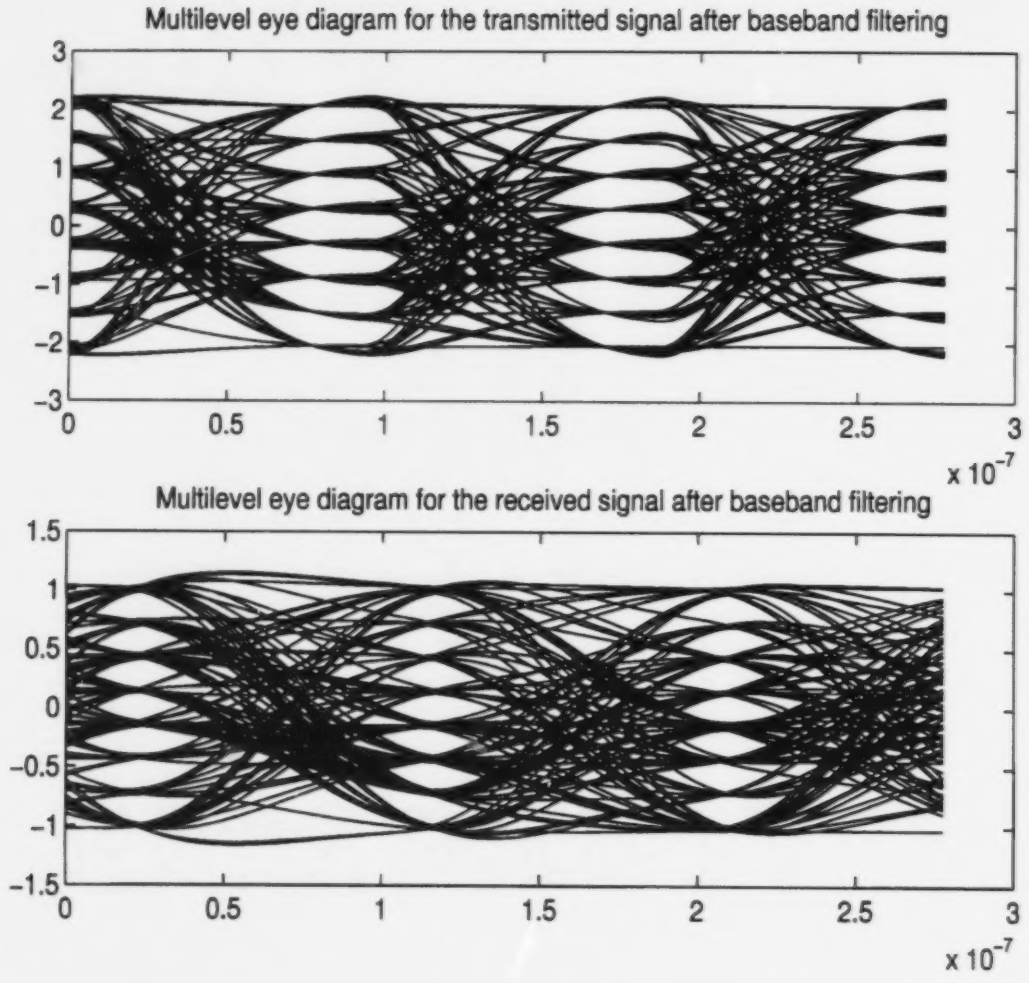

Figure 3.8: Simluated Eye Diagram after Transmitter Baseband Filter and Receiver Baseband Filter with 2nd order Butterworth Filters (f_c = 7 MHz)

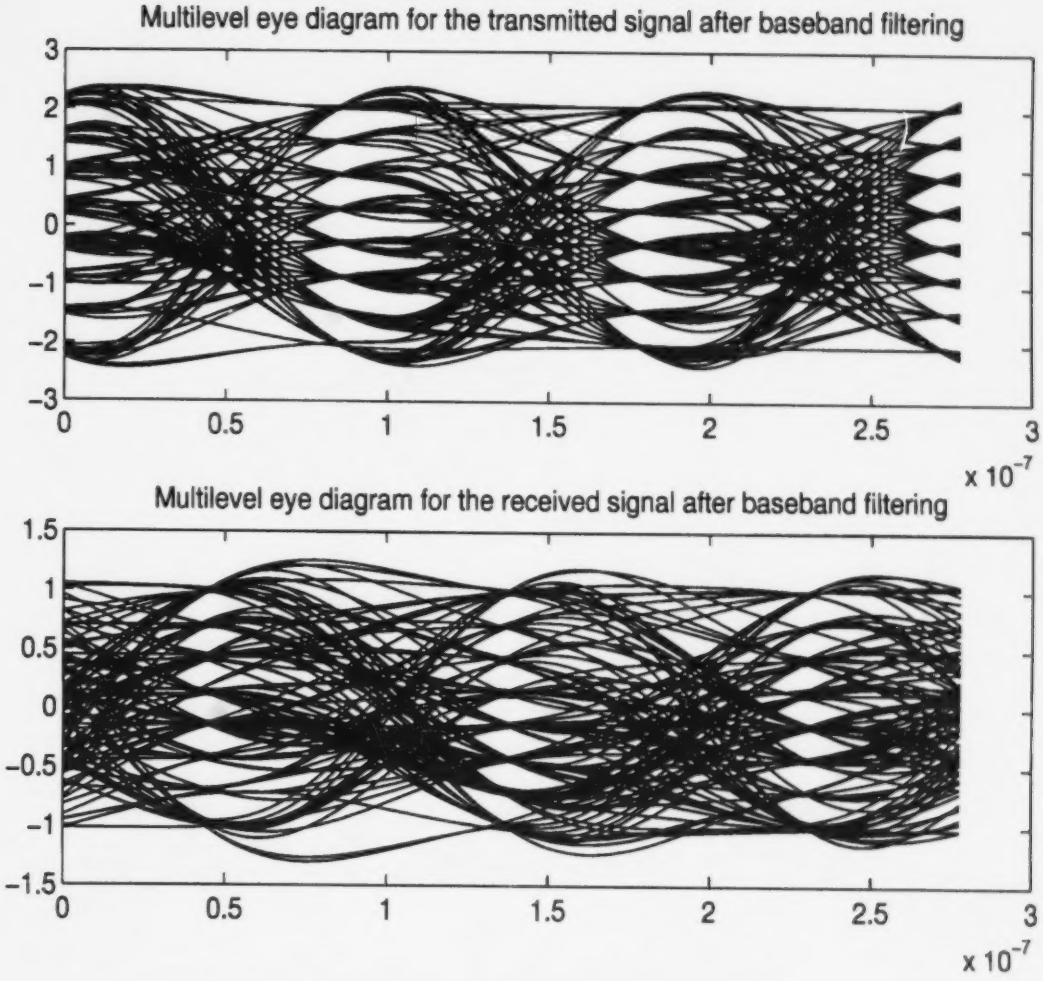

Figure 3.9: Simulated Eye Diagram after Transmitter Baseband Filter and Receiver Baseband Filter with 3rd order Butterworth Filters (f_c = 7 MHz)

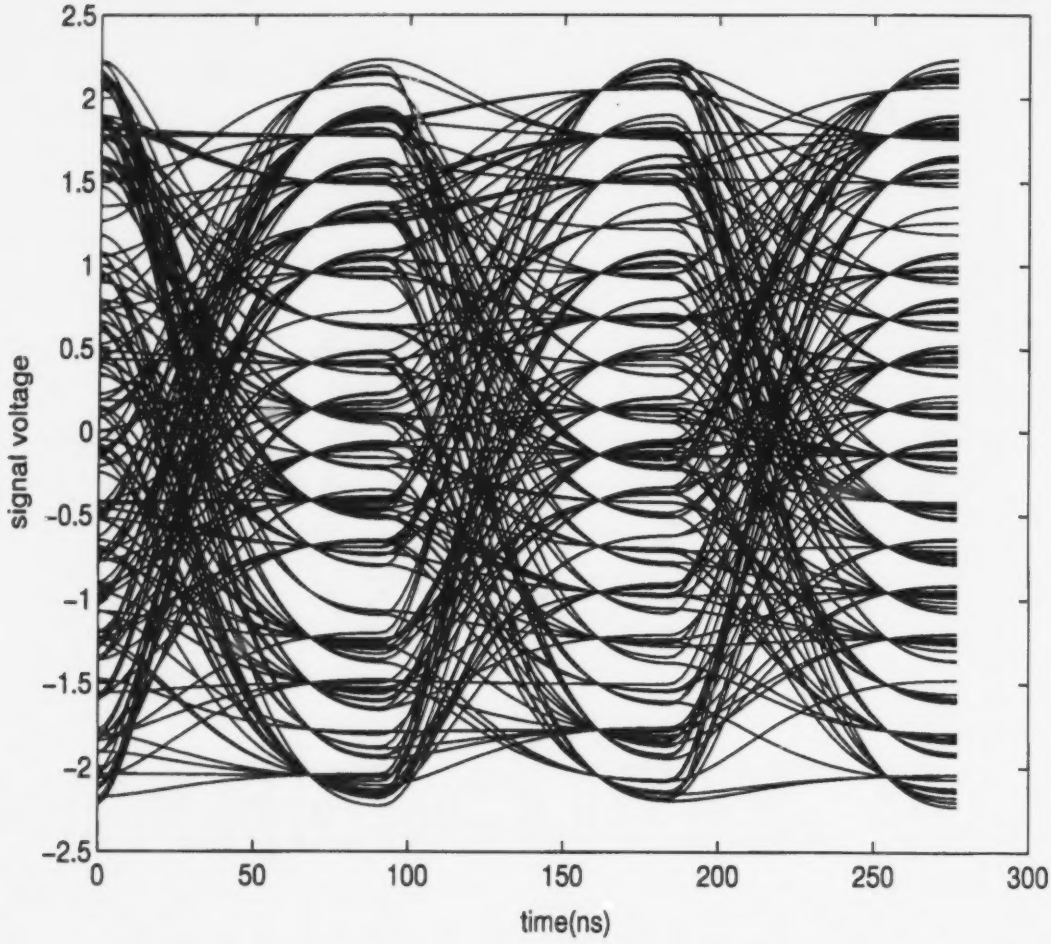

Figure 3.10: 16-level Eye Diagram after Transmitter Baseband Filter

3.5 Impact of Vestigial Sideband Filtering on the Error Performance of Multilevel ASK in Gaussian and Non-Gaussian Impulsive Noise

The proposed HDTV system in North America utilizes a combination of multilevel ASK signaling and vestigial sideband (VSB) filtering to create a spectrally-efficient digital television signal. Root-raised cosine filters are used in both the transmitter and receiver for the dual-purpose of pulse shaping and improving the spectral efficiency of the transmitted signal. In this section of the thesis, the qualitative performance of an ASK/VSB signal

transmitted in the presence of Gaussian noise and non-Gaussian impulsive noise will be examined.

In a multilevel ASK transmission system, an RF sinusoidal carrier is modulated by a baseband multilevel NRZ signal. Generally speaking, the upconverion to an RF frequency occurs via an intermediate frequency (IF), in order to reduce the complexity of channel selection and filtering. The baseband multilevel signal is characterized by a power spectral density (PSD) defined by the $\text{sinc}^2(x)$ function [45] where

$$sinc(x) = \frac{sin(\pi x)}{\pi x} \tag{3.43}$$

Upconversion to an IF or RF frequency does not alter the shape of the power spectral density, but simply shifts the spectral content to a different frequency. Since $\text{sinc}^2(x)$ is symmetric about the origin, the PSD of the upconverted multilevel ASK signal also exhibits even symmetry about the carrier frequency. Consequently, the upper sideband (USB) and lower sideband (LSB) are mirror images of each other. Hence, the bandwidth efficiency is improved if only one of the two sidebands is transmitted. Since it is impossible to implement perfect brickwall filters, vestigial sideband filtering is used instead of single sideband filtering. It is interesesting to note that M-ASK/SSB and M^2-QAM have equivalent bandwidth efficiencies. A QAM system uses quadrature carriers and can therefore transmit twice as much information as a double sideband ASK system. However, only a single sideband needs to be transmitted to demodulate the ASK signal, whereas both sidebands must be transmitted to properly demodulate a QAM signal.

Recall from equation (3.42) that the bit error ratio of a multilevel ASK signal (without vestigial sideband filtering) transmitted in the presence of Gaussian noise and non-Gaussian impulsive noise is a function of the number of levels M, the signal-to-noise ratio SNR_G, the signal-to-nonlinear distortion ratio $SNLD$ and the impulsive index A. Both the impulsive index and number of levels are independent of the type of filtering used in the transmission system. Therefore, in order to determine the impact of vestigial sideband filtering on a multilevel ASK signal transmitted in the same noise environment, it is necessary to examine how vestigial sideband filtering affects the SNR and SNLD.

If the input to the modulator is a random, multilevel data stream, the power spectral density of the baseband signal is equal to [45]

$$S_1(\omega) = k \cdot T_o \cdot sinc^2\left(\frac{\omega \cdot T_o}{2\pi}\right) \tag{3.44}$$

where k is a constant whose value is a function of the number of signaling levels
T_o is the input pulse width

After upconversion to the IF frequency, the PSD of the modulated signal can be written in the following form [45]:

$$S_2(\omega) = \frac{k \cdot T_o}{4} \cdot \left[sinc^2\left(\frac{\{\omega + \omega_{IF}\} \cdot T_o}{2\pi}\right) + sinc^2\left(\frac{\{\omega - \omega_{IF}\} \cdot T_o}{2\pi}\right)\right] \tag{3.45}$$

Upconversion to RF and the corresponding downconversion to IF does not affect the shape of the signal power spectral density, and would be equivalent to equation (3.45) with the addition of a scaling factor. The signal power at the output of the IF filter in the receiver can be found by integrating the input signal power spectral density in the following manner:

$$P_s = \frac{1}{2\pi} \int_{-\infty}^{\infty} S_i(\omega) \cdot |H(\omega)|^2 \cdot d\omega \tag{3.46}$$

where $S_i(\omega)$ is the signal PSD at the filter input
$|H(\omega)|$ is the filter magnitude response

The signal power spectral density given in equation (3.45) has even symmetry about the IF frequency. Consequently, given equation (3.46), the signal power at the output of a double sideband filter is twice as much as at the output of a SSB filter. If a vestigial sideband filter is used with a rolloff at the IF frequency that is fairly steep in comparison to the filter bandwidth, the signal power at the output of a VSB filter is approximately half that of a double sideband filter.

If the noise at the input to the receiver IF filter is additive white Gaussian noise (AWGN), then the noise power at the output of the IF filter is equal to the single-sided noise power spectral density multiplied by the filter bandwidth. Therefore, the noise power at the output of a VSB IF filter is approximately equal to half of the noise power at the

output of a DSB IF filter, assuming that the magnitude response of the VSB filter is 0.5 at the IF frequency and that the VSB filter has a sharp rolloff at the IF frequency. Consequently, given the conclusions of the preceding paragraph, it is evident that both the noise power and the signal power at the output of a vestigial sideband filter are half as large as compared to a double sideband filter. Hence, it is fair to assume that the double sideband SNR is approximately equal to the vestigial sideband SNR.

It is also necessary to evaluate how the SNLD differs for a vestigial sideband system in comparison to a that of a double sideband system. The impact of vestigial sideband filtering on the signal power has already been shown. However, the clipping-induced nonlinear distortion of an SCM lightwave system does not have a flat power spectral density whereas Gaussian noise does. Therefore, the relationship between $SNLD_{DSB}$ and $SNLD_{VSB}$ is not derived as easily as was the relationship between SNR_{DSB} and SNR_{VSB}. Since the nonlinear distortion products occur at discrete frequencies across the CATV band, it is necessary to determine the amount of distortion power that falls within a given channel bandwidth. To this end, a nonlinear distortion model is required that calculates NLD power at each of the intermodulation frequencies. One such model [42] calculates CSO and CTB power as a function of the frequency-dependent intermodulation product count. The analysis is similar to that of Alameh and Minasian [36] in that both analyses start with the autocorrelation function of the laser output. However, unlike the analysis in [36], the autocorrelation function is expressed as a power series, which allows determination of the power contribution of each order of nonlinear distortion when the Fourier transform of the autocorrelation function is taken. The two main forms of intermodulation distortion in a lightwave SCM CATV system were found in [42] to be

$$CSO(\upsilon, N, m) = \frac{K_{2\upsilon}}{8\pi N} \cdot exp\left(\frac{-2}{m^2 \cdot N}\right) \cdot \gamma^{-2} \tag{3.47}$$

$$CTB(\upsilon, N, m) = \frac{K_{3\upsilon}}{16\pi N^3} \cdot m^{-2} \cdot exp\left(\frac{-2}{m^2 \cdot N}\right) \cdot \gamma^{-2} \tag{3.48}$$

where $K_{n\upsilon}$ is the power product count of the n^{th} order nonlinear distortion at frequency υ, N is the number of channels, m is the optical modulation index per channel, and γ^{-2} is a constant that can be derived from the expresssion:

$$\gamma^{-2} = \frac{1 + erf\left(\frac{1}{m \cdot \sqrt{N}}\right)}{2} \tag{3.49}$$

Before equations (3.47) and (3.48) can be used, it is necessary to count all the second order and triple beat products that fall in the CATV band. Figures 3.11 and 3.12 give the CSO and CTB product count, respectively, for a 42-channel CATV system using standard NTSC video carrier frequencies in the range of 55.25 MHz to 337.25 MHz. These carrier frequencies correspond to those that can be generated in the lab through the use of the Matrix signal generator to be described in chapter 4. Computer listings used to create the product count shown in Figures 3.11 and 3.12 are given in Appendix A. Note that CSO products are more prevalent at the lower and upper ends of the CATV band, while the majority of the CTB products reside in the middle of the band. Figure 3.13 displays the amount of CSO and CTB power calculated using equations (3.47) and (3.48) for a 42-channel system with a per channel modulation index of 6%.

A number of observations can be made from examination of Figures 3.11 through 3.13. First, the dominant CSO and CTB products, in terms of intermodulation power, are spaced 6 MHz apart. This is a very important result in comparing the impact of VSB filtering and DSB filtering. Second, the prevalent CSO products between 54 MHz and 216 MHz are placed 1.25 MHz below the video carrier, while the dominant CSO products between 248 MHz and 633 MHz are located 1.25 MHz above the carrier. Finally, the main CTB products located between 55 MHz and 470 MHz occur at the video carrier frequency. Between 501 MHz and 904 MHz, the dominant CTB products are located 0.50 MHz above the video carrier frequency.

Although the CSO and CTB products are spaced 6 MHz apart, the amount of nonlinear distortion power within a single sideband as compared to that within a double sideband is dependent on the filter bandwidth as well as the frequency of the channel of interest. Generally speaking, a VSB filter with a bandwidth close to 6 MHz will capture approximately half as much intermodulation distortion power as will a DSB filter with twice the bandwidth. In Figure 3.14, the amount of CSO and CTB power in a DSB bandwidth of 10.76 MHz is compared with the CSO and CTB power contained within a VSB bandwidth of 5.38 MHz for a carrier near 420 MHz. These bandwidths were used in simulations since Zenith's N-VSB proposal uses a vestigial bandwidth of 5.38 MHz. From this graph, it is apparent that both the CSO and CTB powers in a 5.38 MHz bandwidth are about 3 dB lower than the CSO and CTB powers in a bandwidth of 10.76 MHz.

Therefore, for this scenario, the $SNLD_{VSB}$ is very close to the $SNLD_{DSB}$, since the signal power for DSB is twice as much as for VSB. Earlier it was shown that SNR_{DSB} is nearly equivalent to SNR_{VSB}. Consequently, the error performance of the multilevel ASK signal described in equation (3.42) would not change if the signal was passed through a vestigial sideband filter rather than a double sideband filter.

It should be noted that a different choice of carrier frequency or filter bandwidth may give a different result. Consequently, it would be appropriate to define a multiplying constant that relates the nonlinear distortion power in the attenuated sideband to the nonlinear distortion power in the vestigial sideband. This multiplying constant could then be incorporated into equation (3.42) to account for any mismatches in distortion power on either side of the carrier frequency. Since the impact of vestigial sideband filtering is not analyzed in the experimental section of this thesis, the theoretical analysis into the effects of VSB filtering has only been dealt with in a qualitative manner.

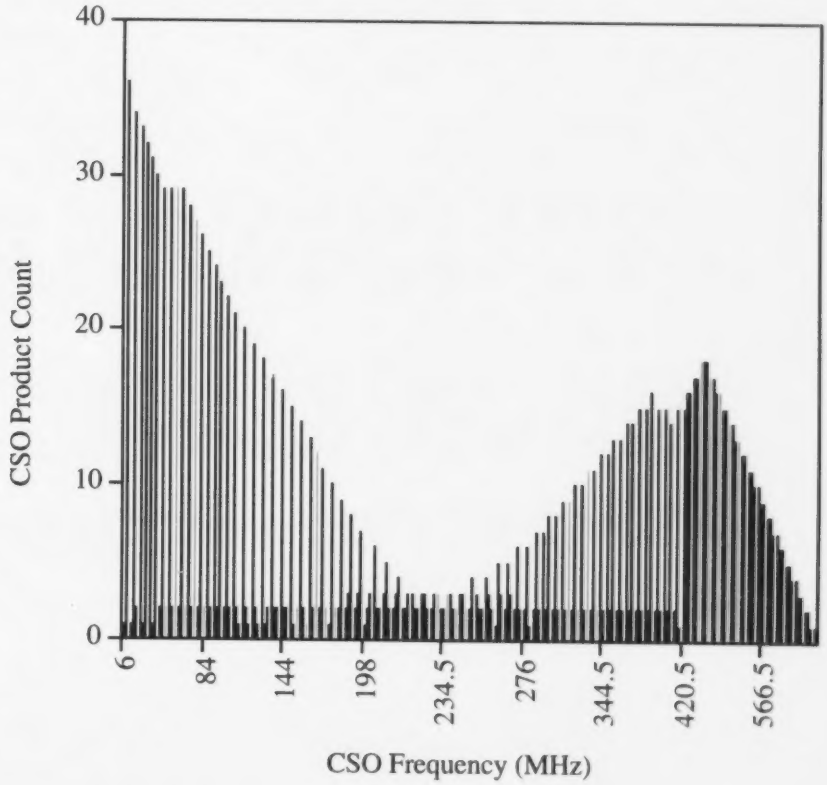

Figure 3.11: CSO Product Count for a 42-Channel CATV System

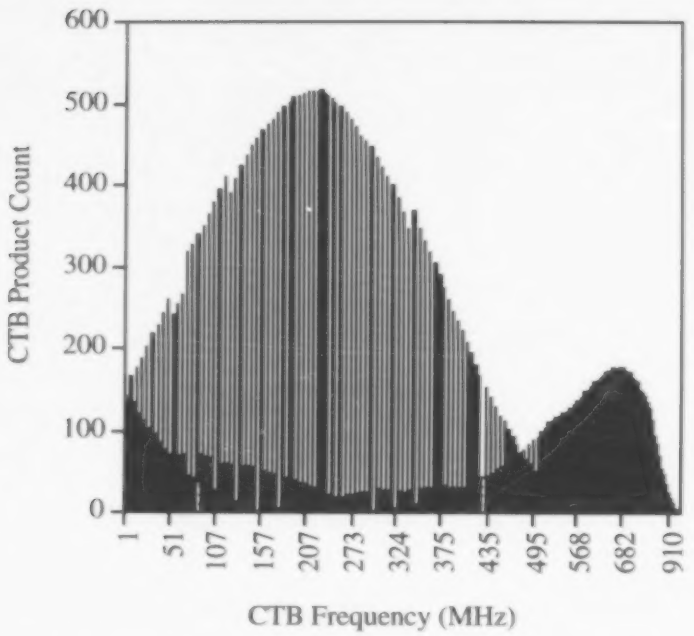

Figure 3.12: CTB Product Count for a 42-Channel CATV System

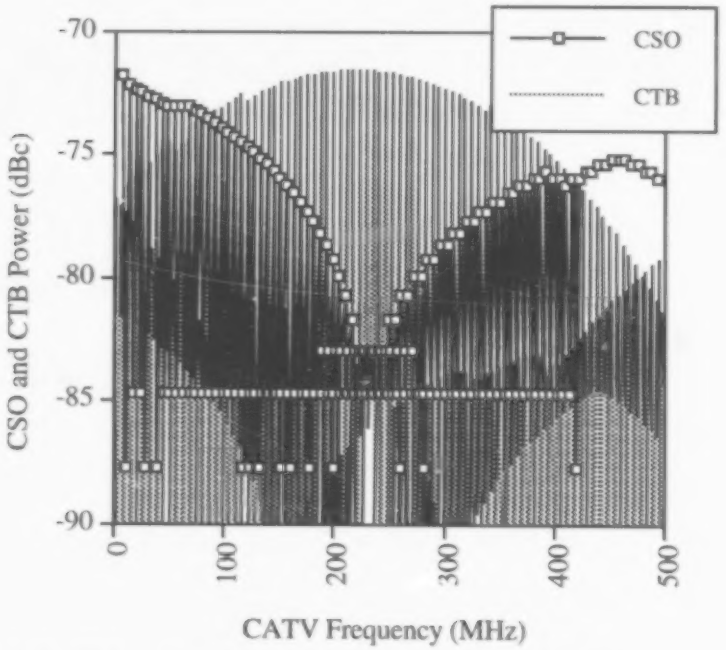

Figure 3.13: CSO and CTB Power for a 42-Channel CATV System

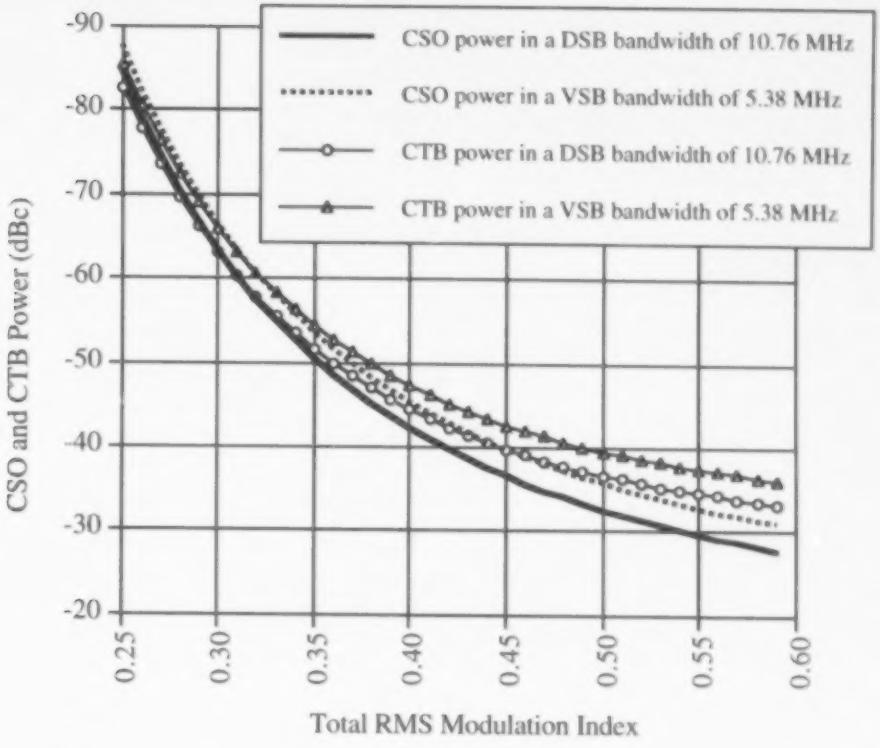

Figure 3.14: Nonlinear Distortion Power of a VSB System Versus that of a DSB System at a Carrier Frequency of 420 MHz

4.0 Design and Characterization of a Fiber Optic Multichannel AM/VSB-Multilevel ASK Transmission System

An optical transmission system utilizing subcarrier multiplexing was designed and built in order to test the validity of the theoretical results. One 8-level ASK signal and 42 analog carriers are combined electrically using frequency division multiplexing. The electrical signal modulates a highly-linear laser diode. The resulting optical signal is then transmitted through a fiber optic link, and converted back to an electrical signal through a photodetector. The 8-level ASK signal is filtered out from the analog carriers, at which point the performance of the digital signal can be experimentally determined. A block diagram of the experimental setup is shown in Figure 4.1.

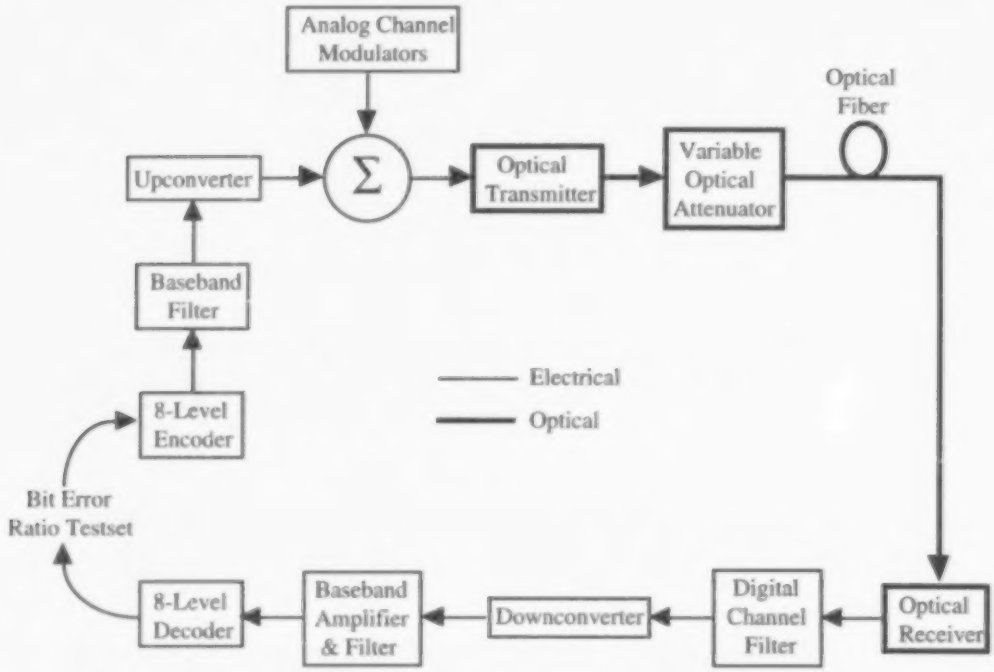

Figure 4.1: Block Diagram of Multichannel AM/VSB-Multilevel ASK Transmission System Experimental Setup

The experimental setup contains a number of key components that will be described in further detail within this chapter. These components include the 8-level ASK encoder and upconverter, 8-level ASK decoder and downconverter, analog channel modulators,

optical transmitter and optical receiver. Optical link characterization such as the nonlinear distortion performance of the laser diode and optical receiver frequency response are included in this chapter. Finally, results of electrical and optical back-to-back calibrations are given for the digital ASK channel.

4.1 Optical Transmission Components

The characteristics and performance of the optical portion of the experimental setup is key to examining the effects of transmitting digital and analog signals side-by-side in a subcarrier multiplexed system. In order to meet the noise and nonlinear distortion criteria placed on the transmission of CATV signals in a fiber optic distribution system, a highly-linear optical transmitter and low-noise optical receiver are required.

4.1.1 Analog Optical Transmitter

The optical transmitter provides the conversion between the electrical input signal and the optical output signal. This conversion needs to be as linear as possible in order to maintain a low level of nonlinear distortion in the system. The linearity of the transmitter is not only a function of the electrical-to-optical conversion, but also the linearity of the supporting circuitry including the biasing and amplifying circuits.

The laser used in the optical transmitter was specifically geared towards CATV applications where very strict requirements on noise and linearity must be met. The optical transmitter contains a distributed feedback (DFB) laser manufactured by Fujitsu (model number FLD150F3ACH-AL). The peak wavelength is 1543 nm at room temperature [52] and is tunable over a 1 nm range by varying the temperature of operation. The relative intensity noise (RIN) specification of the laser is -160 dB/Hz at 50 MHz and -165 dB/Hz at 550 MHz. The laser bias current can be set between 0 and 60 mA with a threshold of 18.7 mA. A plot of the output optical power as a function of the input bias current, generated by Steve Lai of TR*Labs* [53], is shown in Figure 4.2. Note that the laser transfer is quite linear from 20 mA to 55 mA and that the optical power is negligible for bias currents below the threshold value.

The optical transmitter was designed and built by Kinh Pham and Dave Clegg of TR*Labs* for use in experiments involving subcarrier multiplexed transmission of analog AM/VSB and digital QAM signals. A block diagram showing the layout of the optical transmitter is given in Figure 4.3. The CATV amplifier module, which has a power gain of 19 dB and a bandwidth from 40 MHz to 1000 MHz, is only used when the input RF signal needs an increase in power in order to achieve a given modulation depth. The Laser Bias

Insertion Unit applies the modulating RF signal and the DC bias current onto the laser diode. There are two input branches within the Laser Bias Insertion Unit: the AC modulation branch and the DC drive current branch. The AC modulation branch consists of a 0.1 μF capacitor in series with a 67 Ω resistor, which acts as a high pass filter and therefore provides DC isolation. Since the laser module has an intrinsic impedance of 8 Ω, the RF modulation input of the laser becomes 75 Ω. This is necessary in order to match the transmitter input impedance with the 75 Ω line impedance of the coaxial cables used in CATV systems. The DC drive current branch consists of a ferrite bead and a 100 μH inductor in series which function together as an AC block between the laser and the DC Laser Drive Unit. The laser bias current is controlled through the DC Laser Drive Circuit. This module utilizes the back facet photocurrent as a feedback signal in order to maintain a constant laser bias current. The DC Laser Drive Unit also incorporates safety features such as current limit circuits and start-up delay circuits used to avoid bias current overshoot upon turn-on. Finally, the Thermoelectric Cooler Control Unit uses a feedback control mechanism to maintain a constant temperature across the laser diode. The temperature is determined by measuring the voltage across a thermistor, which is a device whose resistance varies with temperature. An error signal is created by comparing the measured temperature with the desired temperature. Based on this error signal, the amount of current that passes through the thermoelectric cooler is adjusted. The thermoelectric cooler is a device that can heat or cool small loads by passing an electric current through it.

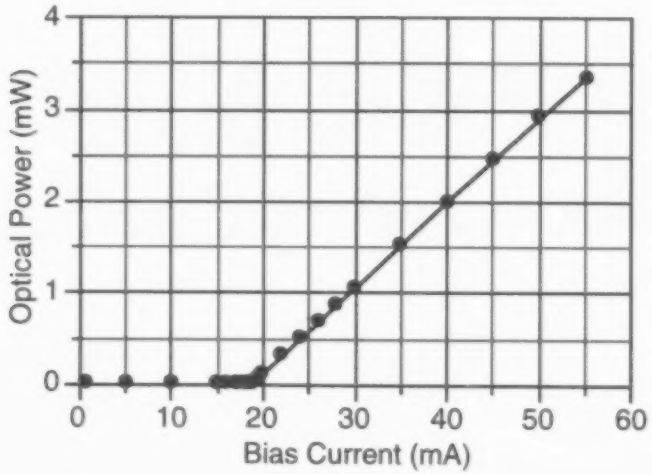

Figure 4.2: Output Optical Power as a Function of Bias Current for Fujitsu Laser

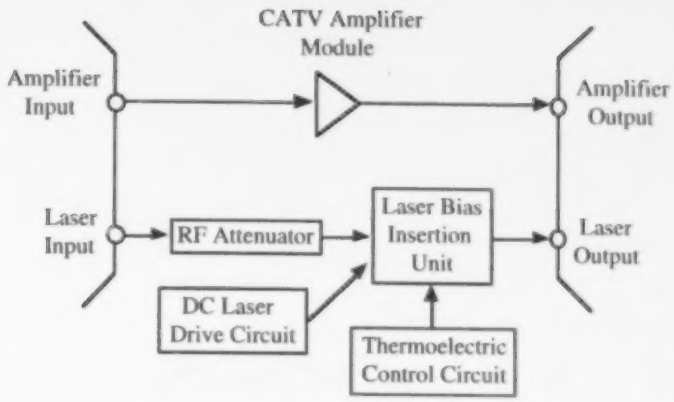

Figure 4.3: Block Diagram Representation of the Analog Optical Transmitter

4.1.2 Analog Optical Receiver

In a fiber optic transmission system, the optical receiver converts the received optical signal into an equivalent electrical signal. In a CATV distribution system, the receiver must have high quality noise and distortion characteristics. For this work, it is especially important to ensure that the intrinsic nonlinear distortion levels of the receiver are quite low since we are attempting to study the impact of nonlinear distortion created through threshold clipping of the laser diode in the transmitter.

The optical receiver used for the transmission experiments was designed and built by Kinh Pham and Dave Clegg. It utilizes an Ortel 2610C photodiode module designed for the stringent requirements of CATV applications. The photodiode module has an impedance transformer built into its package necessary to transform the high output impedance of the photodiode to the 75 Ω impedance of the subsequent stage. The Ortel photodiode is directly coupled to a Philips BGY1085A CATV amplifier module. This is the same type of amplifier that is built into the analog optical transmitter. It has a bandwidth of 1000 MHz, a gain of 19 dB and a noise figure of 6.5 dB.

4.2 Optical Link Characterization

The characteristics of the optical link have a large impact on the performance of multilevel ASK signals transmitted in a hybrid AM/VSB-multilevel ASK subcarrier multiplexed transmission system. Nonlinearities within the laser diode, optical fiber and photodetector result in most of the nonlinear distortion that is observed. In an effort to

analyze the experimental results obtained, it is necessary to fully characterize the optical link, particularly the laser linearity and the receiver frequency response.

4.2.1 Nonlinear Distortion Performance of the Laser Diode

The dominant source of nonlinear distortion in the transmission system is due to the operation of the laser diode itself. The laser linearity is examined by measuring the amount of Composite Second Order (CSO) distortion that exists at the video carrier frequency of channel 62 (451.25 MHz). The nonlinear distortion is measured within channel 62 since the multilevel ASK signal used in the experimental setup has a subcarrier frequency of 450 MHz. This frequency was chosen because it is higher than the largest AM/VSB subcarrier frequency (337.25 MHz) and still lower than the 650 MHz cutoff frequency of the optical receiver. The experimental setup shown in Figure 4.4 is used to measure the CSO at channel 62.

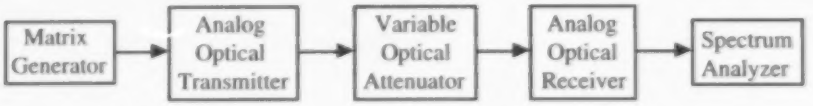

Figure 4.4: Experimental Setup for Measuring Laser Linearity

The Matrix multiple frequency signal generator transmits all of the 42 AM/VSB carriers. The carrier power is set to give a per channel modulation index of 2.0% at a bias current of 50 mA. The bias current is varied between 30 mA and 60 mA in order to visualize how the nonlinear distortion is a function of bias current. Since the composite AM/VSB signal power is not adjusted, the per channel modulation index is 5.6% at 30 mA and 1.5% at 60 mA. The CSO measurements as a function of laser diode bias current are shown in Figure 4.5. Note that the CSO increases as bias current is decreased. This is due to the fact that more nonlinear distortion due to threshold clipping exists for lower bias currents. The measurements were only taken to a bias current of 60 mA since the reliability of the laser at high output optical powers is unknown.

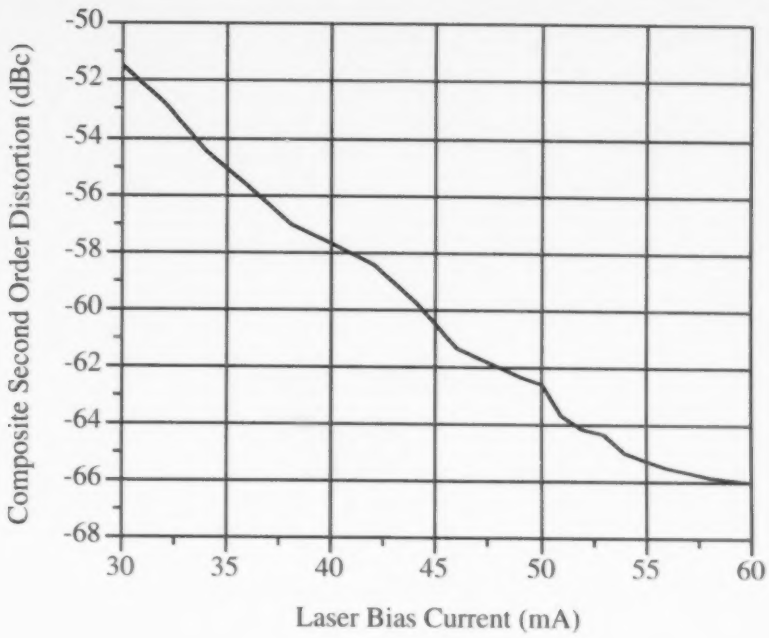

Figure 4.5: Nonlinear Distortion Performance of Laser Diode versus Bias Current

4.2.2 Receiver Frequency Response

In examining the performance of analog and digital signals impacted by clipping-induced nonlinear distortion, the frequency response of the receiver plays a significant role. The combined frequency responses of the photodiode, transimpedance amplifier and supporting circuitry affect the spectrum of the intermodulation distortion power seen at the output of the receiver. It is necessary to characterize the frequency response of the receiver in order to analyze the true impact of threshold clipping on a subcarrier multiplexed signal.

The frequency response of the optical receiver is measured by using an Erbium-Doped Fiber Amplifier (EDFA) as a white noise source. Without an optical signal at the input to the EDFA, the output of the EDFA consists of Amplified Spontaneous Emission (ASE) which can be used to determine the frequency response of a wideband receiver [54]. Spontaneous-spontaneous beat noise is generated at the receiver by interference between electric field components of the Amplified Spontaneous Emission. This noise source has a much wider bandwidth than that of the optical receiver and therefore has a relatively-flat noise spectrum across the bandwidth of the receiver. An RF spectrum analyzer is used to measure the magnitude of the frequency response. The experimental setup used for this measurement is shown in Figure 4.6 with the resulting receiver frequency response given

in Figure 4.7. For this measurement, the drive current for the EDFA is set at 120 mA resulting in a received optical power of -6.8 dBm. Notice that there is approximately 3 dB of gain fluctuation in the passband and that the cutoff frequency is approximately 650 MHz. In a subsequent section of this chapter, a procedure is given for calibrating the modulation index of the transmitted signal. Since the modulation index is defined at the transmitter, the receiver frequency response must be factored out in the calibration process.

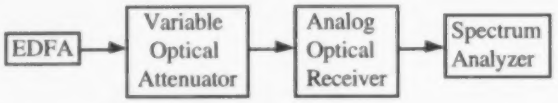

Figure 4.6: Experimental Setup for Measuring Receiver Frequency Response

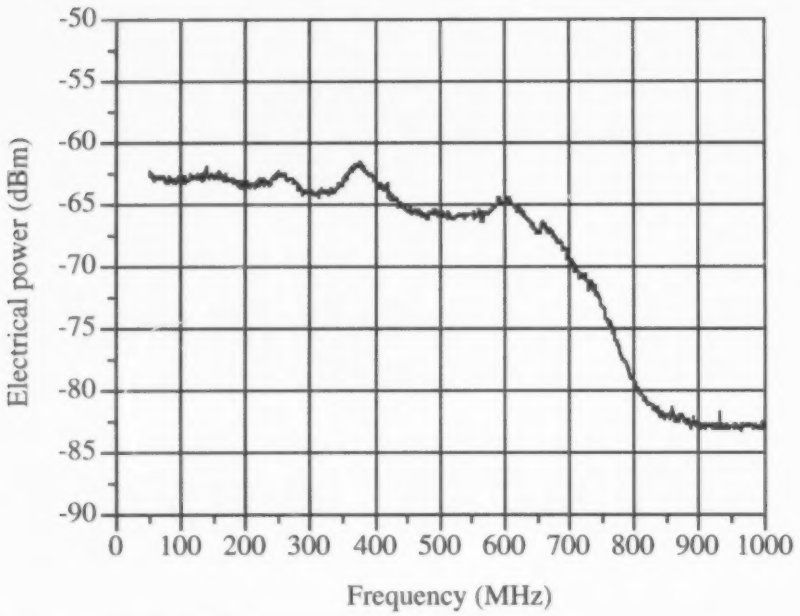

Figure 4.7: Frequency Response of the Ortel Receiver

4.3 Analog Channel Modulators

A Matrix ASX-16 [55] multiple frequency signal generator is used to create the carrier signals that emulate the AM/VSB channels. This instrument contains 42 crystal-controlled oscillators that generate carrier signals from 55.25 MHz to 337.25 MHz. This corresponds to channels 2 and 43, respectively, of the NTSC channel frequency plan. All

of the carriers are spaced 6 MHz apart, with the exceptions being the 10 MHz gap between channels 4 and 5 and the frequencies set aside for the FM radio band. The output power of each carrier can be independently controlled and each carrier signal can be turned on or off without affecting the operation of the remaining carriers. An RF combiner is located within the Matrix signal generator to combine the unmodulated carrier signals together. Since there are no front-panel controls on this instrument, it is operated remotely through the use of an IEEE 488 connection to an automated testing package known as LabVIEW.

4.4 8-Level ASK Encoder

The purpose of the ASK encoder is to generate a pseudorandom 8-level ASK signal that has been Gray encoded. Gray encoding ensures that an error in a detected symbol will only cause a single error in the binary digits transmitted for that symbol. A block diagram representation of the 8-level encoder is given in Figure 4.8.

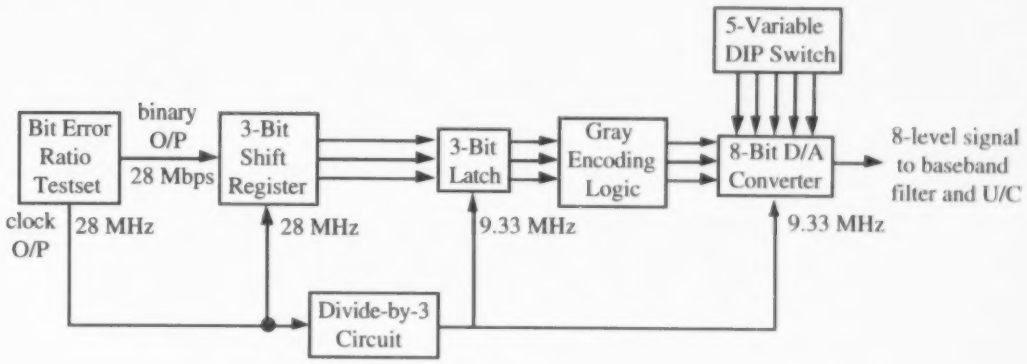

Figure 4.8: Block Diagram of the 8-Level Encoder

The Bit Error Ratio Testset (BERT) outputs a pseudorandom nonreturn-to-zero (NRZ) binary bit stream as well as a clock signal at the same frequency. The BERT used for experimental purposes is the HP3780A Pattern Generator/Error Detector. It has an output bit rate range from 1 kbps to 50 Mbps. The pseudorandom bit stream (PRBS) sequence can have a length of 2^9-1, 2^{15}-1 or 2^{20}-1. For all experimental measurements, a PRBS sequence length of 2^{20}-1 is employed. A bit rate of 28 Mbps is used for the experiments since this is quite close to the bit rate utilized by Zenith in their N-VSB system for high definition television (HDTV) transmission of compressed digital video.

In order to generate an 8-level signal, it is necessary to convert the serial output of the Bit Error Ratio Testset into an equivalent parallel output. This is accomplished via a 74F194 Bidirectional Shift Register. Although this is a 4-bit shift register, only 3 bits are involved for this design. The shift register is used in a 'shift right' mode whereby every 3 consecutive input bits are read in serially, shifted to the right and outputted as 3 separate parallel streams at 1/3 of the input bit rate.

The three parallel data streams are sent to a 74F378 Register which acts as a data latch. This IC consists of 6 edge-triggered D-type flip-flops with a common clock. Therefore, a low-to-high transition of the clock input causes new data to be entered into the register. This is required to ensure that the three parallel bit streams have the same timing before entering the Gray encoding logic. Since the 3-bit data latch operates at one-third the speed of the serial output of the BERT, a divide-by-3 circuit is used to generate a clock at 9.33 MHz that is tied to the 28 MHz clock. To achieve this, a 2-bit counter is employed to generate a 3-state sequence, namely 00, 01, and 10. Since this sequence repeats indefinitely, the first bit is a 1 every third state and can act as a clock signal at one-third the rate of the input clock signal.

The next stage of the 8-level encoder is the Gray encoding logic. Gray encoding establishes the relation between a detected bit error and a symbol error. Table 4.1 shows the input and output of the Gray encoding module. Note that each sequence at the input to the Gray encoder differs from each of its adjacent neighbors by only 1 bit. The logic is implemented using 2-input, 3-input and 4-input NAND gates. FAST TTL integrated circuits are utilized, namely the 74F00, 74F10 and 74F20, respectively. Each of these IC's has a propagation delay of less than 5.0 ns.

The final stage of the 8-level encoder is the digital-to-analog conversion accomplished with an Analog Devices AD9721 8-bit D/A converter. The AD9721 is a high-speed D/A converter that will operate at rates up to 100 Msymbols/sec. It has TTL compatible outputs with fast settling times of 4.5 ns to 1/2 of the least significant bit. Only the first three most significant bits are used to generate the 8-level signal. The remaining bits are connected to a DIP switch that will ground the input pin if the switch is closed or connect the input pin to + 5 V through a resistor if the switch is open. The DIP switch is used so that the DC value of the 8-level D/A output can be controlled. This allows addition of a pilot tone to the 8-level signal, which can be used in the receiver to lock on to the ASK carrier frequency. Since the AD9721 outputs a current between 0 mA (all 0's) and -20.48 mA (all 1's), a current-to-voltage conversion circuit is required at the output. This is accomplished using AD708 and AD9617 high-speed operational amplifiers.

3-Bit Input into Gray Encoder	3-Bit Output of Gray Encoder	Decimal Equivalent at O/P of Gray Encoder
0 0 0	0 0 0	0
0 0 1	0 0 1	1
0 1 1	0 1 0	2
0 1 0	0 1 1	3
1 1 0	1 0 0	4
1 1 1	1 0 1	5
1 0 1	1 1 0	6
1 0 0	1 1 1	7

Table 4.1: Gray Encoding Logic

An HP16500A Digitizing Oscilloscope is used to examine the 8-level eye diagram at the output of the multilevel encoder. The encoder output for bit rates of 5 Mbps and 50 Mbps are shown in Figures 4.9 and 4.10, respectively. For these measurements, the PRBS sequence is set to a length of 2^9-1. Note that the encoder still operates at the 50 MHz maximum frequency of the Bit Error Ratio Testset, although some distortion exists in the transition region between symbols. Figure 4.11 shows a single eye of the 8-level signal with an input bit rate of approximately 30 Mbps. Note that the eye opening between two adjacent levels at the output of the encoder is on the order of 400 mV.

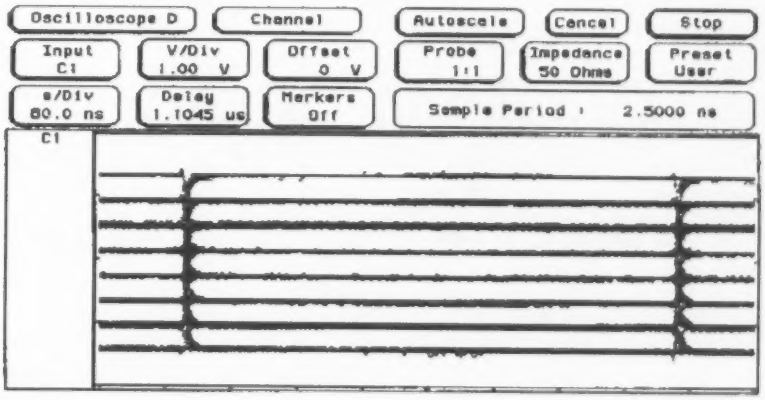

Figure 4.9: Output of 8-Level Encoder with 5 Mbps Binary Input

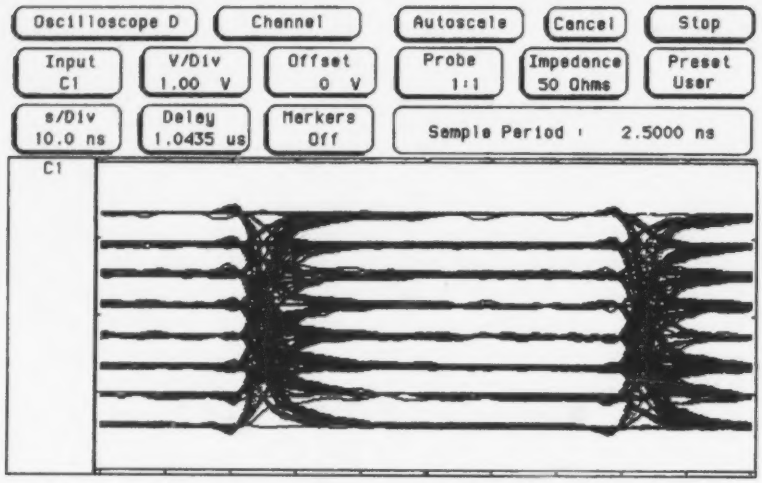

Figure 4.10: Output of 8-Level Encoder with 50 Mbps Binary Input

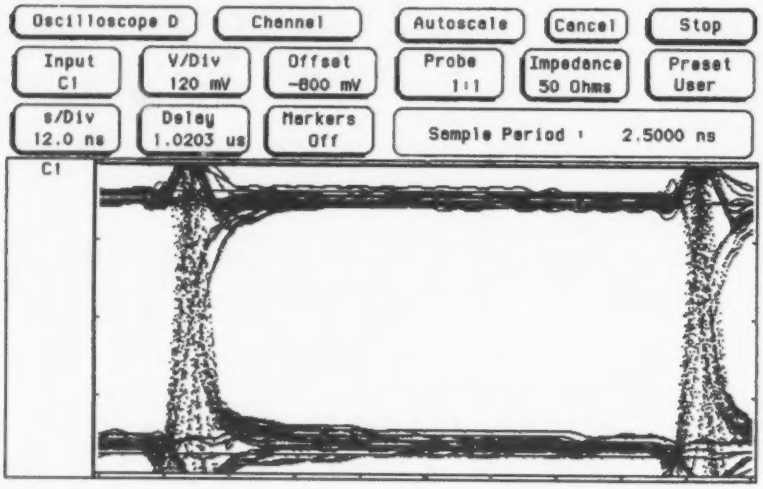

Figure 4.11: Eye Diagram for a Single Eye with a 30 Mbps Binary Input

Baseband filtering is required at the output of the A/D converter to ensure that the ASK signal spectrum does not interfere with any of the analog signals once it has been mixed up to its subcarrier frequency of 450 MHz. Although baseband filtering is often done within the receiver to remove intersymbol interference, it is also used in the transmitter for various reasons. Overall pulse shaping is often split between the transmitter and receiver in an attempt to reduce the filtering requirements of any one stage. Also,

filtering in the transmitter limits the high frequency information that is input into the first mixer, thereby reducing the amount of frequency overlap. Based on simulations discussed in chapter 3, a 2nd order Butterworth filter with a 3-dB cutoff frequency of approximately 7 MHz is used in both the transmitter and receiver to limit the bandwidth of the digital signal. This filter is implemented using tunable inductors and capacitors, with impedance matching to give an input and output impedance of 50 Ω. The power spectral density (PSD) of the 8-level ASK signal before baseband filtering is shown in Figure 4.12. The impact of baseband filtering in the transmitter is evident by looking at the PSD of the 8-level signal after the 7 MHz Butterworth filter, as displayed in Figure 4.13. The eye diagram of an 8-level signal after baseband filtering is presented in Figure 4.14. This multilevel signal is generated using a PRBS sequence at a rate of 32.5 Mbps. Note that although the temporal width of the eye has decreased quite substantially due to filtering, the maximum eye opening is still close to a non-filtered eye.

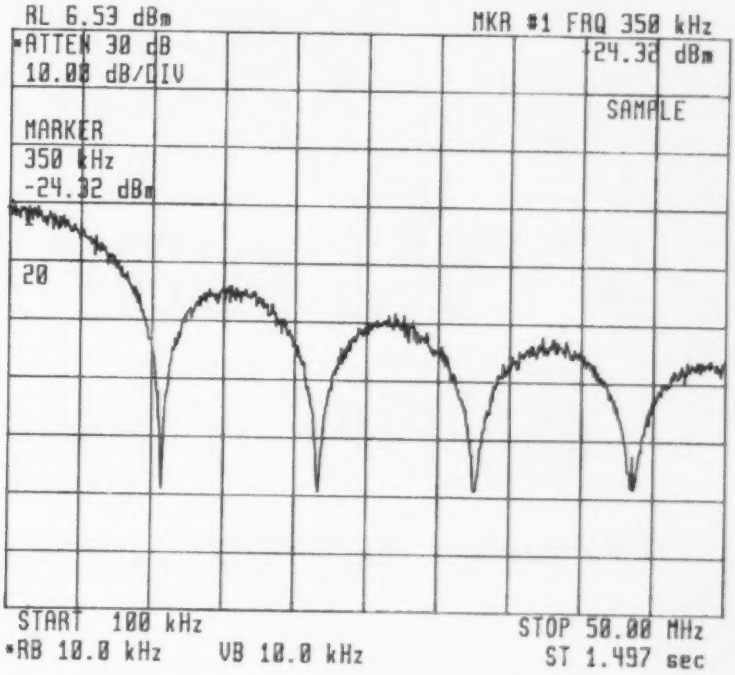

Figure 4.12: Power Spectral Density of 8-Level Signal Before Baseband Filter

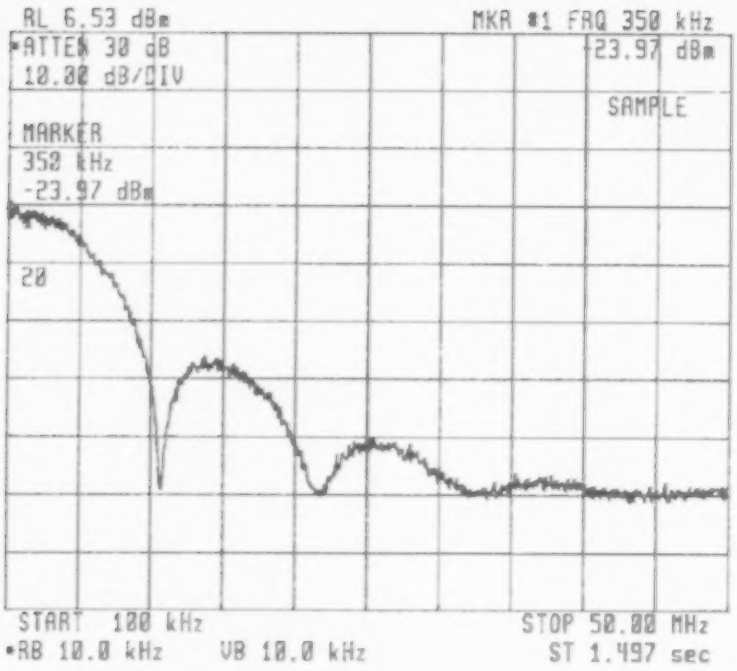

Figure 4.13: Power Spectral Density of 8-Level Signal After Baseband Filter

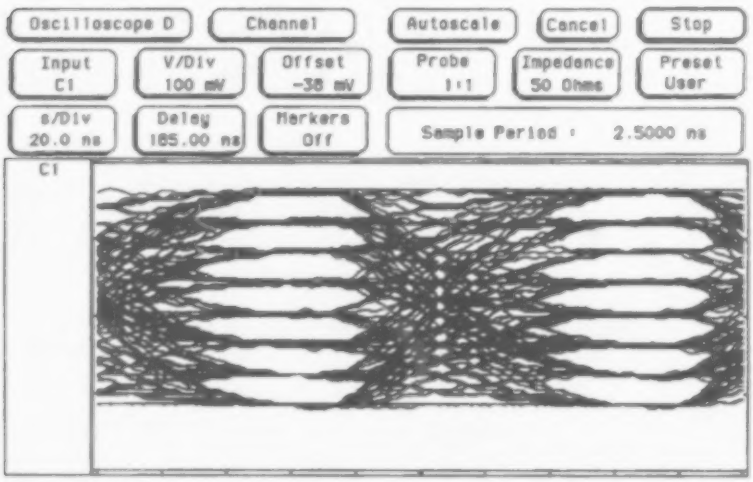

Figure 4.14: Eye Diagram of 8-Level Signal After Baseband Filter

4.5 8-Level ASK Decoder

At the output of the optical receiver, the multilevel digital signal is separated from the analog CATV carriers using bandpass filtering and passes through a series of RF low noise amplifiers. The signal is then mixed down to baseband, at which point it passes through a baseband receiver filter. The filter used at this point is a 2nd order Butterworth filter with a 3-dB cutoff of 7 MHz. The receiver baseband filter is identical in design to the baseband filter employed in the transmitter. The 8-level eye diagram that exists at the input to the decoder board is shown in Figure 4.15. To generate this eye diagram, the output of the encoder is filtered in the transmitter, mixed up to the subcarrier frequency, mixed back down to baseband, and finally passed through the 7 MHz baseband filter in the receiver.

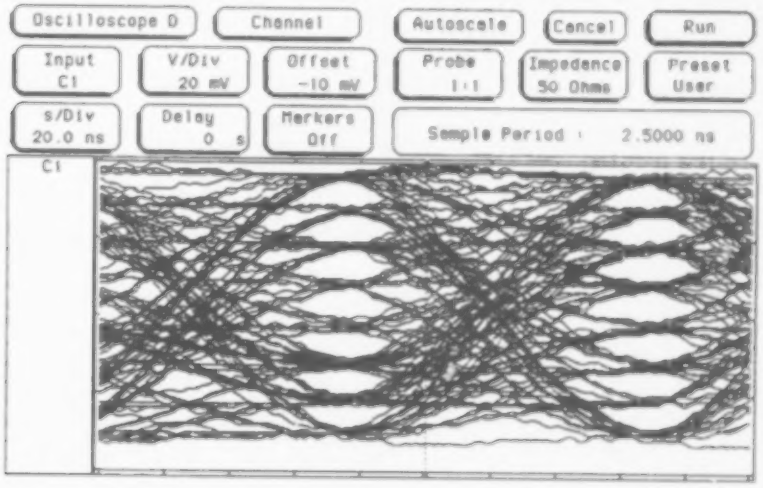

Figure 4.15: Eye Diagram of 8-Level Signal at Input of Decoder Board

In many transmission systems, A/D converters are required to create a digital signal that is an accurate representation of an input analog signal. The A/D converter used in this manner has a sampling rate of at least twice the bandwidth of the analog signal in order to characterize the signal properly. The A/D converter resides in the transmitter since the digital signal is transmitted in binary form through the link. However, for this project, the A/D converter is found in the decoder since it actually converts the received 8-level signal to an equivalent binary representation. The input to the A/D converter is not truly an analog signal since it consists of 8 discrete levels.

The 8-level ASK signal is now ready to be decoded using the design shown in Figure 4.16. The preliminary stage of the decoder scales the peak-to-peak amplitude of the

8-level signal and adjusts its DC offset. The A/D converter requires a peak-to-peak input of 0 to 2 V. Therefore, gain control is utilized at the input of the decoder to meet this requirement. An Analog Devices AD9012 high speed 8-bit A/D converter takes the 2 V full swing 8-level input and converts this signal to a 3-bit digital output. The AD9012 has an analog input bandwidth of 160 MHz and delivers TTL-compatible outputs. Functionally, the A/D converter is comprised of 256 parallel comparator stages whose outputs are decoded to drive the 8 output latches. Although this iC has an 8-bit output, only the 3 most significant bits are needed since the input signal has 8 discrete levels. The other 5 bits are connected to light emitting diodes as a means of verifying the stability of the output signal.

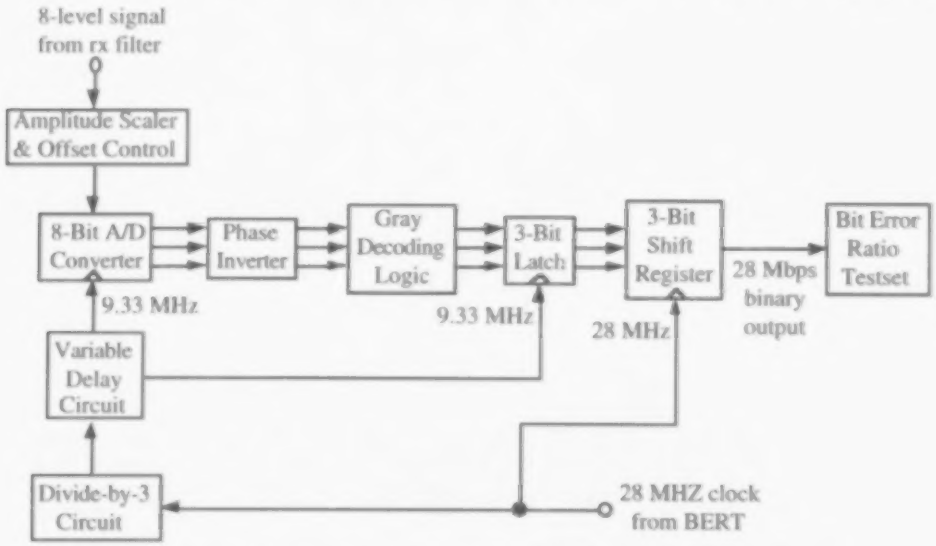

Figure 4.16: Block Diagram Representation of 8-Level ASK Decoder

The clock input for the A/D converter is derived from a divide-by-3 circuit connected to the 28 MHz clock output of the Bit Error Ratio Testset. The divide-by-3 design used in the transmitter to generate a 9.33 MHz clock is also utilized in the decoder. Since the timing of the A/D converter is vital in optimizing the performance of the decoder, a variable delay circuit controls the timing of the clock input into the A/D converter. Dallas Semiconductor DS1000-25 and DS1000-11 delay ICs are arranged to provide up to 100 ns of delay with a resolution of 2 ns. This delay allows control over when the A/D converter samples the 8-level signal, adjusting the sampling time to correspond with the maximum eye opening.

The 3 bits of parallel output from the A/D converter enter the phase inverter circuit. Using a design based on exclusive-OR gates, this circuit can account for a situation in

which the phase of the 8-level signal at the input to the A/D converter has been shifted by 180°. This circuit is used as a preventative measure since multiple stages of upconversion and downconversion may invert the phase of the transmitted signal.

The final three stages of the 8-level decoder are the Gray decoding circuit, 3-bit data latch and 3-bit shift register. These circuits perform the reverse functions of their respective counterparts located in the encoder. The Gray decoder uses 2-input NAND gates to revert the encoded data previously defined in Table 4.1 back to its original state. The 3-bit data latch and 3-bit shift register convert the 3 bits of parallel data to a serial binary data stream at a rate of 28 Mbps. This bit stream enters the return data port of the Bit Error Ratio Testset, at which point the bit error ratio (BER) can be determined.

4.6 Optical Modulation Index (OMI) Calibration

The modulation index of both the analog and digital channels must be determined in order to make comparisons between theory and experiment. To this end, a technique is used to calibrate the per channel modulation index of the 42 analog CATV channels. The results are then extended to determine the modulation index of the single multilevel digital signal.

4.6.1 OMI of the Analog CATV Carriers

In a multichannel SCM optical transmission system, the amount of clipping-induced nonlinear distortion is highly dependent on the per channel modulation index of the analog channels. The theoretical results demonstrate that a slight change in the modulation index can have a huge impact on the amount of system nonlinear distortion, and therefore it is necessary to use an accurate method to determine the per channel modulation index. As previously defined, the modulation index of each channel can be expressed as

$$m = \frac{I_{peak}}{I_{bias} - I_{th}} \tag{4.1}$$

The laser bias current I_{bias} and the laser threshold current I_{th} can be determined quite easily. However, the peak amplitude of the modulation current I_{peak} cannot be determined as easily. Simply measuring the amplitude of the modulating signal at the input to the optical transmitter is not sufficient since electronic interfaces within the transmitter package will alter the signal amplitude that is incident upon the laser diode. To determine the modulation index, a technique proposed by Steve Lai is used. Figure 4.17 gives a block diagram representation of the experimental setup that is utilized to determine the per channel

modulation index. The Matrix generator is set so that only channel 21 at 163.25 MHz is turned on. The bias current of the laser is initially set to a high value so that there is no threshold clipping of the input sinusoidal signal. The peak-to-peak voltage of the channel 21 carrier is measured with a Tektronics 2465A analog oscilloscope at the input to the optical transmitter. This voltage is denoted as $V_{c(p-p)}$. The power of the carrier at the output of the optical receiver is measured with a spectrum analyzer. The laser bias current is slowly decreased until the power at the carrier frequency as measured by the spectrum analyzer starts to drop off. When 100% modulation is reached, the input sinusoidal signal begins to be clipped by the laser diode, and the power in the fundamental frequency measured on the spectrum analyzer begins to shift to higher harmonics. The bias current at the point where 100% modulation is reached, I_c, is determined by a rapid drop in the measured power at 163.25 MHz. This value can be used in a simple transformation to determine the modulation index for an arbitrary bias current I_{bias} and an arbitrary peak-to-peak input voltage $V_{in(p-p)}$ in the following manner:

$$m = \frac{V_{in(p-p)}}{V_{c(p-p)}} \cdot \frac{I_c - I_{th}}{I_{bias} - I_{th}} \tag{4.2}$$

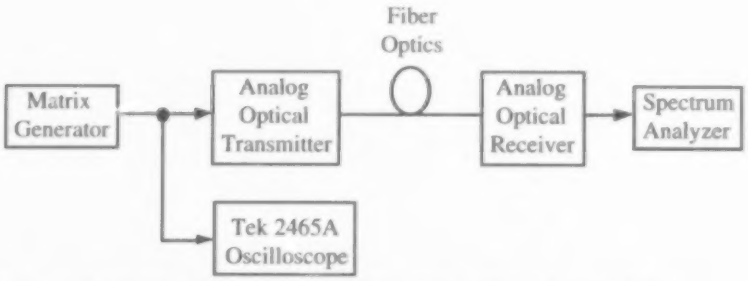

Figure 4.17: Modulation Index Calibration Experimental Setup

The power at 163.25 MHz measured with a spectrum analyzer is shown in Figure 4.18 as a function of laser bias current. The peak-to-peak input voltage swing used to obtain these results was 640 mV. From this graph, the bias current that gives 100% modulation is determined to be 24.5 mA. Recalling that the threshold current for the Fujitsu laser was previously determined to be 18.7 mA, equation (4.2) becomes

$$m = \frac{V_{in(p-p)}}{640\ mV} \cdot \frac{5.8\ mA}{I_{bias} - 18.7\ mA} \tag{4.3}$$

In SCM transmission experiments involving a number of analog channels and a single digital channel, it is desirable to have an identical modulation index for each of the analog channels. This means that all of the carriers would have the same power in the optical fiber since the modulation index is defined at the transmitter. Unfortunately, the frequency response of the optical transmitter is not flat across the bandwidth of the 42 analog carriers, and therefore it is necessary to adjust the transmitted power of each carrier to be equivalent to the channel 21 carrier power in the fiber. The experimental setup previously defined in Figure 4.4 is used for this calibration. All 42 carriers are transmitted through the optical system and the power of each carrier is determined with the spectrum analyzer. This is then compared to the frequency response of the optical receiver that is shown in Figure 4.7. The frequency response of each carrier through the optical transmitter and receiver normalized to channel 21 is compared with the frequency response of the Ortel receiver in Figure 4.19. A LabVIEW program adjusts the power of each carrier within the Matrix generator so that the electrical power of each CATV carrier at the output of the optical receiver follows the frequency response of the receiver. Using this technique, it is quite simple to change the per channel modulation index of the 42 CATV carriers. First, the peak-to-peak voltage swing of the channel 21 carrier at the input to the optical transmitter is set to give a certain modulation index. Then the LabVIEW program is used to automatically adjust the remaining 41 carriers to obtain a given modulation index for all 42 CATV carriers.

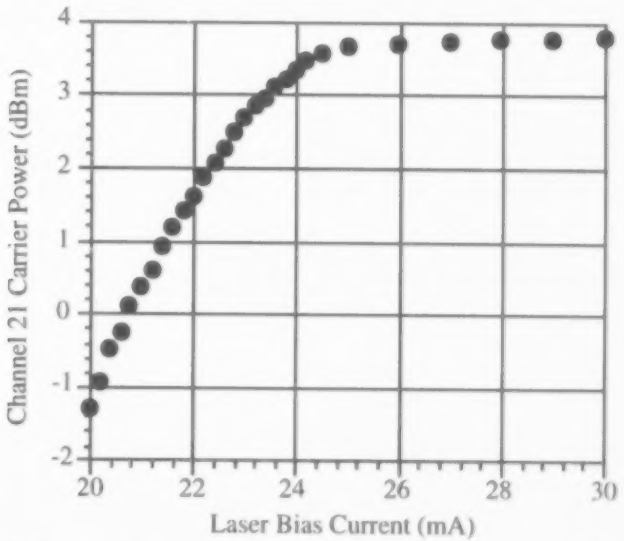

Figure 4.18: Carrier Power of Channel 21 versus Laser Bias Current

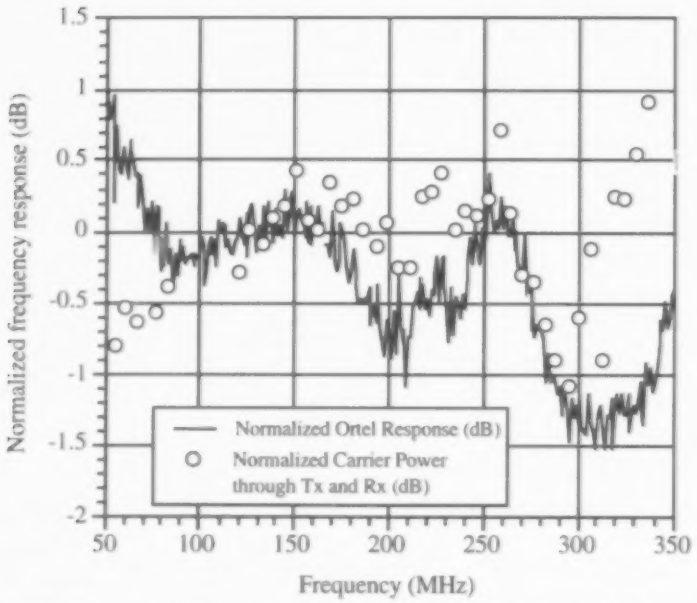

Figure 4.19: Frequency Response of the Optical Receiver and Frequency Response of Each CATV Carrier through the Optical Transmitter and Receiver

4.6.2 OMI of the Multilevel ASK Signal

A few extra steps beyond the previous calibration routine are required to calibrate the modulation index of the digital ASK signal. This is because the multilevel ASK signal is located at a frequency of 450 MHz, cannot be controlled with the Matrix generator, and requires special consideration to determine its average transmitted power since it is an 8-level signal and not a simple sinusoid.

At the output of the optical receiver, the electrical power of a given signal is proportional to the square of the modulation index. If the digital ASK signal and the channel 21 carrier are both transmitted through the optical link, their respective received electrical powers could be related in the following manner:

$$\frac{P_{ASK}}{P_{Ch.21}} = \frac{m_{ASK}{}^2}{m_{Ch.21}{}^2} \tag{4.4}$$

where P_{ASK} is the average electrical power of the multilevel ASK signal at the output of the optical receiver, and $P_{Ch.21}$ is likewise the average electrical power of the Channel 21

carrier after the optical receiver. Equation (4.4) is only valid if the received optical power is the same for both signals, which is the case if they are transmitted simultaneously. The frequency response of the Ortel optical receiver is 2 dB lower at 450 MHz than it is at 163.25 MHz (channel 21 carrier frequency). Therefore, it is necessary to subtract 2 dB, or an absolute factor of 1.58, from the received power of the multilevel ASK signal in order to account for the frequency response of the optical receiver. This is the same technique that was used in section (4.6.1) to normalize all the analog carriers to have the same modulation index as that of channel 21 in the optical fiber. Taking the factor of 1.58 into account, equation (4.4) can be rearranged as

$$m_{ASK} = m_{Ch.21} \cdot \sqrt{\frac{1.58 \cdot P_{ASK}}{P_{Ch.21}}} \tag{4.5}$$

The modulation index of channel 21 $m_{Ch.21}$ is determined using the calibration technique described in section (4.6.1). Since P_{ASK} is the *average* received power of the digital signal, it is easiest to measure the power of a sinusoid at a frequency of 450 MHz that has a known relation to the average power of an 8-level signal. If the Bit Error Ratio Testset is transmitting an all 0's or all 1's pattern, the output of the 8-level encoder is a sinusoid whose magnitude is equivalent to the Peak Signal Envelope S defined in chapter 3. The average power of the digital signal can then be determined by dividing the measured power of the "all 0's" signal by the Peak Power Factor PF of an 8-level ASK signal, i.e. 2.333.

4.7 Multilevel ASK Back-to-Back Calibrations

Before proceeding with experiments, it is necessary to evaluate the performance of the multilevel ASK transmission system in the absence of the 42 AM/VSB carriers. The theoretical examination of a subcarrier multiplexed hybrid AM/VSB-multilevel ASK system presented in chapter 3 assumes that the multilevel ASK portion of the link operates at its theoretical maximum performance level. However, this assumption is based on the use of filters that are perfectly matched to the transmitted pulse and amplifiers that have a perfectly linear phase response. The equipment used in the laboratory does not necessarily meet these criteria and therefore any discrepancies between theory and experiment are partly a reflection of this fact.

4.7.1 Electrical Back-to-Back

A block diagram of the setup used to measure the electrical back-to-back performance of the 8-level ASK link is displayed in Figure 4.20. The baseband filters used in the transmitter and receiver are the 2nd order Butterworth filters described previously. To generate a noise source that has a relatively flat power spectral density at baseband frequencies, two Mini Circuits ZFL-1000LN amplifiers and a Veritek VMA3K10C-232 amplifier are used. Attenuators and 30 MHz low pass filters are placed between each pair of amplifiers to ensure that each subsequent stage is not overdriven by the preceding stage and to minimize reflections back into the output port of each amplifier. The ZFL-1000LN has a 3-dB cutoff of 1.0 GHz, a gain of 20 dB and a 1-dB output compression point of + 3 dBm. The Veritek amplifier has a 3-dB cutoff of 10 GHz, a gain of 32 dB and a 1-dB output compression point of + 17 dBm. The two ZFL-1000LN amplifiers are placed in the first and second stages while the Veritek amplifier constitutes the final stage of the noise source.

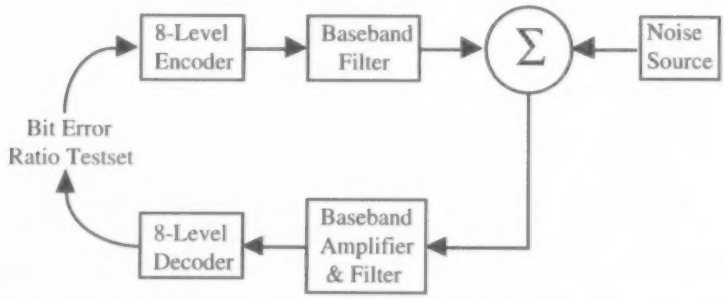

Figure 4.20: Electrical Back-to-Back Experimental Setup

The noise equivalent bandwidth of the Gaussian noise at the input to the 8-level decoder was measured to be approximately 7 MHz. This is because the bandwidth of the noise generated by the noise source is defined by the Butterworth filter located directly before the decoder. In determining the signal-to-noise ratio of the 8-level signal, it is necessary to make two measurements. First, the peak value of the noise power spectral density is measured with a spectrum analyzer, and this value is multiplied by the noise equivalent bandwidth to obtain the total noise power at the input to the decoder. Second, the peak-to-peak voltage of the 8-level signal is measured with an oscilloscope at the output of the 7 MHz receiver filter. The average power is then determined by calculating the peak power and dividing by the peak power factor for an 8-level signal. The bit error ratio for a given signal-to-noise ratio (SNR) can be measured with the Bit Error Ratio Testset.

With a PRBS sequence of length 2^{20}-1, the BER of the electrical back-to-back configuration is shown in Figure 4.21 for bit rates of 24 Mbps, 28 Mbps and 32.5 Mbps. A bit rate of 32.5 Mbps was proposed for this project since this corresponds with the bit rate for Zenith's N-VSB system; however, the back-to-back performance of the digital link is severely degraded at this rate. This is due to the fact that the symbol rate is equal to the bit rate divided by 3 for an 8-level ASK signal. Increasing the bit rate results in increased eye closure due to intersymbol interference for a constant baseband filter bandwidth that is less than the symbol rate. Consequently, a bit rate of 28 Mbps is used for experiments involving simultaneous transmission of analog AM/VSB and multilevel ASK signals.

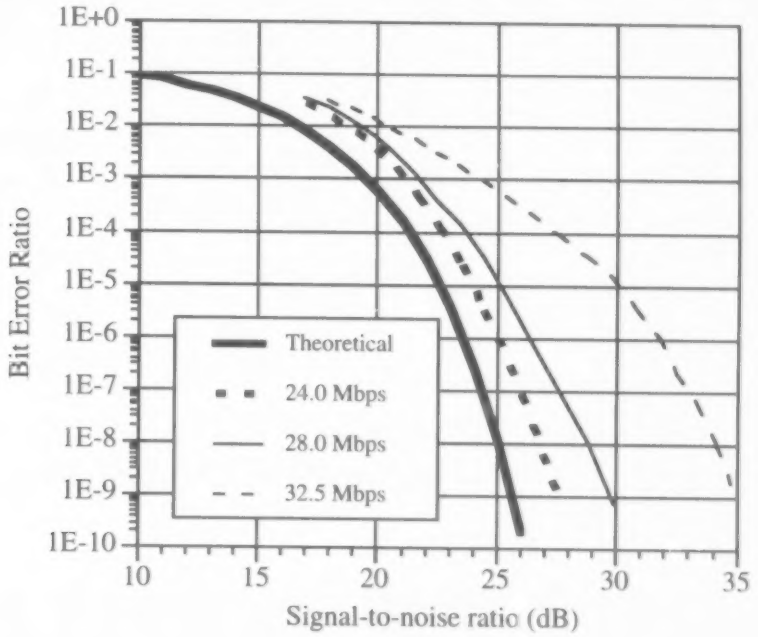

Figure 4.21: Electrical Back-to-Back Performance for three Bit Rates

For interest sake, the binary data stream at the input to the encoder is compared with the bit stream that is sent from the decoder back into the Bit Error Ratio Testset. Figure 4.22 displays the input to the encoder and Figure 4.23 shows the output of the decoder, both measured with a digitizing oscilloscope. Although some ripple due to impedance mismatch exists on the data stream at the output of the decoder, this would have absolutely no effect on the measured bit error ratio. Consequently, any errors that are detected are strictly due to A/D sampling of the 8-level signal at the input to the decoder.

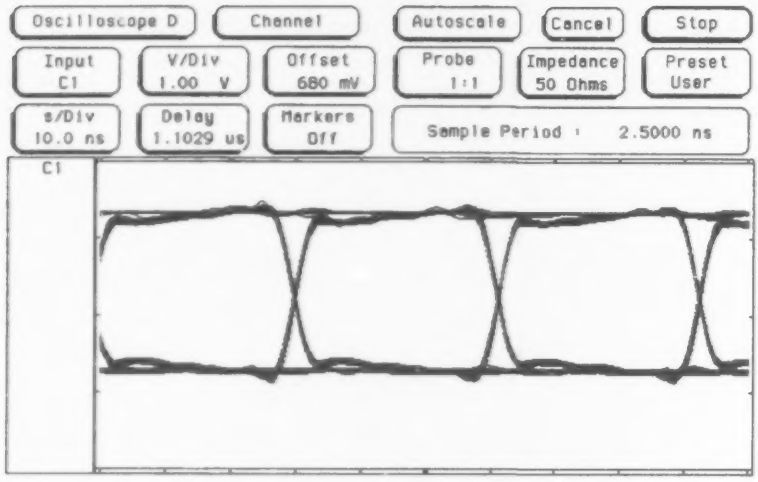

Figure 4.22: Binary Signal at Input to Encoder

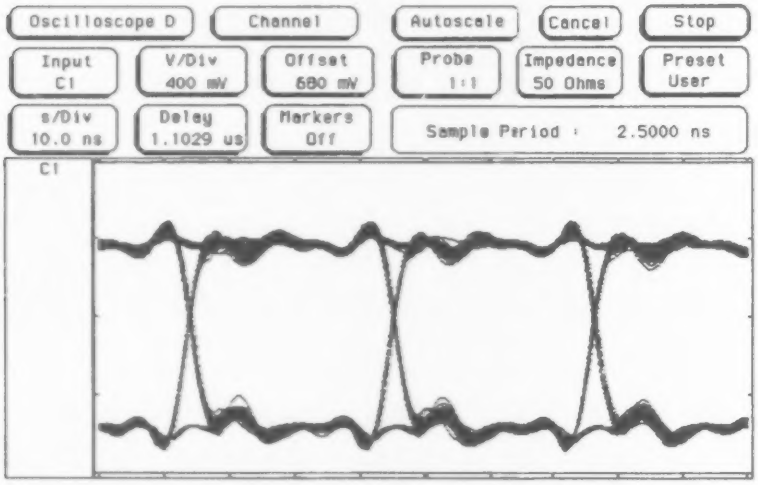

Figure 4.23: Binary Signal at Output of Decoder

4.7.2 Optical Back-to-Back

The multilevel ASK encoder and decoder connected through an optical transmission link is shown in Figure 4.24. This experimental setup constitutes a complete transmission system in which the binary signal is encoded, carried over an optical link, detected with an optical receiver and decoded back to its original state. The setup described herein is identical to that used for experiments on the impact of noise and nonlinear distortion to be discussed in the next chapter.

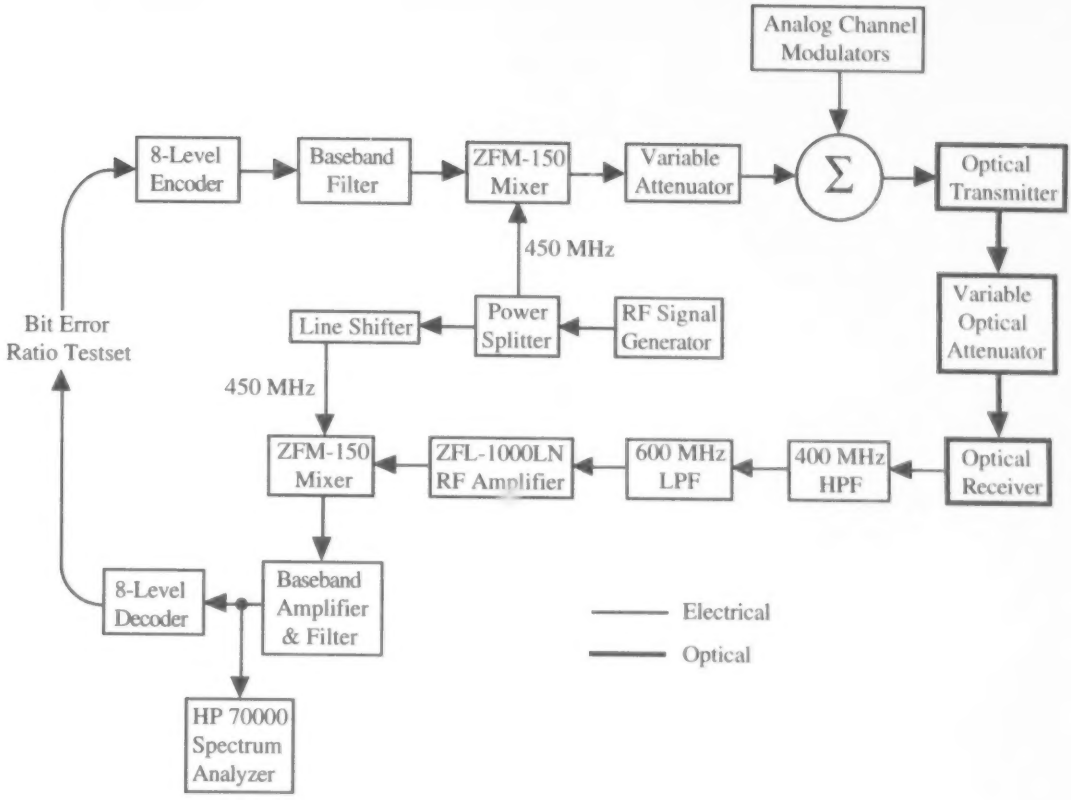

Figure 4.24: Block Diagram of Optical Back-to-Back Experimental Setup

Operation of the 8-level encoder and 8-level decoder has been described in sections 4.4 and 4.5, respectively. An HP8642A RF Signal Generator generates a 450 MHz tone that acts as the carrier for the digital signal. The upconversion process is accomplished via a Mini-Circuits ZFM-150 high dynamic range frequency mixer. This mixer is categorized as level 10, which means that the local oscillator (LO) input should have an RF power of approximately + 10 dBm. The ZFM-150 can handle LO inputs in the range of 10 MHz to 2 GHz and generate RF outputs in the identical frequency range. The IF input port is capable of handling signals right from DC up to 1 GHz. The conversion loss between the input port and output port is approximately 6 dB, and the LO-RF isolation is in the range of 25 to 35 dB. Hewlett Packard HP8494A and HP8494B variable RF attenuators are place after the first mixer to facilitate control over the modulation index of the multilevel signal. The 42 AM/VSB carriers from the Matrix generator are combined with the digital signal, and the composite frequency division multiplexed (FDM) signal directly modulates the Fujitsu laser

diode. Details on the optical components are given in section 4.1. At the output of the optical receiver, the composite FDM signal is passed through a series combination of a 400 MHz high pass filter and a 600 MHz low pass filter both manufactured by Mini-Circuits. The series combination of filters attenuates the power of the analog CATV carriers and removes any high frequency noise that may be present at the output of the optical receiver. The ZFL-1000LN RF amplifier boosts the power of the multilevel signal so that it is within the dynamic range of the ZFM-150 mixer. The RF signal is mixed back down to baseband, where it is again amplified and filtered. The 8-level signal can be viewed at this point with an oscilloscope or spectrum analyzer. Finally, the multilevel signal is converted back to binary in the decoder, at which point the BER can be measured with the Bit Error Ratio Testset.

The BER performance of a digital signal generated from a 28 Mbps pseudorandom input is shown in Figure 4.25. For comparison, the electrical back-to-back performance is also displayed on the same graph. For the optical back-to-back measurement, the optical modulation index of the digital signal is 0.5%, while the per channel modulation index of the 42 AM/VSB channels is 1.4%. The modulation index of the analog channels is low enough that nonlinear distortion due to clipping is negligible.

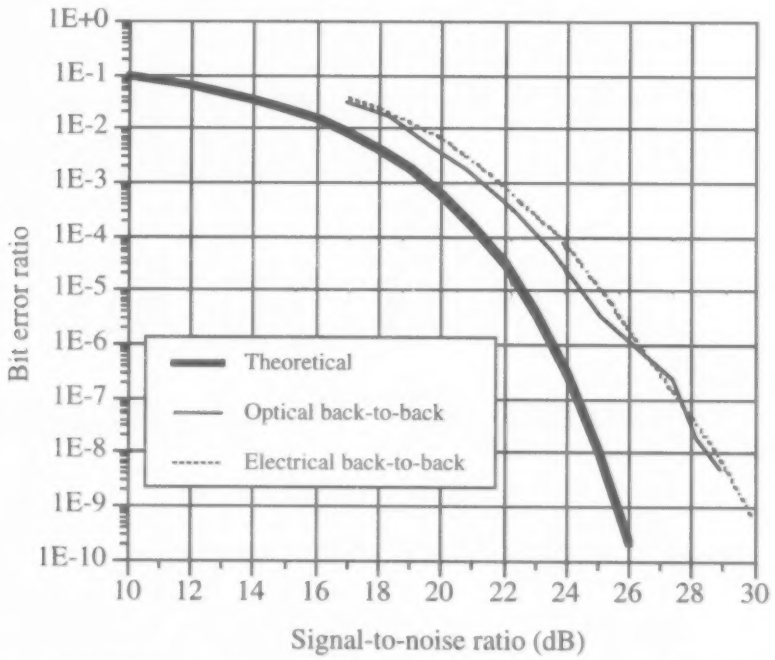

Figure 4.25: BER of 28 Mbps Digital Signal in Back-to-Back Configuration

The BER performance of the multilevel signal in a Gaussian noise environment was also evaluated as a function of received optical power and ASK modulation index. The bit error ratio versus received optical power is plotted in Figure 4.26 for an ASK modulation index of 0.48%. A plot of BER as a function of ASK modulation index is shown in Figure 4.27 for a received optical power of - 6.0 dBm.

The differences between experimental and theoretical results seen in Figures 4.26 and 4.27 are consistent with the results of BER versus signal-to-noise ratio comparisons between experiment and theory. For a 1 dB discrepancy between experiment and theory in Figure 4.26, there is approximately a 2 dB difference at the same BER in Figure 4.25. This is expected since the electrical signal power is proportional to the optical signal power squared. Therefore, 1 dB in the optical domain is equivalent to 2 dB in the electrical domain for a signal of this nature.

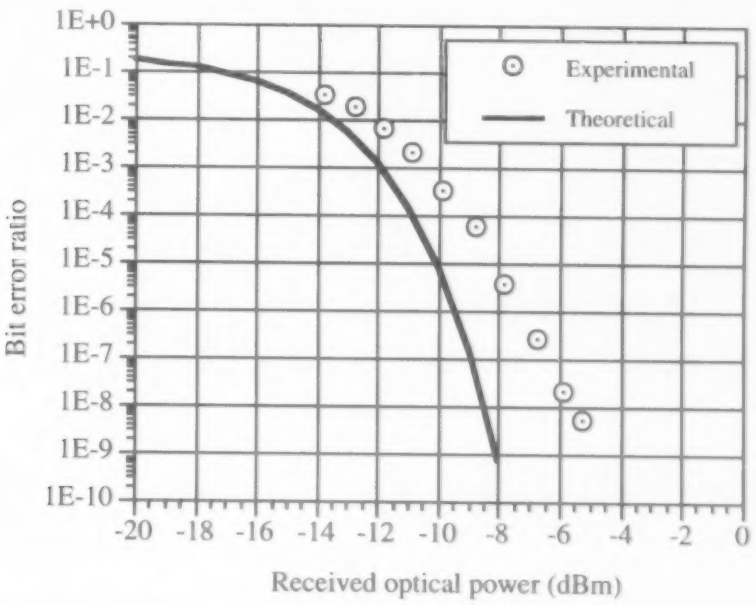

Figure 4.26: Bit Error Ratio as a Function of P_{rx} for an ASK Mod. Index of 0.48%

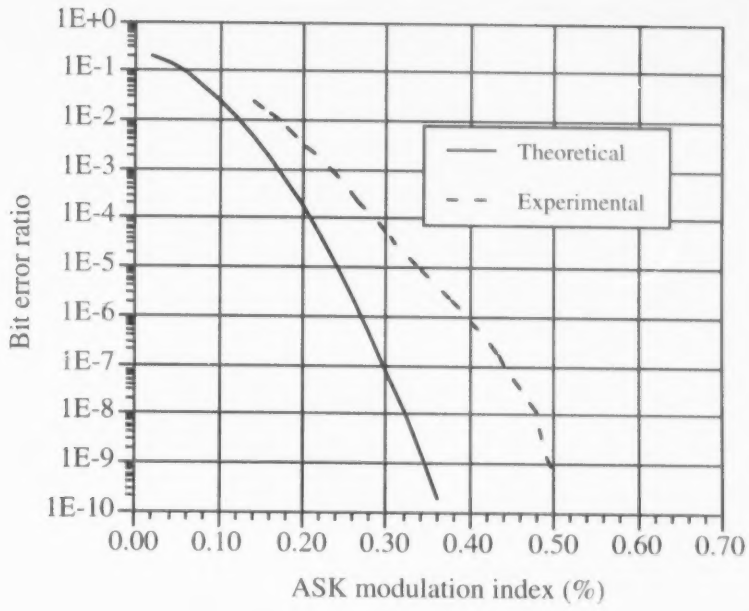

Figure 4.27: BER versus ASK modulation index

The preceding sections outline the design of an optical transmission system and characterize the performance of the multilevel ASK signal in the presence of Gaussian noise. There is a difference of a few dB between the theoretical and experimental performance of the digital encoder and decoder; however, the effort required to improve the performance of this system would be misguided for the upcoming studies. Once nonlinear distortion due to threshold clipping or the combined effects of laser chirp and fiber dispersion is introduced to the system, the performance of the digital signal is degraded substantially. The previous characterization only serves to account for a portion of the discrepancy between theory and experiment for a hybrid AM/VSB-multilevel ASK transmission system.

5.0 Experimental Performance of a Fiber Optic Multichannel AM/VSB-Multilevel ASK Transmission System

The purpose of this chapter is to investigate the performance of an 8-level ASK signal transmitted in a hybrid fiber optic AM/VSB-multilevel ASK transmission system. Experimental results are compared to the theoretical analysis developed in chapter 3. The first section of this chapter examines the noise performance of the AM/VSB carriers. Although the intent of this work is to gain an understanding of the combined effects of noise and nonlinear distortion on a multilevel digital signal, the performance of the analog carriers is also quite important. Following that, a study of nonlinear distortion created in a high-frequency digital channel is undertaken. The next section investigates the performance of the 8-level ASK signal in an environment dominated by Gaussian noise and clipping-induced nonlinear distortion. These two forms of degradation are the most prevalent in a fiber optic transmission system where a large number of carriers are combined together to directly modulate a laser diode. In the final section of this chapter, the impact of nonlinear distortion created through the combination of laser chirp and fiber dispersion is examined.

5.1 Carrier-to-Noise Ratio Performance of an AM/VSB Carrier

The performance of the 42 AM/VSB carriers is examined for an optical transmission system in the absence of the multilevel digital ASK signal. The impact of noise and nonlinear distortion on the analog channels is determined by measuring the carrier-to-noise ratio (CNR), composite second order (CSO) distortion and composite triple beat (CTB) distortion. In this section, the CNR of an analog channel will be investigated. In a later section of this chapter, the CSO and CTB at the subcarrier frequency of the multilevel ASK signal will be examined.

Carrier-to-noise ratio is a common parameter for determining the noise performance of an analog system. The three main sources of Gaussian noise are RIN noise, photodetector shot noise and receiver thermal noise. The carrier-to-noise ratio for a single analog carrier can be represented in the following manner:

$$CNR = \frac{\frac{1}{2}\cdot(m\Re P_o)^2}{RIN\cdot\Re^2 P_o^{\,2}\cdot B + 2q\Re P_o\cdot B + \{i_{th}^{\,2}\}\cdot B} \tag{5.1}$$

The term in the numerator accounts for the received electrical carrier power where m is the peak modulation index per analog channel, $\Re$ is the responsivity of the photodiode and P_o is the received optical power. The denominator of equation (5.1) consists of the three Gaussian noise terms where q is the electron charge, B is the receiver noise bandwidth and $\{i_{th}^2\}$ is the receiver mean square thermal noise current spectral density.

The CNR performance of the experimental transmission system is compared to the theoretical results obtained through the use of equation (5.1). The block diagram of the experimental setup used to make CNR measurements is shown in Figure 5.1. The Matrix generator is set to transmit all 42 AM/VSB carriers. The per channel modulation index can be determined using an analog oscilloscope and spectrum analyzer as described in section (4.6.1). An HP8153A optical power meter is placed directly before the optical receiver in order to measure the received optical power. The Ortel 2610C photodiode within the analog optical receiver has a responsivity of 0.94 A/W and a thermal noise current density at the output of the photodiode of [56]:

$$\{i_{th}\} = 7.3 \cdot 10^{-12} \cdot 10^{\frac{(F-G)}{20}} \quad A/\sqrt{Hz} \tag{5.2}$$

where F is the amplifier noise figure and G is the current gain of the transformer. According to [56], the noise figure for the optical receiver is 6.5 dB and the current gain for this receiver is equal to 7 dB.

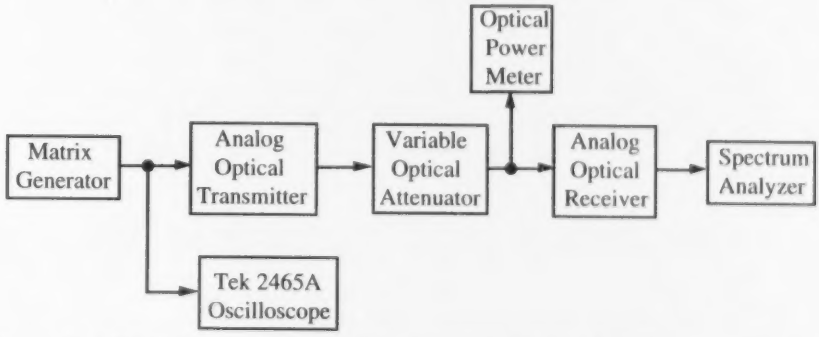

Figure 5.1: Experimental Setup for Measuring Analog CNR

Both the carrier power and noise power can be measured with a spectrum analyzer. According to [3], when measuring the power of a carrier, the spectrum analyzer should be set to a resolution bandwidth of 300 kHz, a video bandwidth of 100 Hz, a frequency span

of 10 MHz and an automatic sweeptime. For measuring CSO and CTB, the spectrum analyzer should have the following settings: resolution bandwidth of 30 kHz, video bandwidth of 10 Hz, frequency span of 500 kHz and a sweeptime of 0.2 sec/division.

When making noise measurements, it is necessary to verify that the noise reading on the spectrum analyzer is from the system under test and not the from the spectrum analyzer itself. This can be determined by noting the value of the noise floor with the spectrum analyzer connected to the system under test. Next, disconnect the system under test from the spectrum analyzer and observe the changes to the noise level. If the noise floor drops dramatically, this indicates that the system itself is the dominant source of the noise. If the noise floor remains unchanged, then the spectrum analyzer noise is greater than that of the system.

The measured noise power is equal to the sum of the spectrum analyzer noise floor and the actual noise power. Since the intent is to determine the actual noise power, the spectrum analyzer noise floor should be subtracted from the measured noise power to obtain an accurate indication of the system noise power. Decreasing the input attenuation of the spectrum analyzer will increase the difference between the spectrum analyzer noise floor and the system noise floor. Unfortunately, if the input attenuation is too low, the front end of the spectrum analyzer will become overloaded and any measurements may be incorrect due to distortion in the spectrum analyzer. The spectrum analyzer can give a reading of noise power spectral density in units of dBm/Hz. Using an AM/VSB bandwidth of 4.25 MHz, the total noise in the AM/VSB channel is equal to

$$N_{tot} = \langle N \rangle + 10 \cdot log(4.25 \cdot 10^6) \tag{5.3}$$

where $\langle N \rangle$ is the noise power spectral density in dBm/Hz.

In Figures 5.2 and 5.3, plots showing measured CNR as a function of received optical power are given for per channel modulation indices of 4.1% and 5.8%, respectively. The carrier power is measured for channel 21 at 163.25 MHz and the noise power is measured within the bandwidth of channel 21. These graphs also display the theoretical carrier-to-noise ratio using equation (5.1), as well as the individual noise contributions arising from laser RIN, receiver thermal noise and photodetector shot noise.

Three main conclusions can be drawn from examination of Figures 5.2 and 5.3. First, there is close agreement between measured CNR and theoretical CNR for both graphs. This indicates that equation (5.1) is a valid means of predicting the noise performance of the system. Second, an increase in the per channel modulation index from

4.1% to 5.8% causes the CNR to increase by approximately 3 dB for any received optical power. This implies that a system CNR requirement can be met simply by increasing the per channel modulation index appropriately. However it will be shown in a later section that an increase in the modulation index of the analog channels causes an increase in the nonlinear distortion products produced across the CATV band. Since these NLD products have a serious impact on the error performance of the digital signals, a compromise exists between reaching a certain analog CNR objective and maintaining an error performance objective for the digital signals. The final conclusion is that three separate noise regimes are observed as the received optical power is increased. For low received powers, thermal noise is the dominant noise source. For high received optical powers, RIN noise dominates over the other two noise sources. In the middle regime, approximately -10 dBm to + 5 dBm for this system, the total noise power at the output of the receiver is essentially determined by the amount of photodetector shot noise that exists.

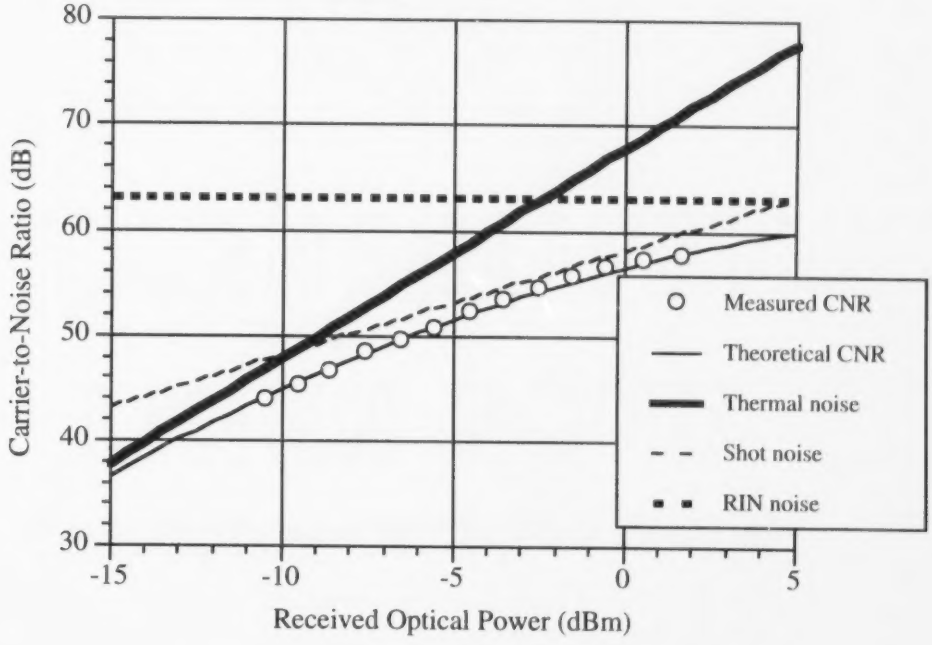

Figure 5.2: CNR versus Received Optical Power for Modulation Index of 4.1%

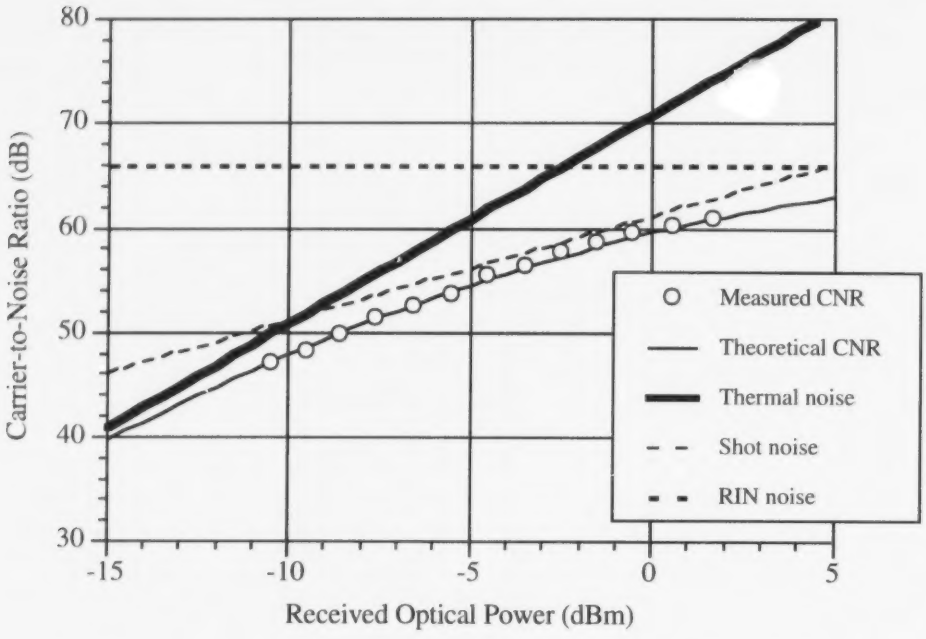

Figure 5.3: CNR versus Received Optical Power for Modulation Index of 5.8%

5.2 Nonlinear Distortion in a High Frequency Digital Channel

In a multichannel subcarrier multiplexed fiber optic system, any nonlinearities in the transmission system will cause nonlinear distortion products at the output of the receiver. The main causes of nonlinear distortion are threshold clipping of a laser diode, intrinsic nonlinearities of the laser, and nonlinearities arising from the combined effect of laser chirp and fiber optic dispersion. In this section, the amount of distortion created by all three types of nonlinearities will be examined.

5.2.1 Nonlinear Distortion in the Absence of Fiber Optics

When a large number of subcarriers are mixed through a nonlinearity, cross-modulation, harmonic distortion and intermodulation distortion (IMD) are created. Of the three, intermodulation distortion tends to dominate in CATV systems. Cross-modulation involves the transfer of modulation from one or more subcarriers to another subcarrier. It occurs as a result of nonlinear gain in the system. Modulation in one channel varies the gain of the laser which in turn causes modulation of other subcarrier signals. Harmonic distortion is when signals are created at multiples of one of the subcarrier frequencies. Intermodulation distortion occurs in multichannel systems due to the interaction of two or

more subcarrier frequencies. Second order distortion products exist at frequencies that are the sum or difference of two subcarrier frequencies. Third order distortion can take the form of two-tone IMD, which refers to a second harmonic of one subcarrier mixing with another subcarrier, or triple beat distortion, which arises from the interaction of three subcarrier frequencies. For a large number of channels, triple beat nonlinear distortion is the dominant form of third order intermodulation distortion.

Two parameters are used to define the amount of intermodulation distortion in a fiber optic system: (i) composite second order (CSO) distortion and (ii) composite triple beat (CTB) distortion. CSO distortion is given by the ratio of the carrier power to the accumulation of second order IMD products within a 6 MHz channel bandwidth. Likewise, CTB distortion equals the ratio of carrier power to the accumulation of triple beat distortion products within a 6 MHz channel bandwidth. For the NTSC frequency allocation plan, the main CSO products tend to fall 1.25 MHz above or below the video carrier frequency, and the main CTB products fall exactly on the video carrier frequency. The setup shown in Figure 5.4 is used to observe the nature of intermodulation distortion. The Matrix generator outputs all 42 AM/VSB carriers between 55.25 MHz and 337.25 MHz. A spectrum analyzer with a 10 MHz span centered on 451.25 MHz and a resolution bandwidth of 30 kHz displays the distortion products created in the vicinity of 450 MHz. Preceding the spectrum analyzer are a 400 MHz highpass filter and a 600 MHz lowpass filter. These filters are required to remove the 42 analog carriers and all the distortion products below 400 MHz and above 600 MHz so that the front end of the spectrum analyzer is not overdriven.

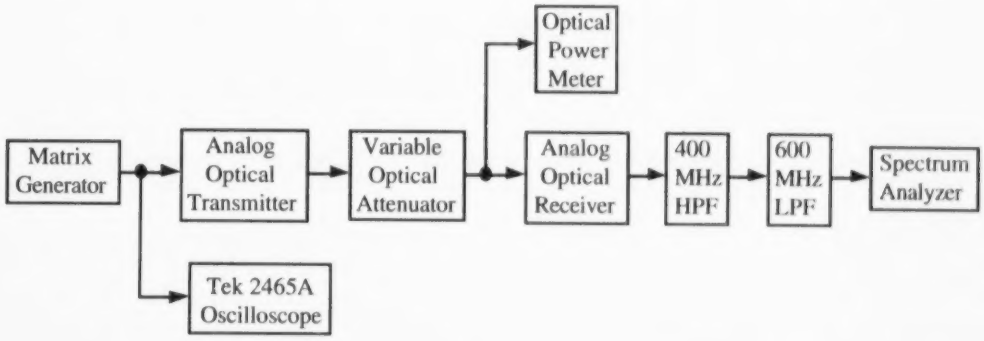

Figure 5.4: Experimental Setup for Viewing Intermodulation Distortion Products

Figures 5.5, 5.6 and 5.7 are plots of the distortion products seen with the spectrum analyzer for modulation indices of 4.1%, 5.8% and 6.5% per channel, respectively. In Figure 5.5, the two spikes at 446.5 MHz and 452.5 MHz are CSO distortion products. As the modulation index is increased to 5.8% per channel, a number of other distortion products rise above the noise floor. The spike in the middle of the plot shown in Figure 5.6 at a frequency of 451.25 MHz is the main CTB product. In Figure 5.7, a large number of intermodulation products are evident. This is because a modulation index of 6.5% per channel will result in a high level of clipping-induced nonlinear distortion. In addition to the previously-mentioned CSO products at 446.5 MHz and 452.5 MHz and the CTB product at 451.25 MHz, there are 7 other triple-beat frequencies that occur between 446.25 MHz and 456.25 MHz. Therefore, approximately a dozen of the smaller spikes in Figure 5.7 are due to harmonic distortion, two-tone third order distortion and higher order intermodulation distortion.

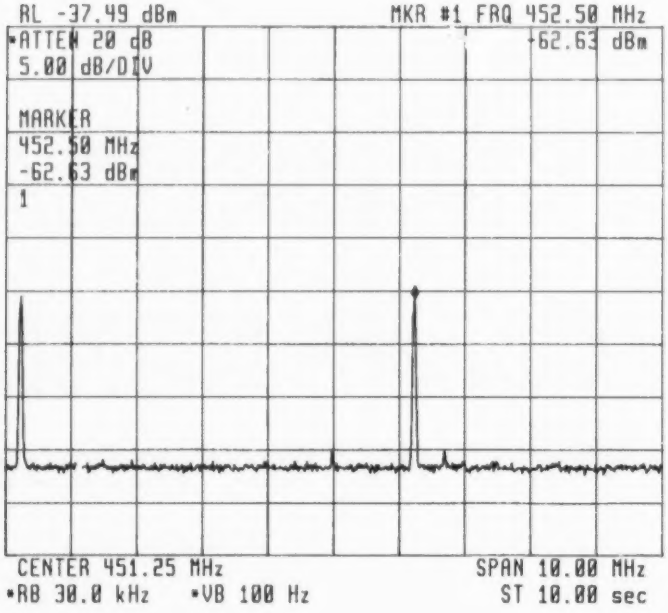

Figure 5.5: Distortion Products near 450 MHz with a Modulation Index of 4.1%

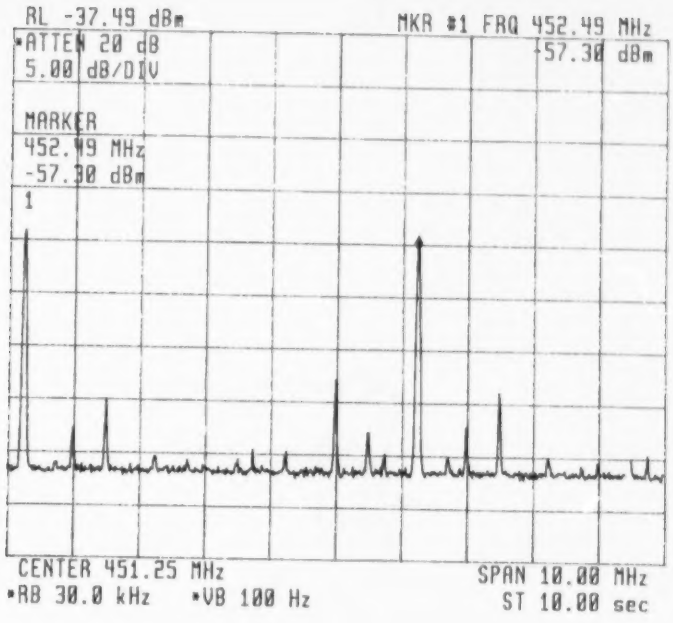

Figure 5.6: Distortion Products near 450 with a Modulation Index of 5.8%

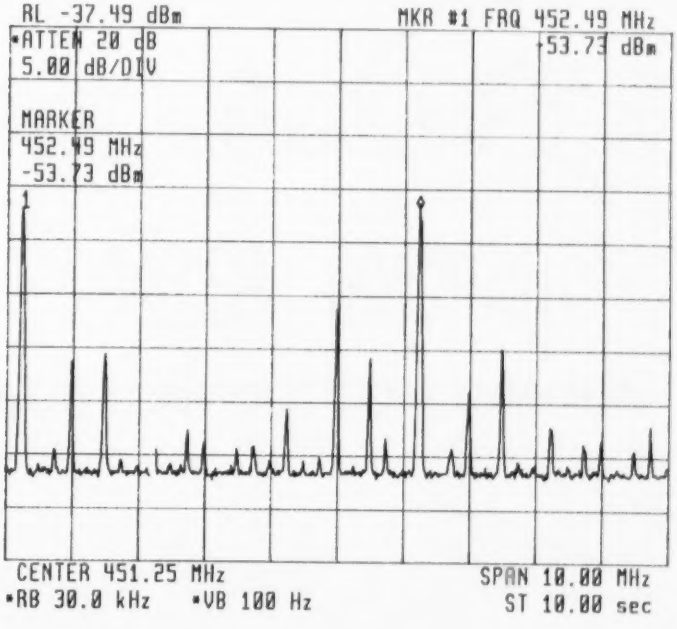

Figure 5.7: Distortion Products near 450 MHz with a Modulation Index of 6.5%

The spectrum analyzer displays shown in Figures 5.5 through 5.7 offer some interesting insight into nonlinear distortion in a fiber optic CATV system. Since a variable optical attenuator is used in the setup, there is no nonlinear distortion resulting from fiber dispersion. Therefore, all the products are due to intrinsic nonlinearities of the laser, receiver nonlinearites and clipping-induced nonlinear distortion. At a modulation index of 4.1%, the CSO products are mostly due to intrinsic nonlinearities. Second order distortion limitations of DFB lasers have been well-investigated in the recent past [57]. As the modulation index is increased to 5.8%, the number of intermodulation distortion products as well as the absolute power of these products increases as clipping-induced nonlinear distortion is introduced. However, a slight increase in the modulation index from 5.8% to 6.5% causes a dramatic increase in the amount of system nonlinear distortion. This is due to the statistics of clipping-induced nonlinear distortion, whereby the relationship between NLD power and modulation index is exponential for high modulation indices.

As the per channel modulation index is increased, the amount of nonlinear distortion power in the system increases. This can be seen by measuring the amount of CSO and CTB power within a given channel as a function of modulation index. Using the same setup as the one shown in Figure 5.4, the intermodulation distortion power that exists near 450 MHz is determined as a function of the total rms modulation index μ. In chapter 3, μ is defined in the following manner:

$$\mu = \sqrt{\frac{N \cdot m^2}{2}} \tag{5.4}$$

where N is the total number of AM/VSB channels and m is the per channel modulation index. A plot of CSO and CTB power as a function of total rms modulation index is given in Figure 5.8. Following NCTA recommended practices for CATV measurements [3], the CSO power is measured at a frequency of 452.5 MHz and CTB power is measured at a frequency of 451.25 MHz. The measured intermodulation distortion powers are referenced to the carrier power of channel 21 at a frequency of 163.25 MHz. All of the nonlinear distortion measurements presented in this chapter are for frequencies outside the band of the 42-channel CATV system. This is because the NLD performance of the analog channels has previously been examined in great detail. In fact, the intermodulation distortion created by a 42-channel SCM system has been determined earlier at TR*Labs* [2] for channels 2 and 30 of the NTSC frequency designation plan. Therefore, it seems more beneficial to

characterize the NLD performance of a high frequency channel in which a digital signal would reside.

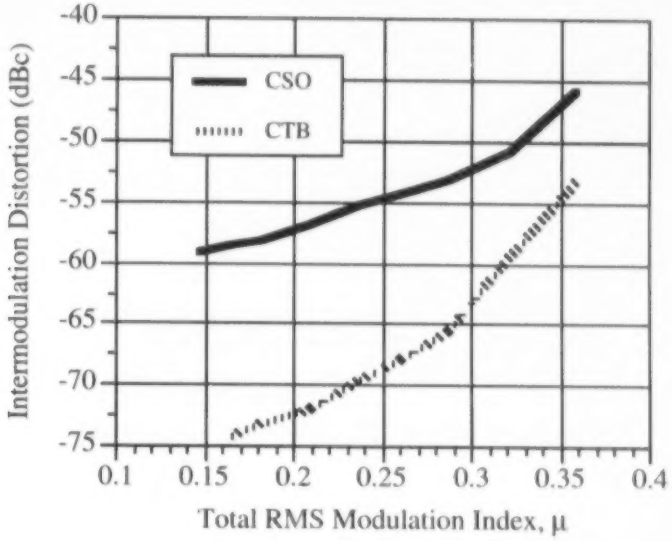

Figure 5.8: CSO and CTB Power near 450 MHz as a Function of μ

The CSO distortion near 450 MHz is much higher than the CTB distortion in the same channel. From analysis on CSO and CTB product counts presented in chapter 3, it is evident that CTB distortion is greatest in the middle of the CATV band and CSO distortion dominates at the lower and upper ends of the CATV band. Since Figure 5.8 displays the distortion power at a frequency above the highest analog channel frequency, it is anticipated that the CSO power will be greater than the CTB power.

For low total rms modulation indices in Figure 5.8 (i.e. $\mu<0.2$), the CSO and CTB distortion power is almost completely due to intrinsic nonlinearities in the laser diode. As μ increases, the curves become more steep since clipping-induced nonlinear is created. This effect is most evident with respect to the increase in CTB power, partly due to the fact that the CTB power resulting from intrinsic nonlinearities is quite low to begin with.

5.2.2 Nonlinear Distortion due to the Combination of Laser Chirp and Fiber Dispersion

When a multichannel subcarrier multiplexed fiber optic transmission system is operating in the 1550 nm wavelength range, second order distortion is created through the combination of laser diode chirp and fiber dispersion. An explanation for how this

nonlinearity is created is quite straightforward. Direct modulation of a laser diode can result in modulation of the output optical frequency, or wavelength. This phenomenon is known as laser diode chirp. Modulation of the injection current causes modulation of the carrier density, which in turn results in variation in the refractive index of the laser's active layer. Since the optical frequency is dependent on the refractive index of the active layer, direct intensity modulation results in a variation of the output optical wavelength.

In single mode fiber optics, intramodal fiber dispersion results in light of different wavelengths traveling through the fiber at different group velocities, where group velocity is defined as the speed at which light in a particular mode travels along the fiber [33]. The two main causes of intramodal dispersion are material dispersion and waveguide dispersion [32], [33]. Material dispersion arises from the variation of the refractive index of the optical fiber core material for different wavelengths. Since the group velocity is a function of refractive index, material dispersion causes different wavelengths to travel through the fiber at different speeds. As a signal is transmitted through dispersive fiber, laser frequency modulation caused by chirp results in modulation of the transmission delay, which in turn results in distortion.

In Figure 5.9, CSO power at 452.5 MHz is shown as a function of total rms modulation index with various lengths of fiber in the link. Likewise, Figure 5.10 displays the CTB power at 451.25 MHz as a function of μ for various fiber lengths. These measurements are taken with the same setup as shown in Figure 5.4, except that fiber is placed between the variable optical attenuator (VOA) and the optical receiver. For the results with fiber, the VOA attenuation is set to 0 dB and the received optical power is measured. The fiber is then removed from the setup and the VOA attenuation is adjusted to give the equivalent received power. When a VOA is used instead of fiber, it is found that the measured CSO and CTB power (in dBc) changes very little with increasing attenuation. This is because the received carrier power and the nonlinear distortion power are both a function of the square of the received optical power. Consequently, only one curve is shown on each graph for the situation in which the VOA emulates fiber loss.

As can be seen in Figure 5.9, the combination of chirp and dispersion causes a large degradation in the CSO performance of the optical link. At a total rms modulation index of 0.25, the CSO has increased by 8 dB with 10 km of fiber in the link, 13 dB with 20 km of fiber and 16 dB with 35 km of fiber. Examination of these curves indicates that clipping-induced distortion is still lower than chirp/dispersion-induced distortion for all but the highest modulation indices. It is well-known that second-order distortion due to chirp and fiber dispersion is more severe for the higher frequency channels than it is for the

lower frequency channels [58]. Previous work at TR*Labs* [2] demonstrated that with 10 km of fiber in a 42-channel SCM system, second order distortion in channel 3 (carrier frequency = 61.25 MHz) and channel 30 (carrier frequency = 259.25 MHz) at high modulation indices is dominated by clipping-induced distortion rather than intrinsic or chirp/dispersion-induced distortion. However, the results of this project indicate that the combination of laser chirp and fiber dispersion is not insignificant in the high-frequency digital channels and would play a role in determining the maximum link distance of directly-modulated systems operating at a wavelength of 1550 nm.

In Figure 5.10 it is observed that chirp and dispersion have a much lower impact on the CTB performance of a digital channel than on the same channel's CSO performance. However, at a fiber length of 35 km, a 3 dB degradation in the CTB performance is evident for all but the highest modulation indices. This indicates that the combination of chirp and dispersion has as strong an impact on CTB performance as does clipping-induced distortion for long fiber lengths. Phillips et al [59] have investigated the degree of CSO and CTB degradation as a result of chirp and dispersion, coming to the conclusion that CTB is more than 30 dB below CSO at all frequencies and can therefore be neglected. However, this work indicates that the CTB degradation may be worse than previous predictions.

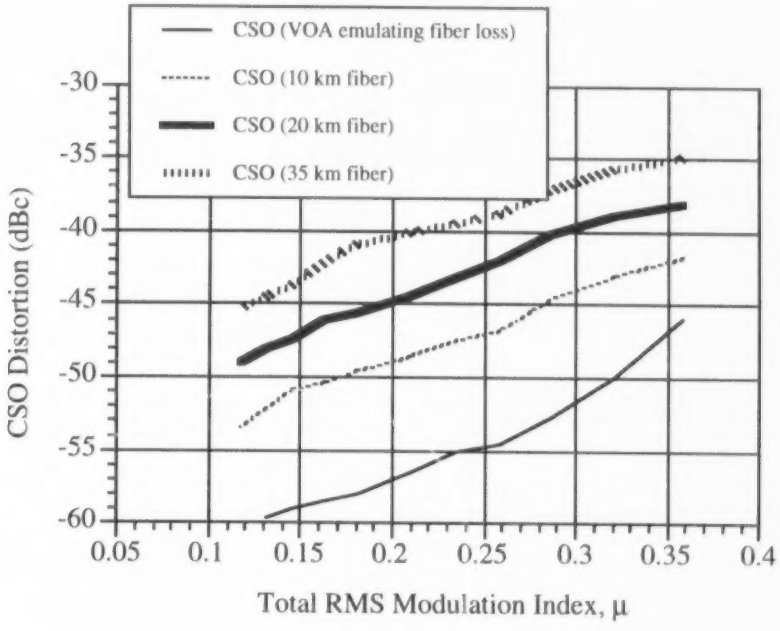

Figure 5.9: CSO Distortion versus μ for Various Fiber Lengths

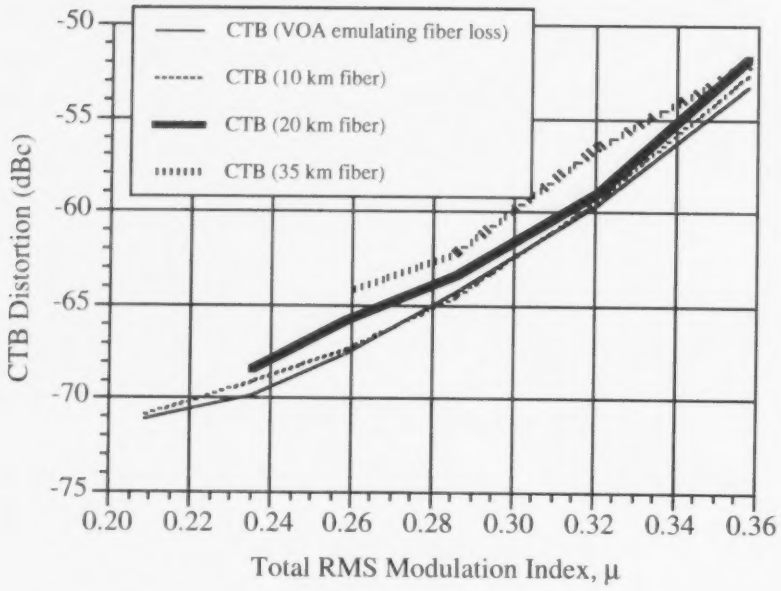

Figure 5.10: CTB Distortion versus μ for Various Fiber Lengths

For hybrid analog-digital subcarrier multiplexed CATV transmission, special consideration is required to avoid the large amount of nonlinear distortion created through the combined impact of laser chirp and fiber dispersion. This distortion can be reduced by limiting transmission lengths to a few kilometers, using dispersion-shifted or dispersion-compensating fiber [60], [61], using optics that operates at the 1300 nm dispersion-minimum of standard single mode fiber, or by using a low-chirp source such as an externally-modulated laser. The problem with using conventional external modulators in subcarrier multiplexed lightwave transmission systems is that these modulators produce a high degree of third order distortion [62]. However, much effort has been directed toward using linearized external modulators in SCM systems to alleviate this problem [29], [63]-[66].

5.3 Performance of 8-Level ASK in a Hybrid SCM Optical Transmission System Dominated by Nonlinear Distortion due to Laser Clipping

In a fiber optic transmission system in which both multichannel AM/VSB and multilevel ASK signals are present, the performance of the digital signals is affected by Gaussian noise and nonlinear distortion. The most common parameter for measuring the

performance of a digital signal is the bit error ratio, defined as the number of received bits that are in error divided by the total number of bits received during a large time interval. The BER of a digital signal is generally a function of the received signal-to-noise ratio. However, in a multichannel SCM system, a large amount of nonlinear distortion may also be present. This nonlinear distortion appears as intermodulation products at discrete frequencies spread across the entire CATV band, with impulsive characteristics in the time domain [24], [26], [31], [41], [53]. As seen in section 5.2, many of these products may exist within the bandwidth of a high-frequency digital channel. Since the intermodulation products do not have a flat spectrum as does Gaussian noise, they can not be treated in the same manner. In chapter 3, Middleton's impulsive noise model was used to determine the bit error ratio of a multilevel ASK signal degraded by both Gaussian noise and impulsive noise. In this section, experimental results are obtained in order to determine the validity of applying Middleton's model to the performance of a multilevel ASK signal impacted by Gaussian noise and impulsive noise.

The experimental setup shown in Figure 5.11 is used to examine the BER performance of an 8-level ASK signal transmitted in an optical fiber hybrid SCM system. There are 42 analog channels with carrier frequencies ranging from 55.25 MHz to 337.25 MHz. The 8-level ASK signal is positioned at a carrier frequency of 450 MHz. Baseband filtering is used to limit the bandwidth of the digital signal before upconversion to the carrier frequency. Operation of the digital encoder, decoder, optical transmitter and optical receiver has been characterized in the previous chapter, where it was shown that the 8-level encoder and decoder operate within 3-4 dB of theoretical limits for an optical back-to-back configuration.

Since a variable optical attenuator is used in the experimental setup shown in Figure 5.11 rather than optical fiber, no nonlinear distortion is created due to the combination of laser chirp and fiber dispersion. Consequently, clipping-induced nonlinear distortion is the main cause of impulsive noise in the digital channel. In this section, the impact of the analog signals on a multilevel ASK signal is evaluated by determining the BER performance of the 8-level ASK signal. The BER performance of the digital signal is investigated with respect to various parameters including the ASK modulation index, signal-to-noise ratio (SNR), signal-to-nonlinear distortion ratio (SNLD) and the received optical power.

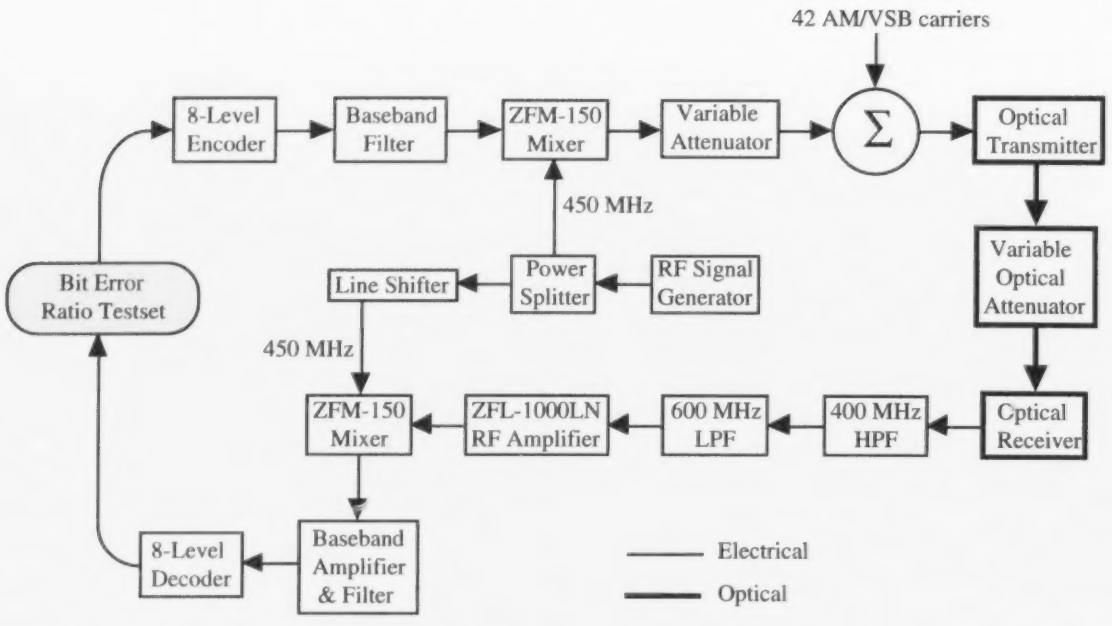

Figure 5.11: Experimental Setup for Measuring BER Performance of an 8-Level ASK Signal in an Optical Fiber Hybrid SCM Transmission System

5.3.1 Error Performance as a Function of ASK Modulation Index

Using the setup shown in Figure 5.11, the error performance of the 8-level ASK signal is measured as a function of the ASK modulation index for AM/VSB modulation indices of 0% (no AM/VSB carriers), 3.85%, 4.80% and 6.00%. The results are shown in Figure 5.12 for a received optical power of -1.0 dBm. The per channel modulation index for the AM/VSB carriers is determined using the calibration technique given in section 4.6.1. The modulation index of the 8-level ASK signal is determined using the procedure described in section 4.6.2 and varied by adjusting the attenuation setting of the variable attenuator located after the first ZFM-150 mixer. The laser diode is set to a bias current of 50 mA for all experimental results.

In Figure 5.12, the experimental results are compared to theoretical results based on the use of Middleton's model for describing combined Gaussian and impulsive noise. Clipping-induced nonlinear distortion results in impulsive intermodulation products across the CATV band and can therefore be modeled using Middleton's noise model. Recall from chapter 3 that the BER of a multilevel ASK signal transmitted in the presence of Gaussian noise and non-Gaussian impulsive noise can be represented in the following form:

$$P_b = \frac{M-1}{M \cdot \log_2 M} \cdot e^{-A} \cdot \sum_{j=0}^{\infty} \frac{A^j}{j!} \cdot erfc\left(\frac{\sqrt{\left(SNR_G^{-1} + SNLD^{-1}\right)^{-1} \cdot PF_M}}{(M-1) \cdot \sqrt{\dfrac{\dfrac{j}{A} + \dfrac{SNLD}{SNR_G}}{1 + \dfrac{SNLD}{SNR_G}}}} \right) \tag{5.5}$$

where M is the number of discrete levels for the ASK signal, A is the impulsive index, SNR_G is the signal-to-Gaussian noise ratio, $SNLD$ is the signal-to-nonlinear distortion ratio and PF_M is the peak power factor for an M-level ASK signal.

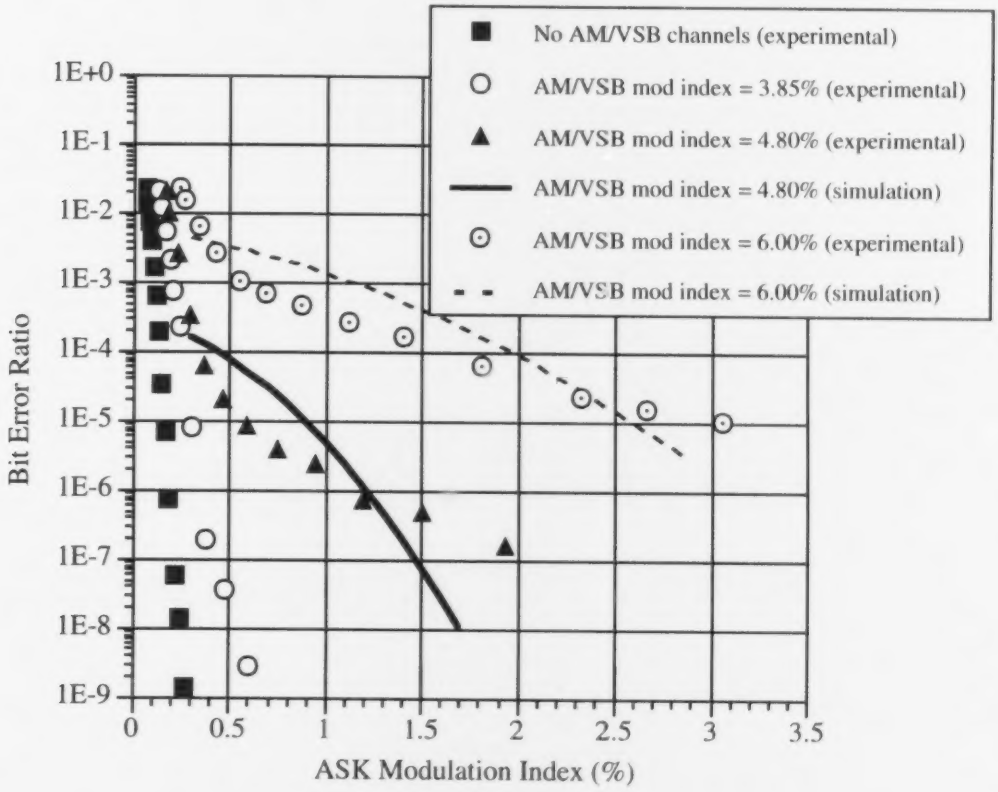

Figure 5.12: BER versus ASK Modulation Index for AM/VSB Modulation Indices of 0%, 3.85%, 4.80%, 6.00%

From Figure 5.12 it is evident that the bit error ratio performance decreases as the modulation index of the AM/VSB carriers is increased. At a per channel modulation index of 3.85%, the BER is mostly a function of the signal-to-noise ratio, since the degree of threshold clipping is very low. At modulation indices of 4.8% and 6.0%, the BER is determined by the impulsive noise degradation within the digital channel. With no AM/VSB channels in the setup, it is possible to obtain a bit error ratio of 1×10^{-9} for an ASK modulation index of only 0.3%. However, as the modulation index of the AM/VSB channels is increased, the ASK modulation index must be increased dramatically to achieve reasonable bit error ratios. Consequently, for large AM/VSB modulation indices, the transmitted power level of the multilevel ASK signal needs to be quite high to offset the BER degradation attributed to the increased amount of nonlinear distortion.

When the bit error ratio is measured as a function of the ASK modulation index, no real BER floor is ever reached. Even with an AM/VSB modulation index of 6%, an increase in the modulation index of the digital signal causes a small increase in the BER performance. This observation can be explained quite simply. For each curve in Figure 5.12, both the received optical power and the AM/VSB modulation index are constant. Therefore, the noise and nonlinear distortion at the receiver does not change. However, the received digital signal power is a function of the ASK modulation index, and an increase in this modulation index results in an increase in both the signal-to-noise ratio and the signal-to-nonlinear distortion ratio. Consequently, an increase in the ASK modulation index will always cause a small increase in the BER performance, even for a high AM/VSB per channel modulation index.

5.3.2 Error Performance as a Function of Signal-to-Noise Ratio and Signal-to-Nonlinear Distortion Ratio

The setup shown in Figure 5.11 is used to examine how the bit error ratio of an 8-level ASK signal is affected by changes in the signal-to-noise and signal-to-nonlinear distortion ratios. Figure 5.13 contains three experimental curves depicting the BER performance of the digital signal as a function of SNR for SNLD ratios of infinity (i.e. no AM/VSB carriers), 39.6 dB and 31.3 dB. For these results, the AM/VSB modulation index is set at 6.0% for all 42 analog channels.

With an analog modulation index of 6.0%, the NLD power within the digital channel is measured. The signal-to-nonlinear distortion ratio is then set by adjusting the attenuation of the variable attenuator located after the first mixer. Since the SNLD does not change with variations in the received optical power, the SNR can be adjusted without

affecting SNLD by increasing or decreasing the attenuation setting of the variable optical attenuator. Experimental results are compared to simulation again based on Middleton's noise model for combined Gaussian and non-Gaussian impulsive noise. For a signal-to-nonlinear distortion ratio of 39.6 dB, there appears to be a large discrepancy between experiment and simulation. This difference is probably due to human error in setting up the decision timing within the decoder circuitry.

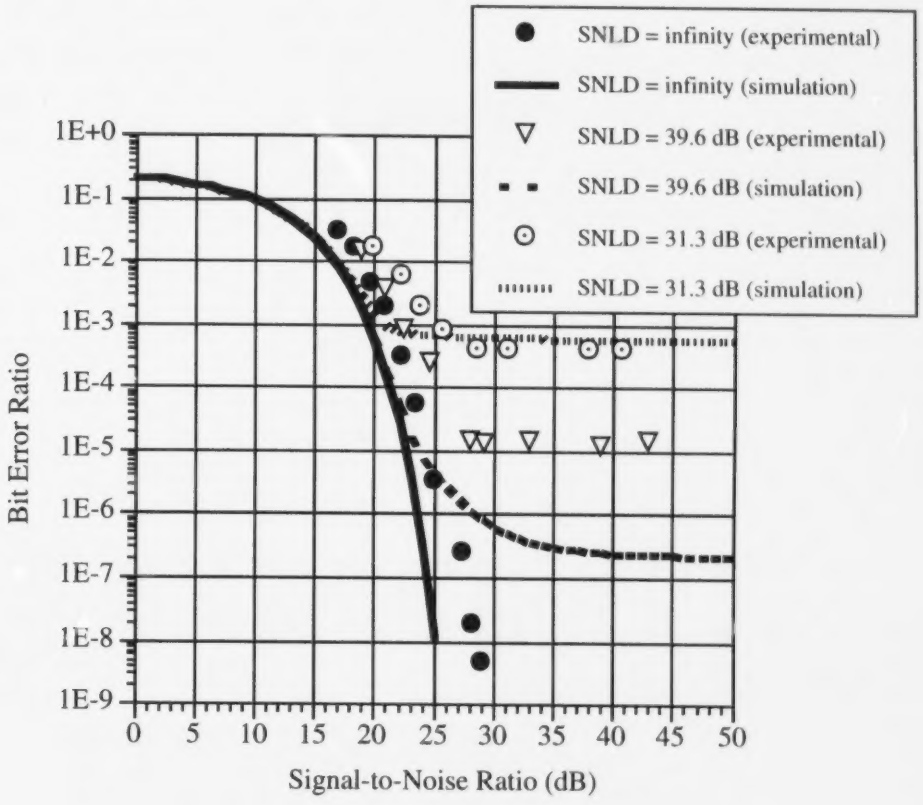

Figure 5.13: BER versus SNR for SNLD's of 31.3 dB, 39.6 dB and infinity

With an SNLD of 31.3 dB or 39.6 dB, a bit error ratio floor exists for both the experimental and theoretical results. For high signal-to-noise ratios, the BER of the 8-level ASK signal is limited by nonlinear distortion within the digital channel. This is obvious since a change in the signal-to-nonlinear distortion ratio from 39.6 dB to 31.3 dB causes the BER floor to shift upwards, while an increase in SNR above 30 dB has almost no impact on the error performance of the signal.

Another interesting observation can be made regarding the relation between SNR and SNLD on the error performance of the digital signal. That is, the 8-level ASK signal requires a lower SNR than SNLD to achieve a given BER objective. A BER floor at approximately 5×10^{-4} is reached for an SNLD of 31.3 dB. In a system with no nonlinear distortion, the same BER is reached for an SNR of only 22 dB. Likewise, an SNLD of 39.6 dB results in a BER floor at ~ 1×10^{-5}. This same bit error ratio is obtained with an SNR of only 24 dB (27 dB theoretically) when there is no nonlinear distortion in the system. Consequently, nonlinear distortion has a more severe impact on the performance of an 8-level ASK signal than does Gaussian noise.

5.3.3 Error Performance as a Function of Received Optical Power and ASK Modulation Index

In Figures 5.14 through 5.16, the effect of variations in the received optical power on the BER is measured. Figure 5.14 plots BER versus ASK modulation index with no AM/VSB carriers in the system for received optical powers of -1.0 dBm and -6.0 dBm. Similar plots are shown in Figures 5.15 and 5.16 but with 42 analog carriers at a per channel modulation index of 4.8% and 6.0%, respectively.

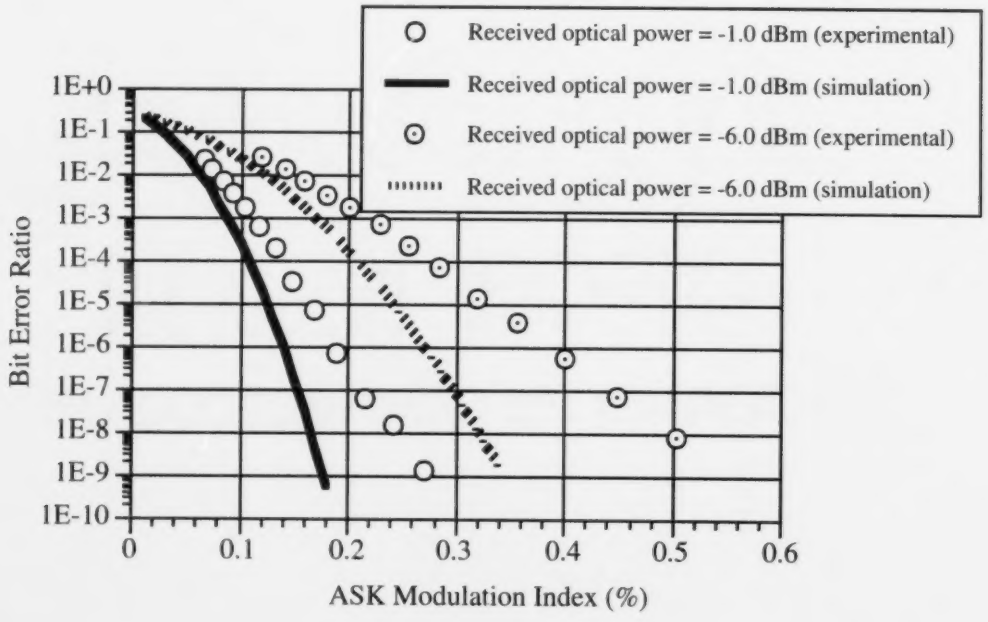

Figure 5.14: BER vs. ASK Modulation Index with no AM/VSB Carriers and with Received Optical Powers of -1.0 dBm and -6.0 dBm

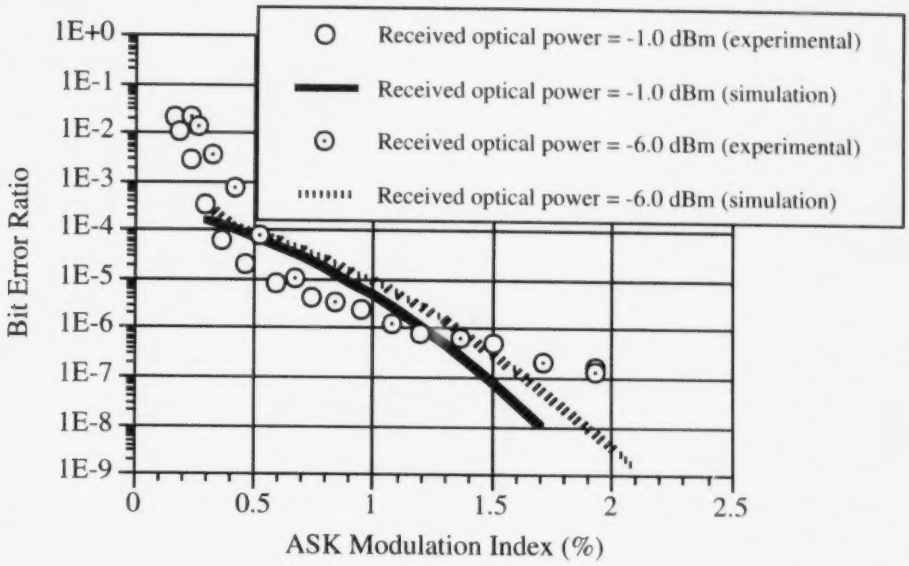

Figure 5.15: BER vs. ASK Modulation Index for an AM/VSB Modulation Index of 4.80% and Received Optical Powers of -1.0 dBm and -6.0 dBm

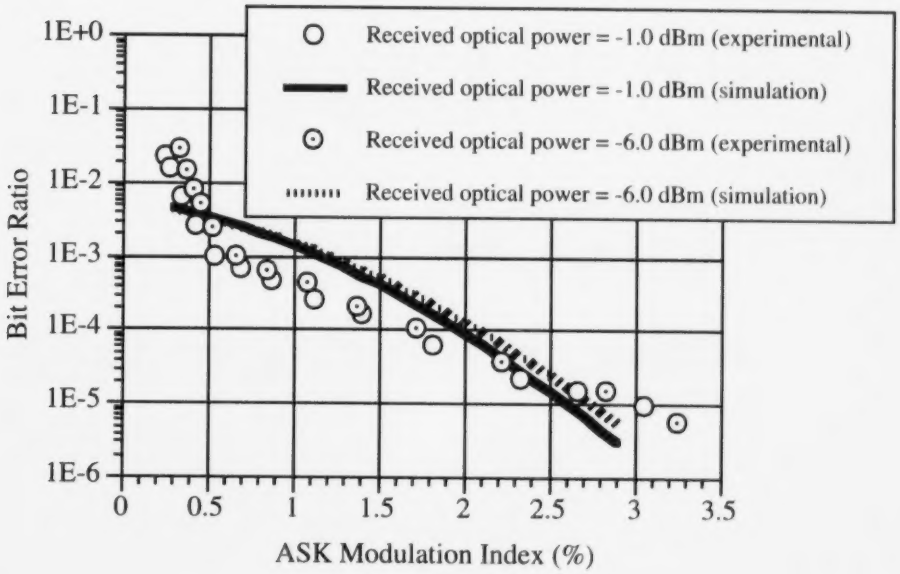

Figure 5.16: BER vs. ASK Modulation Index for an AM/VSB Modulation Index of 6.0% and Received Optical Powers of -1.0 dBm and -6.0 dBm

When there are no AM/VSB carriers in the setup, the BER performance of the digital signal is highly dependent on the received optical power, as is seen in Figure 5.14. Since there is very little nonlinear distortion at the receiver, the BER is defined by the signal-to-noise ratio. SNR increases with increased received optical power when operating in the shot and thermal noise regimes. At optical powers of -1 dBm and -6 dBm, the dominant noise term is shot noise. Hence, a change in the received optical power causes a shift in the error performance of the digital signal.

With 42 AM/VSB carriers at modulation indices of 4.8% and 6.0%, variations in the received optical power have almost no impact on the error performance of the 8-level ASK signal. This is due to the fact that the signal performance is limited by SNLD rather than SNR for high AM/VSB modulation indices. As the received optical power is increased, SNR increases but SNLD remains unchanged. Therefore, if the BER does not change, this indicates that the performance of the digital signal is defined by nonlinear distortion rather than noise.

5.3.4 Alternative Analysis of Clipping-Induced Impulse Noise

The statistical nature of clipping-induced impulse noise in a hybrid SCM transmission system was investigated by a fellow graduate student at TR*Labs*, Steve Lai. The model he developed [40], [53] is based on the initial representation of a clipped SCM signal as a sum of two separate signals: (i) the original modulating signal before clipping, and (ii) an additive noise waveform that represents the clipping events. The original modulating signal is approximated as a Gaussian variable, as long as the number of AM/VSB carriers is greater than 10. The additive noise waveform is modeled using the statistical properties of the threshold crossing behavior of a Gaussian process. In doing so, the clipping events are represented by a Poisson random process. The probability density of the duration of each clipping event follows an asymptotic Rayleigh distribution, and the shape of each clipped pulse is approximated by a parabolic arc. The characteristic function of the resulting clipping-induced impulsive noise waveform is determined by examining the response of the bandlimited digital channel to the clipped signal.

The theoretical model developed by Lai is applied to an M-ary ASK system by modifying the characteristic function of the impulsive noise waveform to include the response of a matched filter demodulator. The probability density function of combined Gaussian noise and clipping-induced impulsive noise is found by taking the Inverse Fourier Transform of the product of their independent characteristic functions. Using the

pdf of combined Gaussian and impulsive noise, the BER of a multilevel ASK signal can then be determined.

This analytical model is used for comparison with experimental results as shown in Figure 5.17. This graph uses the same experimental measurements as those of Figure 5.12, with additional theoretical results based on Lai's model of clipping-induced impulse noise. Simulated error performance based on Middleton's model of combined Gaussian and non-Gaussian impulse noise is also included for comparison.

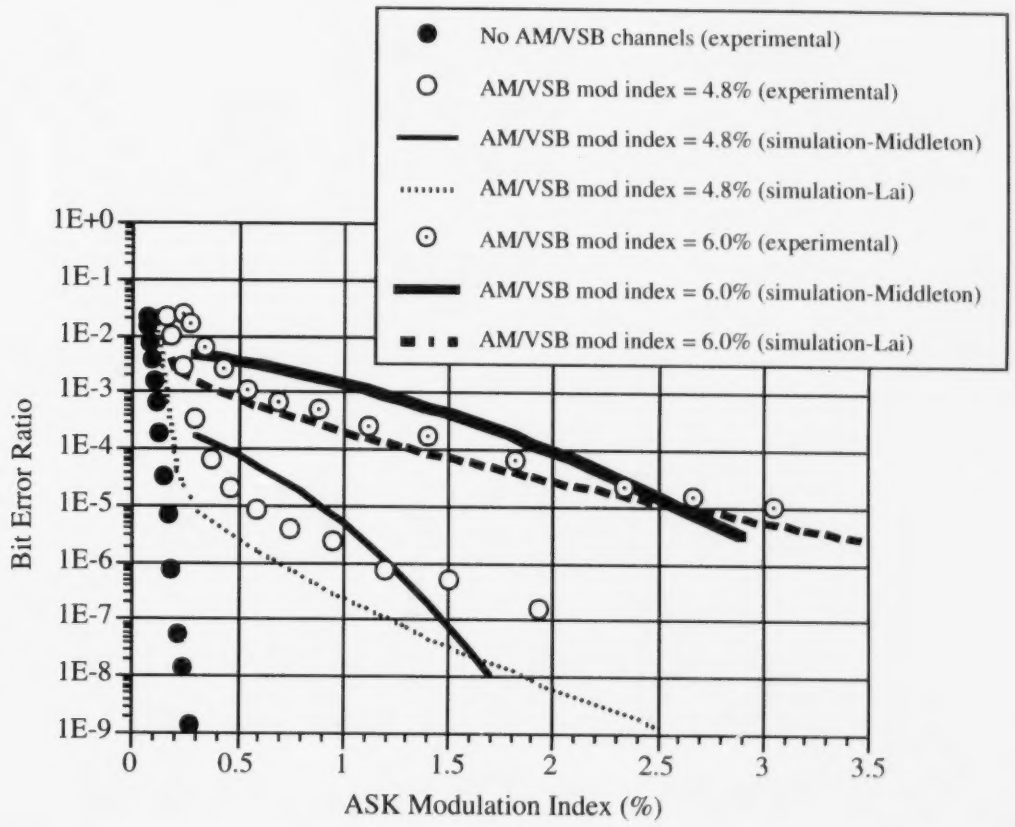

Figure 5.17: BER versus ASK Modulation Index with Comparison to Simulations using Lai's and Middleton's models for Clipping-Induced Impulse Noise

Theoretical error performance based on the noise model developed by Lai is very close to the experimental results. The shape of the theoretical curves is almost identical to that of the curves derived from experiments. Unlike Middleton's model, Lai's model gives

accurate results even at low signal-to-noise ratios. In addition, the simulation does not require measurement of the Impulsive Index parameter, as does simulation based on Middleton's noise model.

5.4 Performance of 8-Level ASK in a Hybrid SCM Optical Transmission System with Nonlinear Distortion due to Laser Clipping and the Combination of Laser Chirp and Fiber Dispersion

In this section, optical fiber is added between the variable optical attenuator and the optical receiver in the experimental setup shown in Figure 5.11. The additional second order distortion created by the combination of laser chirp and fiber dispersion was demonstrated in section 5.2.2. The error performance of an 8-level ASK signal in the presence of Gaussian noise, clipping-induced NLD and chirp/dispersion-induced NLD is investigated as a function of both the ASK modulation index and AM/VSB modulation index.

5.4.1 Error Performance as a Function of ASK Modulation Index

In this section, the BER of an 8-level ASK signal is examined with and without optical fiber in the setup, and for AM/VSB modulation indices of 1.4% and 6.0%. With a received optical power of -6.0 dBm for all experimental measurements, four distortion environments are examined in Figure 5.18: (i) negligible nonlinear distortion, (ii) nonlinear distortion due to laser chirp and fiber dispersion, (iii) nonlinear distortion due to threshold clipping of a laser diode, and (iv) nonlinear distortion due to laser threshold clipping as well as the combination of chirp and dispersion.

The first curve in Figure 5.18 uses a variable optical attenuator (VOA) only in the optical link, and the per channel modulation index for the 42 AM/VSB carriers is 1.4%. Since there is no optical fiber in the link for the results shown in this curve, there is negligible distortion due to chirp and dispersion. Also, with an AM/VSB modulation index of 1.4% per channel, there is very little distortion resulting from laser diode clipping. Consequently, the error performance of the digital signal is entirely dictated by Gaussian noise.

For the second curve of this graph, 10 km of optical fiber is cascaded with the VOA at a lower attenuation setting to give a received optical power of -6.0 dBm. Since the per channel AM/VSB modulation index is still at 1.4%, the dominant source of distortion is from the combination of laser chirp and fiber dispersion. The results of the third curve are

obtained with a per channel modulation index of 6.0% and through using a VOA to emulate fiber loss. The system nonlinear distortion is almost entirely due to threshold clipping. For the final curve of Figure 5.18, 10 km of optical fiber is placed in the setup and the AM/VSB modulation index for the 42 analog carriers is set at 6.0%. The error performance is consequently a function of clipping-induced distortion and chirp/dispersion-induced distortion.

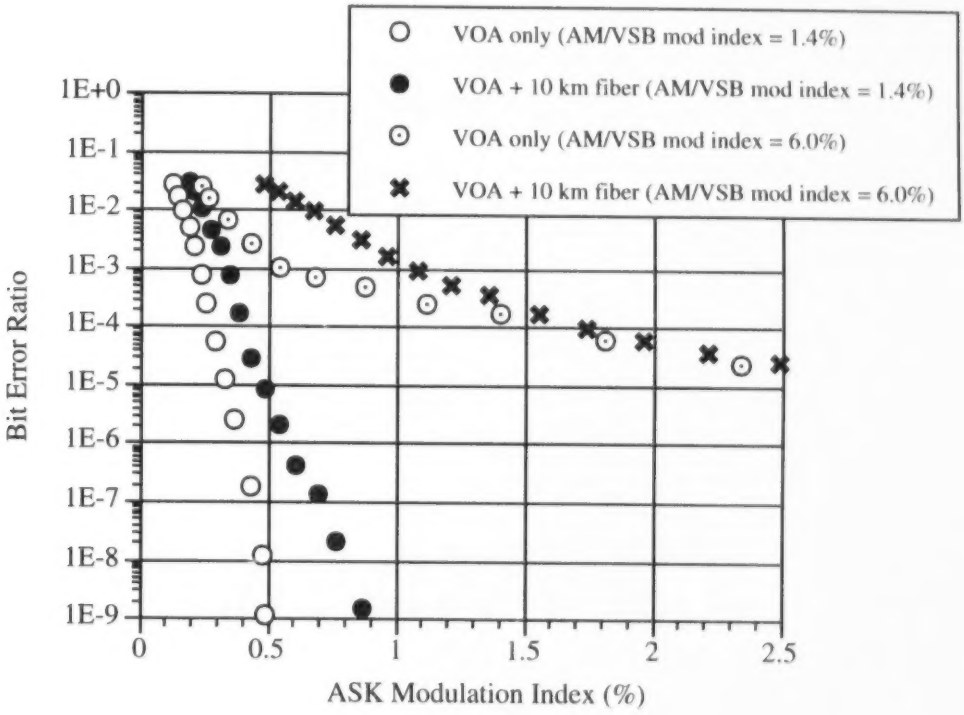

Figure 5.18: BER versus ASK Modulation Index with and without 10 km Fiber

When 10 km of optical fiber is added to the setup while the per channel modulation index is maintained at 1.4%, the error performance is only slightly degraded. However, the error performance of the digital signal decreases quite dramatically when the AM/VSB per channel modulation index is increased to 6.0%. This indicates that the CSO contribution due to 10 km of fiber is substantially less than that due to laser clipping at a modulation index of 6.0%. This corresponds with the results of sections 5.2.1 and 5.2.2. In Figure 5.8, it is observed that the amount of CSO due to clipping-induced NLD for a modulation index of 6.0% (μ=0.275) is approximately -52 dBc. The amount of CSO created with 10 km of fiber in the optical link and a per channel modulation index of 1.4% is seen in Figure

5.9 to be approximately -57 dBc. Therefore, one would expect that an increase in the per channel modulation index to 6.0% would have a greater impact on the BER performance of the digital channel than would addition of 10 km of optical fiber.

5.4.2 Error Performance as a Function of AM/VSB Modulation Index

For Figure 5.19, the BER of the digital signal is determined as the per channel modulation index of the 42 AM/VSB carriers is increased. The signal-to-noise ratio in the ASK channel does not change since the received optical power is set at -6.0 dBm and the ASK modulation index is constant at 0.5%. As the AM/VSB modulation index is increased, the amount of laser chirping and laser clipping both increase. Consequently, chirp/dispersion-induced distortion and clipping-induced distortion will both increase as the AM/VSB modulation index is increased.

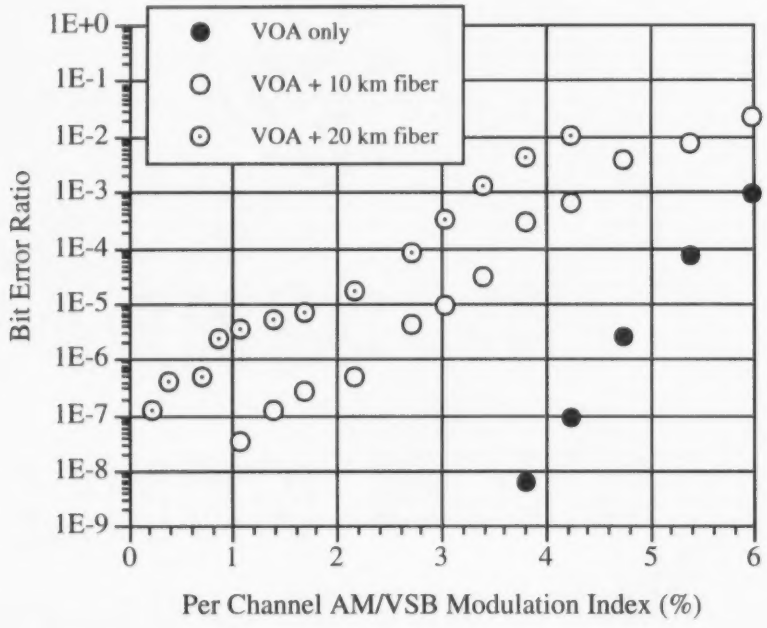

Figure 5.19: BER versus Per Channel AM/VSB Modulation Index for Various Lengths of Optical Fiber

The curves shown in Figure 5.19 have an opposite slope to a standard BER curve because the independent variable shown on the x-axis does not increase the SNR as does ASK modulation index or received optical power. For the curve in which a VOA is used for optical attenuation, note that the BER is quite low when the AM/VSB modulation index

is below 4%. As the modulation index of the 42 analog carriers is increased from 4% to 6%, the error performance degrades rapidly as clipping-induced distortion is introduced to the system. For the other two curves with 10 km and 20 km of optical fiber in the link, a large amount of second-order distortion already exists due to chirp and dispersion. As the per channel modulation index is increased from 0% to 4%, the the bit error ratio performance degrades due to increased chirp/dispersion-induced distortion. As the AM/VSB modulation index is increased beyond 4%, the degradation in error performance due to additional clipping-induced NLD is less dramatic. This is expected since both sources of distortion create intermodulation products at discrete frequencies that are additive on a power basis. A given intermodulation distortion power within the bandwidth of the digital channel has a corresponding impact on the BER performance of the digital signal, regardless of the source of the intermodulation distortion power. That is, whether this nonlinear distortion power is created by threshold clipping or by the combination of chirp and dispersion does not seem to have an impact on the 8-level ASK error performance.

6.0 Conclusions

The main purpose of this thesis has been to evaluate the error performance of a multilevel amplitude shift keyed (ASK) digital signal when transmitted alongside a large number of analog carriers. The analog and digital signals are frequency division multiplexed into a single electrical signal which directly modulates a highly-linear laser diode, thereby resulting in a subcarrier multiplexed (SCM) transmission system. This type of transmission system will be used in the near future for the simultaneous broadcast of analog and digital television signals. In North America, analog television uses AM/VSB modulation while the proposed HDTV format for the delivery of digital television signals is known as N-VSB. This system, designed by Zenith, uses multilevel ASK signaling, combined with a number of forward error correction schemes and vestigial sideband filtering.

In a hybrid optical SCM transmission system, the two main sources of signal degradation are Gaussian noise and nonlinear distortion. In this thesis, the impact of both sources of degradation on the error performance of an 8-level ASK signal is examined. Although 16-level signaling increases the spectral efficiency of the transmitted signal, there is a penalty to be paid due to both noise and distortion. Consequently, hardware implementations focused on 8-level ASK rather than 16-level ASK. Nonlinear distortion resulting from threshold clipping of the laser diode is seen to be a dominant source of distortion in a directly-modulated transmission system. In addition, the impact of nonlinear distortion created through the combined impact of laser chirp and fiber dispersion was also examined and compared to the impact of clipping-induced distortion.

6.1 Summary of Conclusions

A number of more specific conclusions regarding the effects of noise and nonlinear distortion on the performance of multilevel ASK can be made. First of all, throughout this work, it is evident that there is a definite compromise between meeting noise objectives and nonlinear distortion objectives. It was demonstrated that as the modulation index of the analog channels is increased, the CNR of these channels also increases. However, an increase in the per channel modulation index results in a greater degree of threshold clipping. This in turn results in more nonlinear distortion products across the CATV band and a corresponding increase in CSO and CTB (measured in dBc) for both the analog channels and the digital channels. For the digital channels, an increase in the intermodulation products that fall within the channel bandwidth can severely impact the

BER performance of the digital television signals. Consequently, an attempt to meet the CNR objectives of the analog AM/VSB channels may result in a degradation in the CSO and CTB performance of the analog channels as well as a degradation in the error performance of the digital channels.

Secondly, it became evident that composite second order distortion dominates over composite triple beat distortion for the high-frequency channels in which digital HDTV signals would be placed. At a frequency of 450 MHz, the intrinsic CSO at low rms modulation indices is 15 dB higher than CTB. When the rms modulation index is increased to 0.35, CSO is still 8 dB higher than CTB at a frequency of 450 MHz. Since the digital television signals in a hybrid system will be placed at frequencies above the existing NTSC analog CATV band, it is necessary to examine ways of reducing the amount of second order distortion in the system.

Since much of this thesis involved studying the impact of threshold clipping of the SCM signal on the performance of a digital signal, a number of results relating to this effect became evident. First of all, as the signal-to-noise ratio of the multilevel ASK signal is increased, a BER floor is eventually reached. That is, once a certain SNR is obtained, an increase in the SNR does not result in an improvement in the bit error ratio. The level of the BER floor is defined by the signal-to-nonlinear distortion ratio of the ASK signal. In addition, experimental measurements demonstrated that 8-level ASK requires a lower SNR than SNLD to achieve a given BER objective. Therefore, it is reasonable to assume that nonlinear distortion due to clipping degrades a multilevel ASK signal more severely than does Gaussian noise. A further conclusion relating to the impact of clipping-induced distortion is that as the modulation index of the ASK signal is increased, there is an improvement in error performance of the multilevel ASK signal but no BER floor is ever reached. This is due to the fact that an increase in the digital modulation index results in an increase in both the signal-to-noise ratio and the signal-to-nonlinear distortion ratio. Consequently, an increase in the ASK modulation index will always cause an increase in the BER performance, even when the AM/VSB modulation index is high. However, when the AM/VSB modulation index is large, the transmitted power of the ASK signal must be increased in order to offset the BER degradation resulting from clipping-induced NLD.

Finally, it was observed that changes in the received optical power have no impact on the BER performance of the digital signal when the AM/VSB per channel modulation index is high. This is due to the fact that the signal performance is limited by the SNLD and not SNR for high values of the analog per channel modulation index. As the received optical power is increased, SNR increases but SNLD remains fixed. Consequently,

changes in the received optical power level have no impact on the error performance of the digital signal.

Within the scope of this thesis, a number of results were obtained relating to the impact of distortion created through the combined effects of laser chirp and fiber dispersion. First of all, it was observed that chirp/dispersion-induced composite second order (CSO) degradation is quite substantial at high frequency channels. Near 450 MHz, the CSO has increased by 8 dB with 10 km of fiber in the link, 13 dB with 20 km of fiber and 16 dB with 35 km of fiber. Therefore, the combination of chirp and dispersion would play a role in determining the maximum fiber length in a directly-modulated transmission system. Secondly, there also exists a smaller degree of composite triple beat (CTB) degradation for long fiber lengths. Near 450 MHz, there is a 3 dB increase in CTB for a fiber length of 35 km. Traditionally, it has been assumed that only the second order distortion performance of the link is affected by the combined impact of laser chirp and fiber dispersion. However, it was demonstrated in this thesis that a small amount of third order degradation also exists as a result of chirp/dispersion-induced distortion.

The error performance of a multilevel ASK signal was examined in the presence of nonlinear distortion created through threshold clipping and through the interaction of laser diode chirp and fiber dispersion. A number of observations were made as to which cause of distortion has the greatest impact on the BER performance of a digital signal. First, the CSO contribution due to the addition of 10 km of fiber while maintaining a low per channel modulation index is less than the level of CSO distortion caused by threshold clipping at a per channel modulation index of 6%. However, when the fiber length is increased to 20 km, the CSO contribution due to the combination of chirp and dispersion is very close to that resulting from laser diode clipping at high modulation indices. Therefore, if the fiber length is longer than 20 km, the BER performance of the digital signal is determined by second order distortion resulting from the combination of laser chirp and fiber dispersion. It is also interesting to look at how changes in the AM/VSB modulation index impact both causes of nonlinear distortion. Threshold clipping begins to have an effect on the error performance of the multilevel ASK signal when the AM/VSB modulation index is greater than 4%. With fiber in the system, a large amount of CSO already exists independent of the AM/VSB modulation index. Consequently, clipping degradation is much less dramatic when the AM/VSB modulation index is increased from 4% to 6% with optical fiber included in the setup.

In this work, the feasibility of transmitting analog and digital television signals side-by-side in an optical subcarrier multiplexed system is examined. Although the error performance of the digital signals is quite dependent on nonlinear distortion as a result of

SCM techniques, there are numerous advantages to transmitting digital television signals in this manner. For example, subcarrier multiplexing of the analog and digital channels is compatible with the present NTSC television system since the analog channels maintain their current channel locations. Also, the power requirement of the multilevel ASK signals in order to meet the performance objectives is quite a bit lower than that for the AM/VSB channels. This in turn allows a greater channel capacity for the digital signals. These advantages make a hybrid AM/VSB - multilevel ASK transmission system a promising transport scheme for future distribution of CATV video.

6.2 Recommendations for Further Research

This work involved an initial study of the performance of a multilevel ASK signal transmitted in a hybrid SCM lightwave CATV system. A practical extension of this thesis would be to perform a similar analysis using an N-VSB transmitter and receiver. According to Zenith [67], N-VSB kits would be made available early in 1996 for research purposes. It would be particularly interesting to examine the performance of the forward error correction codes used in the N-VSB system designed to combat the effects of impulse noise.

A second possibility for further research would be an investigation of some of the techniques designed to reduce the amount of nonlinear distortion in a subcarrier multiplexed system. For example, it has been suggested that preclipping can be used to remove distortion created through threshold clipping of a laser diode [68], [69]. Using this technique, the multiplexed AM/VSB signal is preclipped by a limiter in order to prevent the multiplexed signal current from falling below the laser diode threshold. The resulting nonlinear distortion products created within the bandwidth of the digital signals are removed with a low pass filter, and then the digital signals are multiplexed with the analog signals before modulation of the laser. A preclipping circuit could be added to the experimental setup used in this thesis to examine its impact on the BER of a multilevel ASK signal transmitted alongside a number of analog signals.

Finally, it would be useful to apply Lai's model of impulsive noise [40], [53] to experimental measurements taken with an N-VSB modulator and demodulator. It would appear that using the statistics of asymptotic clipping to describe the impulsive noise term results in an accurate representation of the resulting impact of threshold clipping on the error performance of a multilevel ASK signal. Therefore, extension of these early results to an actual HDTV transmitter and receiver would prove invaluable.

REFERENCES

[1] T. E. Darcie, "Subcarrier Multiplexing for Lightwave Networks and Video Distribution Systems", *IEEE Journal on Selected Areas in Communications*, vol. 8, no. 7, pp. 1240-1248, Sept. 1990.

[2] K. Pham, Performance of 64-QAM Signals in a Hybrid AM-VSB/QAM Optical Fiber Transmission System, M.Sc. Thesis, University of Alberta, Spring 1994.

[3] National Cable Television Association, *NCTA Recommended Practices for Measurements on Cable Television Systems*, 2nd ed., Nov. 1989.

[4] S. S. Wagner, "Recent Progress in Fiber/Coax Local Access Networks", *OFC '95 Technical Digest*, TuK1, pp. 50-51.

[5] C. Lin, S. Ovadia, W. T. Anderson, "Multichannel AM/QAM Video Lightwave Systems for Hybrid Fiber/Coax Distribution Networks", *IOOC '95 Technical Digest*, FC1-4, pp. 70-71.

[6] S. Ramanathan, R. Gusella, "Toward Management Systems for Emerging Hybrid Fiber-Coax Access Networks", *IEEE Network*, pp. 58-68, Sept. 1995.

[7] M. Huffaker, "Take the Coax Route", *Telephony*, pp. 44-51, Nov. 27, 1995.

[8] L. Stark, "Entering the Interactive Echelons", *Telephony*, pp. 24-34, Nov. 27, 1995.

[9] W. I. Way, "Subcarrier Multiplexed Lightwave System Design Considerations for Subscriber Loop Applications", *Journal of Lightwave Technology*, vol. 7, no. 11, pp. 1806-1818, Nov. 1989.

[10] R. Olshansky, V. A. Lanzisera, P. M. Hill, "Subcarrier Multiplexed Lightwave Systems for Broadband Distribution", *Journal of Lightwave Technology*, vol. 7, no. 9, pp. 1329-1341, Sept. 1989.

[11] T. E. Darcie, G. E. Bodeep, "Lightwave Subcarrier CATV Transmission Systems", *IEEE Transactions on Microwave Theory and Techniques*, vol. 38, no. 5, pp. 524-533, May 1990.

[12] L. W. Couch II, Modern Communications Systems, Prentice Hall, pp. 28-29, 177-183, 468-471, 1995.

[13] W. Iversen, "U.S. Gropes for Unity on HDTV", *Electronics*, pp. 70-75, March 1989.

[14] G. Beakley, "Channel Coding for Digital HDTV Terrestrial Broadcasting", *IEEE Transactions on Broadcasting*, vol. 37, no. 4, pp. 137-140, Dec. 1991.

[15] R. Hopkins, "Digital HDTV Broadcasting", *IEEE Transactions on Broadcasting*, vol. 37, no. 4, pp. 123-127, Dec. 1991.

[16] W. Zou, "Comparison of Proposed Digital HDTV Terrestrial Broadcasting Systems", *IEEE Transactions on Broadcasting*, vol. 37, no. 4, pp. 145-147, Dec. 1991.

[17] E. Kohn, "Modulation for Terrestrial Broadcasting of Digital HDTV", *IEEE Transactions on Broadcasting*, vol. 37, no. 4, pp. 141-144, Dec. 1991.

[18] Zenith corporation, "VSB Transmission System Grand Alliance - Technical Details", Dec.7, 1994.

[19] R. Citta, R. Lee, "Practical Implementation of a 43 Mbit/s Digital Modem for Cable Television", *1993 NCTA Technical Digest*, pp. 271-279.

[20] K. Kerpez, "A Comparison of QAM and VSB for Hybrid Fiber/Coax Digital Transmission", *IEEE Transactions on Broadcasting*, vol. 41, no. 1, pp. 9-16, March 1995.

[21] H. Samueli, L. Montreuil, W. Paik, R. Lee, "Which is the Best Modulation? QAM vs. VSB", *Communications Engineering and Design*, pp. 47-53, Dec. 1994.

[22] G. Sgrignoli, R. Citta, "VSB Modulation used for Terrestrial Broadcasts", *1995 IEEE International Conference on Consumer Electronics*, WAM 1.2, pp. 4-5, June 7-9, 1995.

[23] M. Roden, Analog and Digital Communication Systems, 4th ed., Prentice Hall, pp. 257, 517, 1996.

[24] Q. Shi, "Performance Limits on M-QAM Transmission in Hybrid Multichannel AM/QAM Fiber Optic Systems", *IEEE Photonics Technology Letters*, vol. 5, no. 12, Dec. 1993.

[25] S. Ovadia, L. Eskildsen, J. Sciarabba, C. Lin, W. Anderson, "Bit Error Rate Impairment in Hybrid AM-VSB/16-QAM Multichannel Video Lightwave Transmission Systems", *IEEE Photonics Technology Letters*, vol. 6, no. 7, pp. 869-871, July 1994.

[26] X. Lu, G. E. Bodeep, T. E. Darcie, "Clipping-induced Impulse Noise and its Effect on Bit-Error Performance in AM-VSB/64QAM Hybrid Lightwave Systems", *IEEE Photonics Technology Letters*, vol. 6, no. 7, pp. 866-868, July 1994.

[27] K. Pham, J. Conradi, G. Cormack, B. Thomas, C. Anderson, "Performance of 64-QAM Signals in a Hybrid AM-VSB/QAM Optical Transmission System", *OFC '94 Technical Digest*, WH2, pp. 107-108.

[28] X. Lu, G.E. Bodeep, T.E. Darcie, "Broad-band AM-VSB/64 QAM Cable TV System over Hybrid Fiber/Coax Network", *IEEE Photonics Technology Letters*, vol. 7, no. 4, pp. 330-332, April 1995.

[29] S. Ovadia, H. Dai, C. Lin, W. Anderson, "Performance of Hybrid Multichannel AM/256-QAM Video Lightwave Transmission Systems", *IEEE Photonics Technology Letters*, vol. 7, no. 11, pp. 1351-1353, Nov. 1995.

[30] Q. Shi, "Asymptotic Clipping Noise Distribution and its Impact on M-ary QAM Transmission over Optical Fiber", *IEEE Transactions on Communications*, vol. 43, no. 6, pp. 2077-2084, June 1995.

[31] K. Pham, J. Conradi, G. Cormack, B. Thomas, C. Anderson, "Impact of Noise and Nonlinear Distortion due to Clipping on the BER Performance of a 64-QAM Signal in Hybrid AM-VSB/QAM Optical Fiber Transmission System", *Journal of Lightwave Technology*, vol. 13, no. 11, pp. 2197-2201, Nov. 1995.

[32] J. Senior, Optical Fiber Communications: Principles and Practice, 2nd ed., Prentice Hall, New York, p. 107, 468-469, 1992.

[33] G. Keiser, Optical Fiber Communications, 2nd ed., McGraw-Hill, New York, pp.97, 359-369, 1991.

[34] G. R. Joyce, R. Olshansky, "Subcarrier Transmission of Compressed Digital Video," *IEEE Photonics Technology Letters*, vol. 4, no. 6, pp.665-667, June 1992.

[35] A. A. Saleh, "Fundamental Limit on Number of Channels in Subcarrier-Multiplexed Lightwave CATV System," *Electronics Letters*, vol. 25, no. 12, pp. 776-777, June 1989.

[36] K. E. Alameh, R. A. Minasian, "Ultimate Limits of Subcarrier Multiplexed Lightwave Transmission," *Electronics Letters*, vol. 27, no. 14, pp. 1260-1262, July 1991.

[37] N. J. Frigo, G. E. Bodeep, "Clipping Distortion in AM-VSB CATV Subcarrier Multiplex Lightwave Systems," *IEEE Photonics Technology Letters*, vol. 4, no. 7, pp. 781-784, July 1992.

[38] N. J. Frigo, M. R. Phillips, G. E. Bodeep, "Clipping Distortion in Lightwave CATV Systems: Models, Simulations, and Measurements," *Journal of Lightwave Technology*, vol. 11, no.1, pp.138-146, Jan. 1993.

[39] J. E. Mazo, "Asymptotic Distortion Spectrum of Clipped, dc-Biased, Gaussian Noise," *IEEE Transactions on Communications*, vol. 40, no. 8, pp. 1339-1343, Aug. 1992.

[40] S. Lai, J. Conradi, "Theoretical and Experimental Analysis of Clipping-Induced Impulsive Noise in AM-VSB Subcarrier Multiplexed Lightwave Systems", to be published in *Journal of Lightwave Technology*.

[41] Q. Pan, R. Green, "Bit-Error-Rate Performance of Lightwave Hybrid AM/OFDM Systems with Comparison with AM/QAM systems in the Presence of Clipping Impulse Noise", *IEEE Photonics Technology Letters*, vol. 8, no. 2, pp. 278-280, Feb. 1996.

[42] Q. Shi, R. Burroughs, D. Lewis, "An Alternative Model for Laser Clipping-Induced Nonlinear Distortion for Analog Lightwave CATV Systems", *IEEE Photonics Technology Letters*, vol. 4, no. 7, pp. 784-788, July 1992.

[43] C. Yuo, "Fundamental Nonlinear Distortions in Analog Links with Fiber Amplifiers", *Journal of Lightwave Technology*, vol. 11, no. 1, pp.7-15, Jan. 1993.

[44] J. G. Proakis, Digital Communications, 2nd ed., McGraw-Hill Book Company, New York, pp. 272-277, 396-399, 1989.

[45] B. P. Lathi, Modern Digital and Analog Communication Systems, 2nd ed., Holt, Rinehart and Winston, Inc., Philadelphia, pp. 111, 208-209, 514-516, 536-539, 1989.

[46] D. Middleton, "Statistical-Physical Models of Electromagnetic Interference", *IEEE Transactions on Electromagnetic Compatibility*, vol. 19, no. 3, pp. 106-127, Aug. 1977.

[47] A. Spaulding, D. Middleton, "Optimum Reception in an Impulsive Interference Environment - Part I: Coherent Detection", *IEEE Transactions on Communications*, vol. 25, no. 9, pp. 910-923, Sept. 1977.

[48] J. Seo, S. Cho, K. Feher, "Impact of Non-Gaussian Impulsive Noise on the Performance of High-Level QAM", *IEEE Transactions on Electromagnetic Compatibility*, vol. 31, no. 2, pp.177-180, May 1989.

[49] K. Maeda, H. Nakata, K. Fujito, "Analysis of BER of 16QAM Signal in AM/16QAM Hybrid Optical Transmission System", *Electronic Letters*, vol. 29, no. 7, pp. 640-642, April 1993.

[50] F. Stremler, Introduction to Communication Systems, 3rd ed., Addison-Wesley Publishing Company, Massachusetts, p. 390, 1990.

[51] M. Jeruchim, P. Balaban, S. Shanmugan, Simulation of Communication Systems, Plenum Press, New York, pp. 350-351, 1992.

[52] Fujitsu Limited, *FLD150F3ACH-AL Data Sheet*, 1992.

[53] S. Lai, Clipping-Induced Impulsive Noise in Directly Modulated Fiber Optic CATV Transmission Systems, M.Sc. Thesis, University of Alberta, Spring 1996.

[54] E. Eichen, J. Schlafer, W. Rideout, J. McCabe, "Wide-Bandwidth Receiver/Photodetector Frequency Response Measurements Using Amplified Spontaneous Emission from a Semiconductor Optical Amplifier" *Journal of Lightwave Technology*, vol. 8, no. 6, pp.912-916, June 1990.

[55] Matrix Test Equipment Inc., *Model ASX-16, AR-12, and DTS Operating Manual.*

[56] Ortel Corporation, *Photodiode Module Model 2610C Operator's Manual.*

[57] J. C. Froidure, C. Lebrun, P. Megret, E. Jaunart, P. Goerg, T. Tasia, M. Lamquin, M. Blondel, "Theoretical and Experimental Study of Second-Order Distortions in CATV DFB Laser Diodes", *IEEE Photonics Technology Letters*, vol. 7, no. 3, pp. 266-268, Mar. 1995.

[58] H. A. Blauvelt, N. S. Kwong, P. C. Chen, I. Ury, "Optimum Range for DFB Laser Chirp for Fiber-Optic AM Video Transmission", *Journal of Lightwave Technology*, vol. 11, no. 1, pp. 55-59, Jan. 1993.

[59] M. R. Philips, T. E. Darcie, D. Marcuse, G. E. Bodeep, N. J. Frigo, "Nonlinear Distortion Generated by Dispersive Transmission of Chirped Intensity-Modulated Signals", *IEEE Photonics Technology Letters*, vol. 3, no. 5, pp. 481-483, May 1991.

[60] W. Muys, J. C. van der Plaats, F. W. Willems, A. M. Vengsarkar, C. E. Soccolich, M. J. Andrejco, D. J. DiGiovanni, D. W. Peckham, S. G. Kosinski, P. F. Wysocki, "Directly Modulated AM-VSB Lightwave Video Transmission System Using Dispersion-Compensating Fiber and Three Cascaded EDFAs, Providing 50 dB Power Budget over 38 km of Standard Single-Mode Fiber", *OFC '96 Technical Digest*, WN4, pp. 198-199.

[61] H. Yoshinaga, E. Yoneda, "40-channel VSB-AM Video Transmission through 70 km of High-Dispersion Fiber by using Dispersion-Compensating Fiber", *OFC '95 Technical Digest*, TuN6, pp. 66-67.

[62] R. Olshansky, "Optimal Design of Subcarrier Multiplexed Lightwave Systems Employing Linearized External Modulators", *Journal of Lightwave Technology*, vol. 10, no. 3, pp. 378-382, Mar. 1992.

[63] R. B. Childs, V. A. O'Byrne, "Multichannel AM Video Transmission Using a High-Power Nd:YAG Laser and Linearized External Modulator", *IEEE Journal on Selected Areas in Communications*, vol. 8, no. 7, pp. 1369-1376, Sept. 1990.

[64] K. E. Alameh, R. A. Minasian, "Optimization of Fiber Amplifier SCM Lightwave Video Systems using Direct and External Modulation", *Journal of Lightwave Technology*, vol. 11, no. 1, pp. 76-81, Jan. 1993.

[65] M. Nazarathy, J. Berger, A. J. Ley, I. M. Levi, Y. Kagan, "Progress in Externally Modulated AM CATV Transmission Systems", *Journal of Lightwave Technology*, vol. 11, no. 1, pp. 82-105, Jan. 1993.

[66] M. K. Jackson, V. Smith, W. Hallam, J. Maycock, "Chirp in Optically-Linearized External Modulators and its Effect on Analog Transmission", *OFC '96 Technical Digest*, ThR2, pp. 279-280.

[67] Ron Lee, Zenith Electronics Corporation, Personal Correspondence, Nov. 1994.

[68] Q. Jiang, M. Kavehrad, "Eliminating Clipping-Induced Transmission Impairment in QAM Channels in a Hybrid AM-VSB/QAM Fiber-Optic System by Preclipping", *OFC '95 Technical Digest*, TuN7, pp. 67-68.

[69] A. Kanazawa, M. Shibutani, K. Emura, "Pre-Clipping Method to Reduce Clipping-Induced Degradation in Hybrid Analog/Digital Subcarrier Multiplexed Optical Transmission Systems", *IEEE Photonics Technology Letters*, vol. 7, no. 9, pp. 1069-1071, Sept. 1995.

Appendix A: Computer Program Listings

A.1 CNR vs. Received Optical Power for AM/VSB Carrier (Mathematica)

```
(* This program calculates the carrier-to-noise ratio of an AM/VSB carrier transmitted in *)
(* an optical fiber system. The impact of RIN noise, shot noise and thermal noise are *)
(* each evaluated separately. *)

(* Set input parameters *)

q = 1.602*10^-19;                    (* Electronic charge in C *)
Ro = 0.94;                           (* Photodetector responsivity in A/W *)
BW = 4.25*10^6;                      (* Channel bandwidth in Hz *)
ith = 6.0*10^-12;                    (* Thermal noise in A/sqrt [Hz] *)
m = 0.058;                           (* AM/VSB per channel modulation index *)
RINdB = -160;                        (* RIN noise parameter in dB/Hz *)
RIN = 10^(RINdB / 10);               (* RIN noise *)

(* Initialize lists *)

PrxdBmlist = { };
CNRrindBlist = { };
CNRthdBlist = { };
CNRshotdBlist = { };
CNRtotaldBlist = { };
SetDirectory [ "~/simulations/CNR_AMVSB" ];

(* Calculate the carrier power and noise powers as a function of optical received power, *)
(* and place each calculated CNR into a list. *)

For [PrxdBm = -15.0, PrxdBm <= +5.0, PrxdBm = PrxdBm + 0.5,

        Prx = N[10^(PrxdBm/10)*1*10^-3];
        PrxdBmlist  = Append [PrxdBmlist, PrxdBm];

        (* Received carrier power *)
        Pcarr = N[0.5*(m*Prx*Ro)^2];

        (* Determine carrier-to-thermal noise ratio *)
        Nth = N[ith^2*BW];
        CNRth = N[Pcarr/Nth];
        CNRthdB = 10*Log[10, CNRth];
        CNRthdBlist = Append [CNRthdBlist,CNRthdB];

        (* Determine carrier-to-shot noise ratio *)
        Nshot = N[2*q*Ro*Prx*BW];
        CNRshot = N[Pcarr/Nshot];
        CNRshotdB = 10*Log[10, CNRshot];
        CNRshotdBlist = Append [CNRshotdBlist,CNRshotdB];
```

```
        (* Determine carrier-to-RIN noise ratio *)
        Nrin = N[RIN*(Ro*Prx)^2*BW];
        CNRrin = N[Pcarr/Nrin];
        CNRrindB = 10*Log[10, CNRrin];
        CNRrindBlist = Append [CNRrindBlist,CNRrindB];

        (* Determine carrier-to-total noise ratio *)
        Ntotal = N[Nth+Nrin+Nshot];
        CNRtotal = N[Pcarr/Ntotal];
        CNRtotaldB = 10*Log[10, CNRtotal];
        CNRtotaldBlist = Append [CNRtotaldBlist,CNRtotaldB];

    ]

(* Write the four CNRlists to a file. Each line contains the CNRth, CNRshot, CNRrin, *)
(* and CNRtotal for a given received power with a tab between each entry. *)

{x} = Dimensions [ PrxdBmlist ];
outfile = OpenWrite["CNR_amvsbvsPrx-n"];
For [i=1, i<(x+1), i++,
        WriteString[ outfile, CNRthdBlist[[i]], "\t",
        CNRshotdBlist[[i]], "\t", CNRrindBlist[[i]], "\t",
        CNRtotaldBlist[[i]], "\n" ];
    ]
Close["CNR_amvsbvsPrx-n"];
```

A.2 BER vs. ASK Modulation Index for Gaussian Noise Environment (Mathematica)

```
(* This program calculates the bit error ratio of an M-ary ASK signal as a function of *)
(* ASK modulation index. The noise environment is Gaussian only. *)

(* Set input parameters *)

M = 8;                                  (* Number of signaling levels *)
q = 1.602*10^-19;                       (* Electronic charge in C *)
Ro = 0.94;                              (* Photodetector responsivity in A/W *)
BW = 7.0*10^6;                          (* Channel bandwidth in Hz *)
F = 6.5;                                (* Receiver amplifier noise figure in dB *)
G = 7;                                  (* Current gain of the transformer in dB *)
RINdB = -160;                           (* RIN noise parameter in dB/Hz *)
RIN = 10^(RINdB / 10);                  (* RIN noise *)
PrxdBm = -10.0;                         (* Received optical power in dBm *)

Pelist = {};
mASKlist = {};
SetDirectory [ "~/simulations/BER_MaryASK/gaussian" ];
```

```
(* This loop calculates the SNR for each value of the ASK modulation index and then *)
(* uses the calculated SNR to determine the bit error ratio. *)

For [mASK = 0.0005, mASK <= 0.010, mASK = mASK + 0.0005,

        Prx = N[10^(PrxdBm/10)*1*10^-3];

        (* Received signal power *)
        Psig = N[0.5*(mASK*Ro*Prx)^2];

        (* Thermal /amplifier noise *)
        Nth = N[(7.3*10^-12*10^((F-G)/20))^2*BW];

        (* Shot noise *)
        Nshot = N[2*q*Ro*Prx*BW];

        (* RIN noise *)
        Nrin = N[RIN*(Ro*Prx)^2*BW];

        (* Gaussian Signal-to-noise ratio *)
        SNRg = N[Psig / ( Nth + Nshot + Nrin)];

        (* BER of M-ary ASK with Gaussian noise *)
        Pe = N[((M-1)/(M*Log[2,M]))*Erfc[Sqrt[(3*SNRg)/(M^2 - 1)]]];

        Pelist = Append [Pelist,Pe];
        mASKlist = Append [mASKlist,mASK];

    ]

(* Write Pelist to a file with a new entry on each line. *)

{x} = Dimensions [Pelist];
outfile=OpenWrite["BERvsmASK_gaussian-n"];
For[i=1, i<(x+1), i++,
        WriteString[ outfile, Pelist[[i]], "\n" ];
    ]
Close["BERvsmASK_gaussian-n"];

(* Plot bit error ratio versus mASK. *)

newlist  = Transpose[{mASKlist, Log[10, Pelist]}];
ListPlot [newlist,  PlotJoined -> True];
```

A.3 BER vs. Received Optical Power for Gaussian Noise Environment (Mathematica)

```
(* This program calculates the bit error ratio of an M-ary ASK signal as a function of *)
(* received optical power. The noise environment is Gaussian only. *)
```

```
(* Set input parameters *)

M = 8;                                  (* Number of signaling levels *)
q = 1.602*10^-19;                       (* Electronic charge in C *)
Ro = 0.94;                              (* Photodetector responsivity in A/W *)
BW = 7.0*10^6;                          (* Channel bandwidth in Hz *)
F = 6.5;                                (* Receiver amplifier noise figure in dB *)
G = 7;                                  (* Current gain of the transformer in dB *)
RINdB = -160;                           (* RIN noise parameter in dB/Hz *)
RIN = 10^(RINdB / 10);                  (* RIN noise *)
mASK = 0.0048;                          (* ASK modulation index *)

Pelist = {};
PrxdBmlist = {};
SetDirectory [ "~/simulations/BER_MaryASK/gaussian" ];

(* This loop calculates the SNR for each value of received optical power and then uses *)
(* these values to calculate the bit error ratio. *)

For [PrxdBm = -20, PrxdBm <= -5, PrxdBm++,

        Prx = N[10^(PrxdBm/10)*1*10^-3];

        (* Received signal power *)
        Psig = N[0.5*(mASK*Ro*Prx)^2];

        (* Thermal /amplifier noise *)
        Nth = N[(7.3*10^-12*10^((F-G)/20))^2*BW];

        (* Shot noise *)
        Nshot = N[2*q*Ro*Prx*BW];

        (* RIN noise *)
        Nrin = N[RIN*(Ro*Prx)^2*BW];

        (* Gaussian Signal-to-noise ratio *)
        SNRg = N[Psig / ( Nth + Nshot + Nrin)];

        (* BER of M-ary ASK with Gaussian noise *)
        Pe = N[((M-1)/(M*Log[2,M]))*Erfc[Sqrt[(3*SNRg)/(M^2 - 1)]]];

        Pelist = Append [Pelist,Pe];
        PrxdBmlist = Append [PrxdBmlist,PrxdBm];

    ]

(* Write Pelist to a file with a new entry on each line. *)

{x} = Dimensions [Pelist];
outfile=OpenWrite["BERvsPrx_gaussian-n"];
For[i=1, i<(x+1), i++,
        WriteString[ outfile, Pelist[[i]], "\n" ];
```

```
    ]
Close["BERvsPrx_gaussian-n"];

(* Plot bit error ratio versus mASK *)

newlist  = Transpose[{PrxdBmlist, Log[10, Pelist]}];
ListPlot [newlist,  PlotJoined -> True];
```

A.4 BER vs. Gaussian SNR for a Noise Environment that includes both Gaussian and Impulsive Noise (Mathematica)

```
(* This program calculates the bit error ratio of an M-ary ASK signal in an environment *)
(* that  includes both Gaussian and non-Gaussian impulsive noise. Middleton's pdf is *)
(* used to characterize the noise. The independent variables are the impulsive index, A, *)
(* the gaussian SNR, SNRg, and the signal-to-nonlinear distortion, SNLD. M and *)
(* SNLD  are set, and the BER is computed as a function of average signal-to-noise *)
(* ratio. It is assumed that Gray encoding is used in determining the relationship *)
(* between  a bit error and a symbol error.  *)

(* Set input parameters *)

M = 8;                                  (* Number of signaling levels *)
A = 0.022;                              (* Impulsive index for mod. index of 6% *)
SNLDdB = 100;                           (* Signal-to-nonlinear distortion ratio in dB*)
PF = 3*(M-1)/(M+1);                     (* Peak power factor *)

SNRgdBlist = {};
Pelist ={};
SetDirectory [ "~/simulations/BER_MaryASK/middleton" ];

(* A loop is used to calculate BER as a function of Gaussian SNR. *)

For [SNRgdB = 0, SNRgdB <= 50, SNRgdB++,

        SNRg = 10^(SNRgdB / 10);
        SNLD = 10^(SNLDdB / 10);

        (* BER of M-ary ASK with Gaussian and impulsive noise *)

        SNR = (SNRg^-1 + SNLD^-1)^-1;

        Pe = N[((M-1)/(M*Log[2,M]))*Exp[-A]*Sum[((A^j)/j!)*
                Erfc[(Sqrt[(SNR*PF)])/((M-1)*Sqrt[((j/A) + (SNLD/SNRg))
                /(1 + (SNLD/SNRg))])], {j,0,20}]];

        Pelist = Append [Pelist,Pe];
        SNRgdBlist = Append [SNRgdBlist,SNRgdB];

    ]
```

```
(* Write Pelist to a file with a new entry on each line. *)

{x} = Dimensions [Pelist];
outfile=OpenWrite["VSB-BERvsSNRg-n"];
For[i=1, i<(x+1), i++,
        WriteString[ outfile, Pelist[[i]], "\n" ];
    ]
Close["VSB-BERvsSNRg-n"];

(* Plot bit error ratio versus SNRg *)

newlist  = Transpose[{SNRgdBlist, Log[10, Pelist]}];
ListPlot [newlist,  PlotJoined -> True];
```

A.5 BER vs. SNLD for a Noise Environment that includes both Gaussian and Impulsive Noise (Mathematica)

```
(* This program calculates the bit error ratio of an M-ary ASK signal in an environment *)
(* that includes both Gaussian and non-Gaussian impulsive noise. Middleton's pdf is *)
(* used to characterize the noise.  The independent variables are the impulsive index, A, *)
(* the gaussian SNR, SNRg, and the signal-to-nonlinear distortion, SNLD. M and *)
(* SNRg are set, and the BER is computed as a function of signal-to-nonlinear *)
(* distortion. Determination of the bit error ratio is based on the assumption that Gray *)
(*  encoding is used.  *)

(* Set input parameters *)

M = 8;                                  (* Number of signaling levels *)
A = 0.022;                              (* Impulsive index for mod. index of 6% *)
SNRgdB = 47;                            (* Signal-to-Gaussian noise ratio in dB*)
PF = 3*(M-1)/(M+1);                     (* Peak power factor *)

SNLDdBlist = {};
Pelist ={};
SetDirectory [ "~/simulations/BER_MaryASK/middleton" ];

(* A loop is used to calculate BER as a function of SNLD. *)

For [SNLDdB = 40, SNLDdB <= 50, SNLDdB++,

        SNRg = 10^(SNRgdB / 10);
        SNLD = 10^(SNLDdB / 10);

        (* BER of M-ary ASK with Gaussian and impulsive noise *)

        SNR = (SNRg^-1 + SNLD^-1)^-1;

        Pe = N[((M-1)/(M*Log[2,M]))*Exp[-A]*Sum[((A^j)/j!)*
                Erfc[(Sqrt[(SNR*PF)])/((M-1)*Sqrt[((j/A) + (SNLD/SNRg))
```

```
                /(1 + (SNLD/SNRg))])], {j,0,20}]];

        Pelist = Append [Pelist,Pe];
        SNLDdBlist = Append [SNLDdBlist,SNLDdB];

    ]

(* Write Pelist to a file with a new entry on each line. *)

{x} = Dimensions [Pelist];
outfile=OpenWrite["BERvsSNLD-n"];
For[i=1, i<(x+1), i++,
        WriteString[ outfile, Pelist[[i]], "\n" ];
    ]
Close["BERvsSNLD-n"];

(* Plot bit error ratio versus SNLD. *)

newlist  = Transpose[{SNLDdBlist, Log[10, Pelist]}];
ListPlot [newlist,  PlotJoined -> True];
```

A.6 BER vs. ASK Modulation Index for a Noise Environment that includes both Gaussian and Impulsive Noise (Mathematica)

```
(* This program calculates the bit error ratio of an M-ary ASK signal in an environment *)
(* that  includes both Gaussian and non-Gaussian impulsive noise. Middleton's pdf is *)
(* used to characterize the noise.  The BER is calculated as a function of the ASK *)
(* modulation index. Determination of the bit error ratio is based on the assumption that *)
(* Gray encoding is used.  *)

(* Set input parameters *)

M = 8;                                  (* Number of signaling levels *)
A = 0.022;                              (* Impulsive index for mod. index of 6% *)
PF = 3*(M-1)/(M+1);                     (* Peak power factor *)

q = 1.602*10^-19;                       (* Electronic charge in C *)
Ro = 0.94;                              (* Photodetector responsivity in A/W *)
BW = 7.0*10^6;                          (* Channel bandwidth in Hz *)
F = 6.5;                                (* Receiver amplifier noise figure in dB *)
G = 7;                                  (* Current gain of the transformer in dB *)
RINdB = -160;                           (* RIN noise parameter in dB/Hz *)
RIN = 10^(RINdB / 10);                  (* RIN noise *)
PrxdBm = -1.0;                          (* Received optical power in dBm *)

NLDpower = 3.8416*10^-14;       (* This is calculated from A.9 for A = 0.022, *)
                                (*  carrier freq. = 450 MHz, and Prx = -1 dBm *)

SNRglist = {};
```

```
SNLDlist = { };
Pelist = { };
mASKlist = { };
SetDirectory [ "~/simulations/BER_MaryASK/middleton" ];

(* This loop calculates the SNRg and SNLD for each value of ASK modulation index *)
(* and then uses these values to deterimine the corresponding bit error ratio. *)

For [mASK = 0.003, mASK <= 0.03, mASK = mASK + 0.001,

        Prx = N[10^(PrxdBm/10)*1*10^-3];

        (* Received signal power *)
        Psig = N[0.5*(mASK*Ro*Prx)^2];

        (* Thermal /amplifier noise *)
        Nth = N[(7.3*10^-12*10^((F-G)/20))^2*BW];

        (* Shot noise *)
        Nshot = N[2*q*Ro*Prx*BW];

        (* RIN noise *)
        Nrin = N[RIN*(Ro*Prx)^2*BW];

        (* Gaussian Signal-to-noise ratio *)
        SNRg = N[Psig / ( Nth + Nshot + Nrin)];

        (* Signal-to-nonlinear distortion ratio *)
        SNLD = N[ Psig / NLDpower ];

        (* BER of M-ary ASK with Gaussian and impulsive noise *)

        SNRave = N[(SNRg^-1 + SNLD^-1)^-1];

        Pe = N[((M-1)/(M*Log[2,M]))*Exp[-A]*Sum[((A^j)/j!)*
                Erfc[(Sqrt[(SNRave*PF)])/((M-1)*Sqrt[((j/A) + (SNLD/SNRg))
                /(1 + (SNLD/SNRg))])], {j,0,20}]];

        Pelist = Append [Pelist,Pe];
        SNRglist = Append [SNRglist,SNRg];
        SNLDlist = Append [SNLDlist,SNLD];
        mASKlist = Append [mASKlist,mASK];

    ]

(* Write Pelist to a file with a new entry on each line. *)

{x} = Dimensions [Pelist];
outfile=OpenWrite["BERvsmASK-n"];
For[i=1, i<(x+1), i++,
        WriteString[ outfile, Pelist[[i]], "\n" ];
    ]
```

```
Close["BERvsmASK-n"];

(* Plot bit error ratio versus mASK. *)

newlist  = Transpose[{mASKlist, Log[10, Pelist]}];
ListPlot [newlist,  PlotJoined -> True];
```

A.7 CSO count: Determination of Second Order Nonlinear Distortion Products for NTSC 42-Channel Frequency Plan (Mathematica)

```
(* This program counts all the second order distortion products that exists in a *)
(* subcarrier multiplexed CATV system. The frequency locations of each CSO product *)
(* and the number of products that exist at each frequency are both determined. *)


(* Input a list of all AM/VSB carrier frequencies in MHz. *)

ch = {55.25, 61.25, 67.25, 77.25, 83.25, 121.25, 127.25, 133.25, 139.25, 145.25,
151.25, 157.25, 163.25, 169.25, 175.25, 181.25, 187.25, 193.25, 199.25, 205.25,
211.25, 217.25, 223.25, 229.25, 235.25, 241.25, 247.25, 253.25, 259.25, 265.25,
271.25, 277.25, 283.25, 289.25, 295.25, 301.25, 307.25, 313.25, 319.25, 325.25,
331.25, 337.25};

(* Initialize arrays *)

ct1 = { };              (* List of all CSO products due to a summation of two carriers *)
ct2 = { };              (* List of CSO products due to the difference between 2 carriers *)
ct = { };               (* Combination of ct1 and ct2 *)
pcountlist = { };       (* List of no. of CSO products at each frequency in productlist *)
productlist = { };      (* List of all CSO frequencies *)
{n} = Dimensions[ch];
SetDirectory [ "~/simulations/NLD" ];


(* A nested FOR loop is used to determine the CSO distortion product frequencies.  *)

For [ j = 2, j <= n, j++,

        For [ i = j, i <= n, i++,

                r = Abs[ch[[j-1]] + ch[[i]]];
                s = Abs[ch[[j-1]] - ch[[i]]];

                ct1 = Append[ct1, r];
                ct2 = Append[ct2, s];

            ]
    ]
```

```
ct = Join[ct1,ct2];
productlist = Union[ct];
{v} = Dimensions[productlist];


(* This loop counts the number of products that exist at each of the distortion *)
(* frequencies given in productlist. *)

For [k = 1, k <= v, k++,

        pcount = Count[ct,productlist[[k]]];
        pcountlist = Append[pcountlist,pcount];

    ]

(* Plot the CSO products versus frequency. *)

newlist  = Transpose[{productlist,pcountlist}];
ListPlot [newlist,  PlotJoined -> True];
```

A.8 CTB count: Determination of Triple Beat Nonlinear Distortion Products for NTSC 42-Channel Frequency Plan (Mathematica)

```
(* This program counts all the triple beat distortion products that exists in a subcarrier *)
(* multiplexed CATV system. The frequency locations of each CTB product and the *)
(* number of products that exist at each frequency are both determined. *)


(* Input a list of all AM/VSB carrier frequencies in MHz. *)

ch = {55.25, 61.25, 67.25, 77.25, 83.25, 121.25, 127.25, 133.25, 139.25, 145.25,
151.25, 157.25, 163.25, 169.25, 175.25, 181.25, 187.25, 193.25, 199.25, 205.25,
211.25, 217.25, 223.25, 229.25, 235.25, 241.25, 247.25, 253.25, 259.25, 265.25,
271.25, 277.25, 283.25, 289.25, 295.25, 301.25, 307.25, 313.25, 319.25, 325.25,
331.25, 337.25};

(* Initialize arrays *)

ct1 = { };      (* CTB products resulting from [A + B + C] *)
ct2 = { };      (* CTB products resulting from [A - B + C] *)
ct3 = { };      (* CTB products resulting from [A + B - C] *)
ct4 = { };      (* CTB products resulting from [A - B - C] *)
ct = { };       (* Combination of ct1, ct2, ct3 and ct4 *)

pcountlist = { };       (* List of no. of CTB products at each frequency in productlist *)
productlist = { };      (* List of all CTB frequencies *)
{n} = Dimensions[ch];
SetDirectory [ "~/simulations/NLD" ];

(* A nested FOR loop is used to calculate the triple beat distortion product frequencies.*)
```

```
For [ k = 2, k < n, k++,

        For [ j = k, j < n, j++,

                For [ i = j+1, i <= n, i++,

                        a = Abs[ch[[k-1]] + ch[[j]] + ch[[i]]];
                        b = Abs[ch[[k-1]] - ch[[j]] + ch[[i]]];
                        c = Abs[ch[[k-1]] + ch[[j]] - ch[[i]]];
                        d = Abs[ch[[k-1]] - ch[[j]] - ch[[i]]];

                        ct1 = Append[ct1, a];
                        ct2 = Append[ct2, b];
                        ct3 = Append[ct3, c];
                        ct4 = Append[ct4, d];
                ]
        ]
    ]

ct = Join[ct1,ct2,ct3,ct4];
productlist = Union[ct];
{v} = Dimensions[productlist];

(* This loop counts the number of products that exist at each of the CTB distortion *)
(* frequencies given in productlist. *)

For [l = 1, l <= v, l++,

        pcount = Count[ct,productlist[[l]]];
        pcountlist = Append[pcountlist,pcount];

    ]

(* Plot the CTB products versus frequency. *)

newlist  = Transpose[{productlist,pcountlist}];
ListPlot [newlist,  PlotJoined -> True];
```

A.9 Nonlinear Distortion Power at each CSO and CTB Frequency [based on Ref. 42] for NTSC 42-Channel Frequency Plan (Mathematica)

```
(* This program calculates the CSO and CTB power (in dBc) of an SCM CATV system *)
(* as a function of the CATV frequency. It is based on Shi et. al.'s model [reference 42] *)
(* for finding n^th order NLD through a power series expansion of the laser output *)
(* autocorrelation function. *)


(* Set input parameters *)
```

```
NN = 42;                (* Number of AM/VSB channels *)
m = 0.06;               (* Optical modulation index per channel *)

(* Read in CSO and CTB product count information. *)

SetDirectory [ "~/simulations/NLD/productcounts" ];
CSOproductlist = ReadList ["CSOproductlist-42", Number];
CSOpcountlist = ReadList ["CSOpcountlist-42", Number];
CTBproductlist = ReadList ["CTBproductlist-42", Number];
CTBpcountlist = ReadList ["CTBpcountlist-42", Number];

{a} = Dimensions [CSOproductlist];
{b} = Dimensions [CTBproductlist];

(* Initialize arrays *)

CSOdBlist = { };        (* List of CSO power (in dBc) at each CSO frequency *)
CTBdBlist = { };        (* List of CTB power (in dBc) at each CTB frequency *)
SetDirectory [ "~/simulations/NLD" ];

L = N[(1 + Erf[1/(m*Sqrt[NN])]) / 2];          (* A constant derived from m and NN *)

(* A loop is used to calculate the CSO power (in dBc) at each CSO frequency. *)

 For [ fCSO = 1, fCSO <= a, fCSO++,

        CSO = N[(CSOpcountlist[[fCSO]] / (8*Pi*NN)) * Exp[-2/(m^2*NN)] * L];
        CSOdB = 10*Log[10, CSO];
        CSOdBlist = Append [CSOdBlist,CSOdB];

     ]

(* A loop is used to calculate the CTB power (in dBc) at each CTB frequency. *)

For [ fCTB = 1, fCTB <= b, fCTB++,

        CTB = N[(CTBpcountlist[[fCTB]] / (16*Pi*NN^3)) * m^-2 * Exp
                [-2/(m^2*NN)] * L];

        CTBdB = 10*Log[10, CTB];
        CTBdBlist = Append [CTBdBlist,CTBdB];

    ]

(* Write CSOdBlist to a file with a new entry on each line. *)

outfile=OpenWrite["CSOvsfreq-n"];
For[ i=1, i<(a+1), i++,
        WriteString[ outfile, CSOdBlist[[i]], "\n" ];
    ]
Close["CSOvsfreq-n"];
```

```
(* Write CTBdBlist to a file with a new entry on each line. *)

outfile=OpenWrite["CTBvsfreq-n"];
For[ j=1, j<(b+1), j++,
        WriteString[ outfile, CTBdBlist[[j]], "\n" ];
    ]
Close["CTBvsfreq-n"];
```

A.10 Nonlinear Distortion Power Within a Given Channel Bandwidth [based on Ref. 36] (Mathematica)

```
(* This program calculates nonlinear distortion power in a given bandwidth for a CATV *)
(* system with a large number of channels. It is based on Alameh and Minasian's NLD *)
(* model given in reference 36 and a simluation program written by Kinh Pham of *)
(* TRLabs  [ref.2] *)


(* Set input parameters *)

AMmodIndex = 0.060;          (* Modulation index per AM/VSB channel *)
NN=42;                       (* Number of AM/VSB channels *)
B=7.0*10^6;                  (* Bandwidth of channel under test in MHz *)
fo=199.25*10^6;              (* Frequency of the center channel in MHz *)
fp=450*10^6;                 (* Frequency of the channel under test in MHz *)
Po= -6;                      (* Received optical power in dBm *)
Resp= 0.94;                  (* Photodetector responsivity in A/W*)

(* Calculate the total RMS modulation index. *)

mu=N[Sqrt[(NN*AMmodIndex^2)/2]];

(* Calculation of sigma (variance of the multiplexed input current) *)

sigma:=mu*Resp*(10^(Po/10))*0.001;

(* Formula for G[k]  *)
(* G[k] is a parameter within hh[k] *)

G[k_]:=Sum[Binomial[k-2,j]*(I/((2^0.5)*mu))^j*Integrate
                [Exp[-u^2]*u^(k-j),{u,-10,10}],{j,0,k}];

(* Formula for hh[k] *)
(* hh[k] is a parameter used to determine the NLD autocorrelation *)

hh[k_]:=((1/(2*Pi))*(I^((k-2)))*((2^0.5/sigma)^(k-1))*
                (Exp[-1/(2*mu^2)])*G[k])^2*1/k!*(sigma^(2*k));


(* Formula for Shape[y,k] *)
```

```
(* Shape[y,k] is a parameter used to determine the NLD autocorrelation. *)

Shape[y_,k_]:= (((Sin[Pi*y])/(Pi*y))^k)*(Cos[(2*fo*y)/(NN*B)]^k)*
                                    Cos[(2*fp*y)/(NN*B)];

(* The power spectral density is determined by taking the Fourier Transform of the *)
(* autocorrelation function. Sum the infinite series from k=2 to k=100. Note that 'temp' *)
(* is the incremental addition to the power spectral density and 'total' is the cumulative *)
(* power spectral density *)

store={};
total=0;

For[ x=2,x<100,x=x+1,
        temp=hh[x]*(NIntegrate[Shape[t,x],{t,0,5}])*2/Pi/NN/B;
        total=total+N[temp];
        Print["x: ",x, "  temp: ",N[temp],"    total: ",total];
        store=Append[store,temp];
   ];

(* Calculate NLD power within the channel under test. *)

NLDpower = total*(2B);
```

A.11 Multilevel Transmission System Simulation (MATLAB)

```
% Program description: This program simulates a multilevel ASK signal that is baseband
% filtered in the transmitter, mixed to an RF frequency, mixed back to baseband, baseband
% filtered in the receiver, and then decoded back to a binary sequence. Note: Gaussian
% noise is added to the signal at the input to the receiver baseband filter.
%
% Date created: Nov.8/95
%

% ------  Program inputs  ------

clear
% 'num_levels' is the number of signal levels (power of 2) to be transmitted.
num_levels = 8;

% 'bit_rate' is the bit rate (in MHz) of the pseudorandom input binary data stream.
bit_rate = 32.25e6;

% 'min_value' is the D/A output in the encoder for all zeros.
min_value = -2.048;

% 'max_value' is the D/A output in the encoder for all ones.
max_value = 2.048;

% 'pilot_tone' denotes the increase in the D/A output due to addition of a digital pilot tone.
```

```
pilot_tone = 0.5;


% ------ Obtain all inputs from the user ------

num_symbs = input(' Length of pseudorandom bit stream: ');
f_sampling = input(' Number of samples to be taken for each symbol: ');
f_cutoff = input(' 3-dB cutoff freq of the tx baseband Butterworth filter (Hz): ');
order = input(' Order of the tx baseband Butterworth filter: ');
orderrx = input(' Order of the rx baseband Butterworth filter: ');
f_cutoffrx = input(' 3-dB cutoff freq of the rx baseband Butterworth filter (Hz): ');
f_RF = input(' RF frequency in Hertz (less than one-fifth of sampling rate): ');
phase_deg = input(' Phase error between the first L.O. and the second L.O. (degrees): ');
SNRdb = input(' Average signal-to-noise ratio at input to the rx baseband filter (dB): ');

% ------ Generate a pseudorandom bit stream ------

% Create a pseudorandom bit stream using a maximal-length shift register technique as
% given on pages 396-399 of Proakis (ref. 44). A function called 'PN_seq' creates a
% pseudorandom sequence with a length equal to 'num_symbs', where 'num_symbs' is
% required input for this function. Note that this function was created by Sheldon Walklin
% of TRLabs and is described in the FOCSS programmer's guide.

bin_PN_input = PN_seq(num_symbs);


% ------ Convert binary stream to a multilevel signal ------

% After determining how many levels are required (2^m levels), every m bits of input are
% converted to a decimal equivalent. The multilevel signal is then scaled so as to give the
% appropriate output of the D/A. A time record is then created with a sampling rate that is
% atleast ten times the symbol rate. The FFT and PSD of the multilevel signal are obtained
% and the PSD can be plotted.

a = 0;
% 'm' is the number of bits/symbol
m = log10(num_levels)/log10(2);

multi_PN_inputa=zeros(1,floor(length(bin_PN_input)/m));

for i = 1:floor(length(bin_PN_input)/m)

        for j = 1:m

                y = m*(i-1) + j;
                A = bin_PN_input(y) * pow2(m-j);
                multi_PN_inputa(i) = multi_PN_inputa(i) + A;
        end
end

% Scale the multilevel signal so that a linear swing across the output of the D/A converter is
% acheived. Note that 'multi_PN_input' is the multilevel pseudorandom input data stream.
```

```
weight_factor = (max_value - min_value)/(pow2(m)-1);

multi_PN_input = multi_PN_inputa * weight_factor;

if min_value < 0
        multi_PN_input = multi_PN_input - abs(min_value);
end


% ------ Create a time record of the multilevel input signal ------

for k = 1:length(multi_PN_input)

        for ll = 1:f_sampling

                r = (k-1)*f_sampling + ll;
                multi_PN_input_tr(r) = multi_PN_input(k);
        end
end

% Compute  the FFT and plot the PSD of the multilevel signal. Note that the sampling rate
% is equal to the symbol rate multiplied by 'f_sampling'. Since the number of elements in
% 'multi_PN_input_tr' is denoted as N, the period of the complete time record is N
% multiplied by the sampling period. The power spectral density of the multilevel signal is
% equal to the magnitude squared of the FFT of 'multi_PN_input_tr' divided by 'tr_per'.
% The frequency points that correspond to each value of the computed PSD are linearly
% spaced between freq=0 and freq=samp_rate - samp_int.


symb_rate = bit_rate / m;                % Compute the symbol rate
symb_per = 1 / symb_rate;                % Compute the symbol period
N = length(multi_PN_input_tr);           % Number of elements in time record
samp_per = symb_per / f_sampling;        % Compute sampling period
samp_rate = 1 / samp_per;                % Compute sampling rate
tr_per = N * samp_per;                   % Length of total time record
samp_int = 1 / tr_per;                   % Compute the sampling interval
freq = [0:N-1]/tr_per;                   % Frequency points for PSD

F_multi = fft(multi_PN_input_tr)/N;
PSD_multi = ((abs(F_multi)).^2);

figure(1);
subplot(2,2,1), plot(freq,10*log10(PSD_multi),'-');
axis([-freq(N/50) freq(N/5) -80 0]);
title ('PSD of multilevel baseband signal');


% ------ Pass the multilevel signal through a transmitter baseband filter ------

[a,b] = butter(order, (f_cutoff/(samp_rate/2)) );

Tx_LPF_tr = filter(a,b,multi_PN_input_tr);
```

```
F_Tx_LPF = fft(Tx_LPF_tr) / N;
PSD_Tx_LPF = (abs(F_Tx_LPF)).^2;

% Plot the PSD after baseband filtering
subplot(2,2,2), plot(freq,10*log10(PSD_Tx_LPF),'-');
axis([-freq(N/50) freq(N/5) -80 0]);
title ('PSD of multilevel baseband signal after tx baseband filtering');


% ------ Multiply the baseband signal by an RF carrier ------

t = [0:samp_per:(tr_per - samp_per)];
multi_PN_RF_tr = Tx_LPF_tr .* cos(2*pi*f_RF*t);
F_multi_PN_RF = fft(multi_PN_RF_tr)/N;
PSD_multi_PN_RF = ((abs(F_multi_PN_RF)).^2);

% Plot the PSD at RF
subplot(2,2,3), plot(freq,10*log10(PSD_multi_PN_RF) ,'-');
axis([(f_RF - 4*symb_rate) (f_RF + 4*symb_rate) -80 0]);
title ('PSD of multilevel signal at RF');


% ------ Mix the received signal down to baseband ------

% Multiply the RF signal by a sine term at RF with a slight phase offset from the local
% oscillator signal used for upconversion

phase_rad = (phase_deg*2*pi)/360;
multi_PN_rx_tr = multi_PN_RF_tr .* cos((2*pi*f_RF*t) + phase_rad);
F_multi_PN_rx = fft(multi_PN_rx_tr) / N;
PSD_multi_PN_rx = (abs(F_multi_PN_rx)).^2;


% ------ Add noise to the received signal ------

% Procedure: Find the average value of the amplitude for the highest level of the multilevel
% signal. This is the 'peak signal envelope', PSE, and can be used to find the average
% signal power. For a given average SNR, the noise power that is required can be
% determined from knowing the average signal power. A Gaussian random variable with a
% mean of 0 and a variance of 1 is used to simulate noise. Therefore, multiply this vector
% by the required average noise power and then add the new vector to the multilevel signal
% time record.

% First determine the 'peak signal envelope'

sps = f_sampling;
YY = floor(N/(sps*20));
PSE = zeros(1,YY);

for kk = 1:YY

        PSE(kk) = max(multi_PN_rx_tr(((kk-1)*sps*20 + 1) : (kk*sps*20)));
```

```
end

PSEave = mean(PSE);

% Determine the 'peak power factor', PF, and the average signal power, Pave

PF = 3*(num_levels-1) / (num_levels+1);
Pave = (PSEave^2)/PF;

% From the given SNR specification, determine the average noise power or noise variance

SNRave = 10^(SNRdb / 10);
noise_power = Pave / SNRave;

% Create a zero-mean Gaussian random variable with a variance equal to 'noise_power'.
% Since the randn function is a zero-mean with a variance of 1, in order for the variance to
% be equal to noise_power, we need to multiply each element of the random variable by the
% square root of noise_power. Finally, add the 'noise' vector to the multilevel received
% signal on an element-by-element basis.

noise = sqrt(noise_power)*randn(1,N);
multi_PN_rx_noise_tr = noise + multi_PN_rx_tr;


% ------ Pass the multilevel signal (w/noise) through a receiver baseband filter ------

[aa,bb] = butter(orderrx, (f_cutoffrx/(samp_rate/2)) );

Rx_LPF_tr = filter(aa,bb,multi_PN_rx_noise_tr);
F_Rx_LPF = fft(Rx_LPF_tr) / N;
PSD_Rx_LPF = (abs(F_Rx_LPF)).^2;

% Plot the PSD of the multilevel signal after baseband filtering
subplot(2,2,4), plot(freq,10*log10(PSD_Rx_LPF),'-');
axis([-freq(N/50) freq(N/5) -80 0]);
title ('PSD of multilevel baseband signal (w/noise) after rx baseband filtering');


% ------ Recover the received multilevel signal from the sampled time record ----

for jj = 1:(num_symbs/m)

        multi_PN_filtout(jj) = Rx_LPF_tr((sps/2) + (jj-1)*sps);
end


% ------ Obtain the multilevel eye diagrams for the transmitted and received signals ----
% Plot eye diagram showing three multilevel eyes

input = Tx_LPF_tr(3*f_sampling:(N - 3*f_sampling));
NN = length(input);
output_w_noise = Rx_LPF_tr(3*f_sampling:(N - 3*f_sampling));
```

```
eyes = 3;
time = [0:samp_per:((eyes*f_sampling*samp_per)-samp_per)];

figure(2);
for runs = 1:floor(NN/(f_sampling*eyes))

        subplot(3,1,1),plot(time,input(((runs-1)*f_sampling*eyes +1) :
        (runs*f_sampling*eyes)));
        hold on;

end
title('Multilevel eye diagram for the transmitted signal after baseband filtering');
hold off;

for runs = 1:floor(NN/(f_sampling*eyes))

        subplot(3,1,3), plot(time,output_w_noise(((runs-1)*f_sampling*eyes +1) :
        (runs*f_sampling*eyes)));
        hold on;
end
title('Multilevel eye diagram (w/ noise) for the received signal after baseband filtering');
hold off;
```

Appendix B: Encoder / Decoder Circuit Diagrams

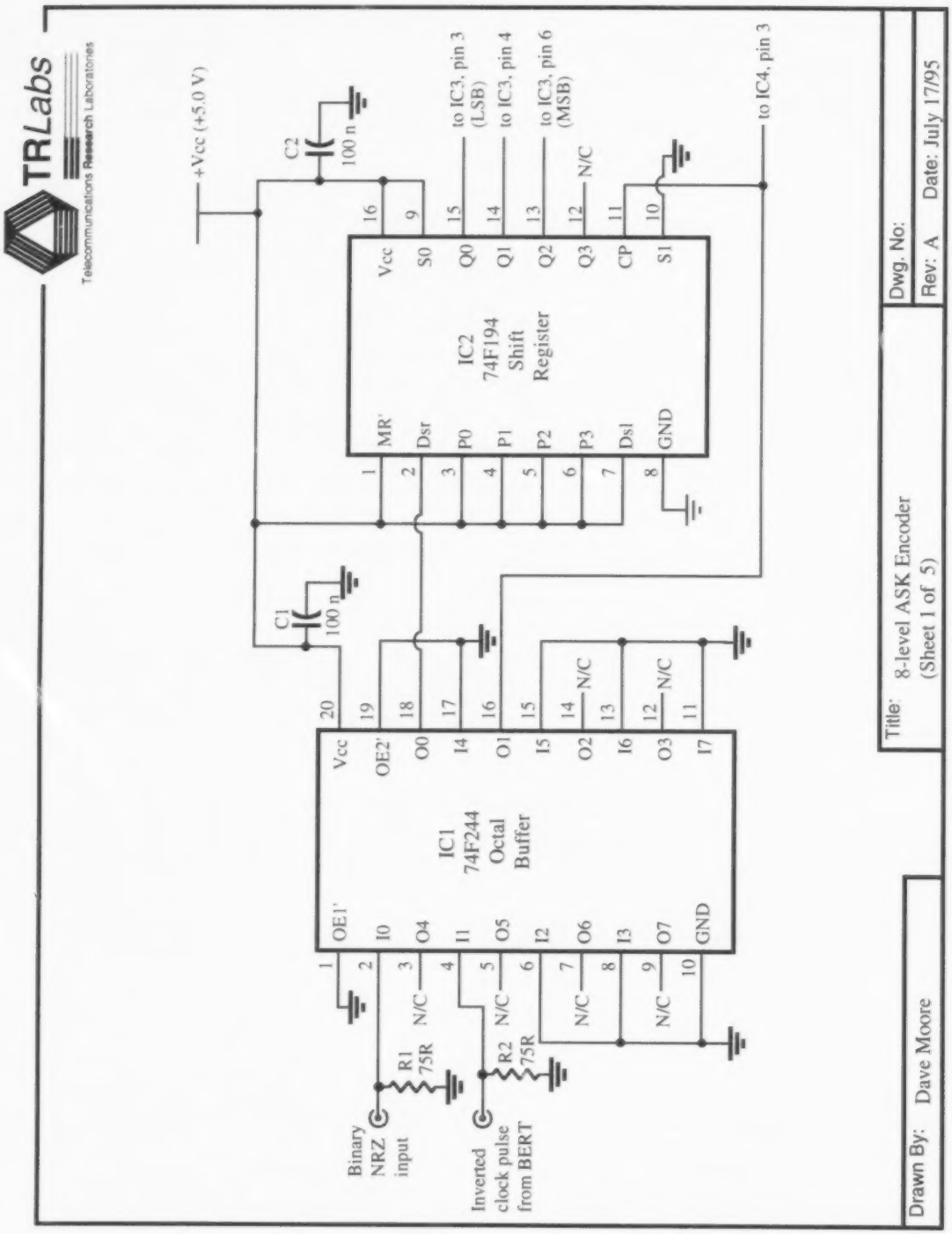

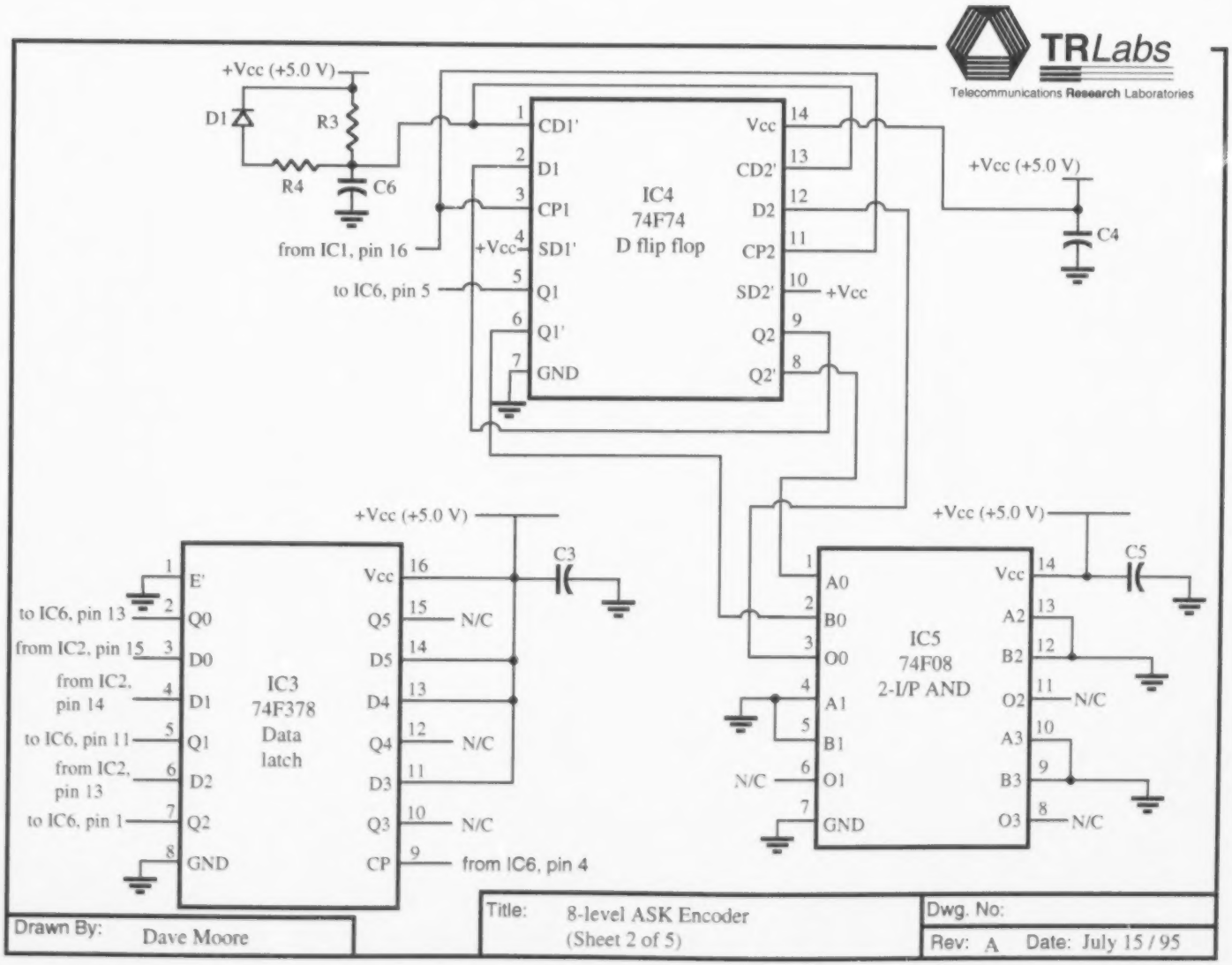
TRLabs
Telecommunications Research Laboratories
+Vcc (+5.0 V)
D1
R3
R4
C6
from IC1, pin 16
to IC6, pin 5
IC4
74F74
D flip flop
CD1'
D1
CP1
+Vcc
SD1'
Q1
Q1'
GND
Vcc
CD2'
D2
CP2
SD2'
Q2
Q2'
+Vcc
C4
IC3
74F378
Data
latch
E'
Q0
D0
D1
Q1
D2
Q2
GND
Vcc
Q5
D5
D4
Q4
D3
Q3
CP
N/C
from IC6, pin 4
to IC6, pin 13
from IC2, pin 15
from IC2, pin 14
to IC6, pin 11
from IC2, pin 13
to IC6, pin 1
C3
IC5
74F08
2-I/P AND
A0
B0
O0
A1
B1
O1
GND
Vcc
A2
B2
O2
A3
B3
O3
N/C
C5
Drawn By: Dave Moore
Title: 8-level ASK Encoder
(Sheet 2 of 5)
Dwg. No:
Rev: A Date: July 15 / 95

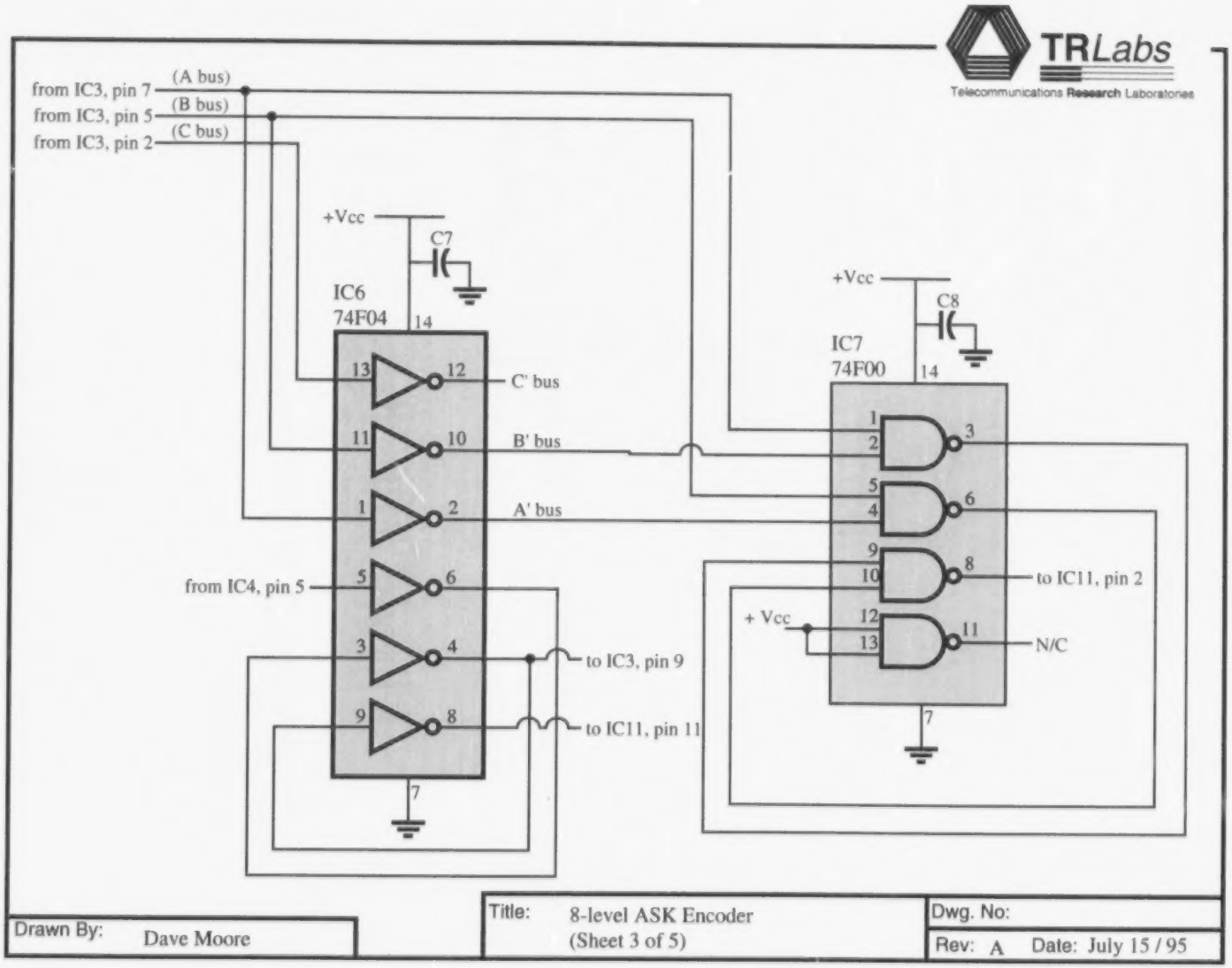
TRLabs
Telecommunications Research Laboratories
from IC3, pin 7
(A bus)
from IC3, pin 5
(B bus)
from IC3, pin 2
(C bus)
+Vcc
C7
IC6
74F04
14
13
12
C' bus
11
10
B' bus
1
2
A' bus
from IC4, pin 5
5
6
3
4
to IC3, pin 9
9
8
to IC11, pin 11
7
+Vcc
C8
IC7
74F00
14
1
2
3
5
4
6
9
10
8
to IC11, pin 2
+ Vcc
12
13
11
N/C
7
Drawn By:
Dave Moore
Title:
8-level ASK Encoder
(Sheet 3 of 5)
Dwg. No:
Rev: A
Date: July 15 / 95

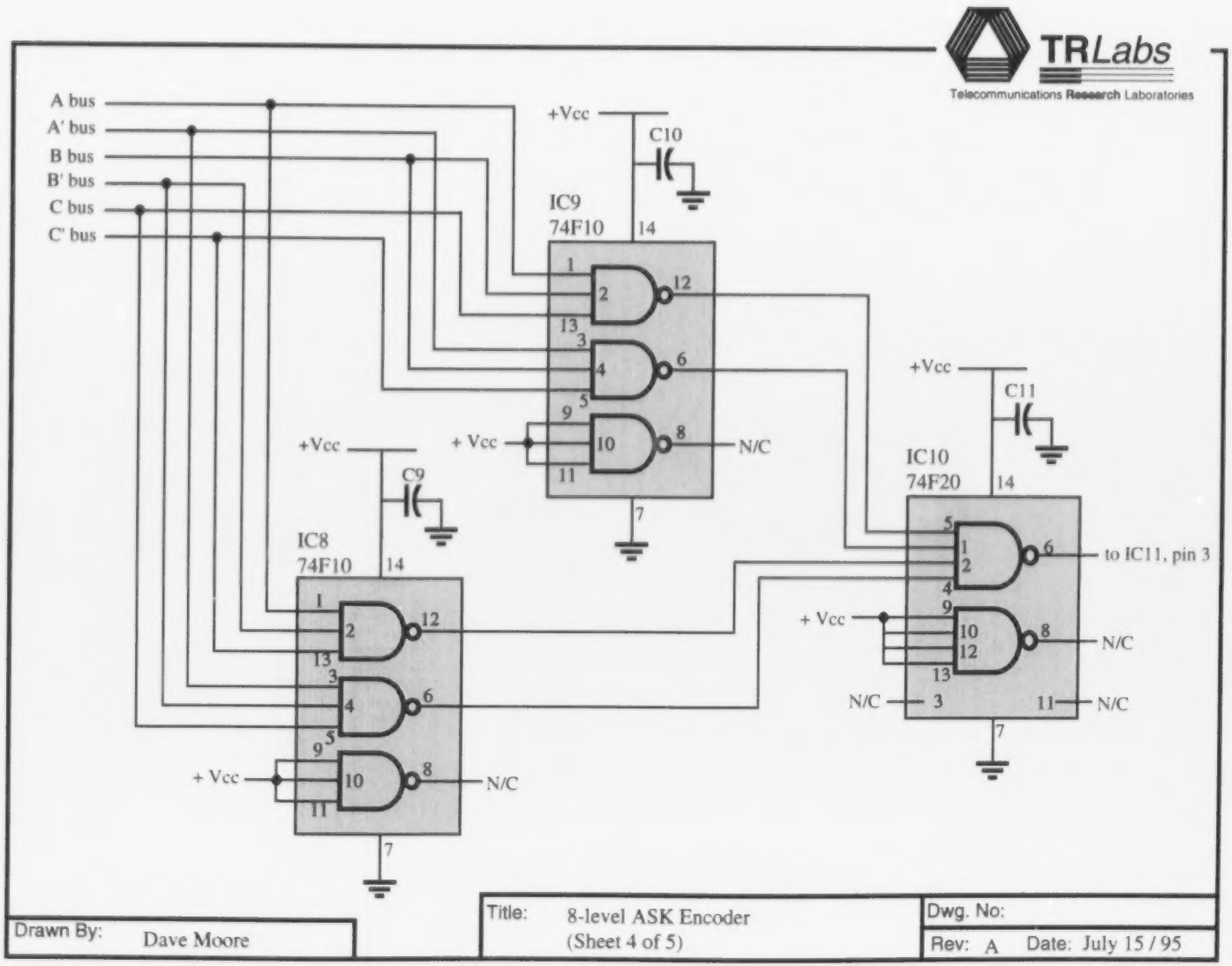
TRLabs
Telecommunications Research Laboratories
A bus
A' bus
B bus
B' bus
C bus
C' bus
+Vcc
C10
IC9
74F10
14
1
2
12
13
3
4
6
9
5
10
8
N/C
11
7
+ Vcc
+Vcc
C9
IC8
74F10
14
1
2
12
13
3
4
6
9
5
10
8
N/C
11
7
+ Vcc
+Vcc
C11
IC10
74F20
14
5
1
2
6
to IC11, pin 3
4
9
10
12
8
N/C
13
+ Vcc
N/C
3
11
N/C
7
Drawn By:
Dave Moore
Title:
8-level ASK Encoder
(Sheet 4 of 5)
Dwg. No:
Rev: A
Date: July 15 / 95

TRLabs
Telecommunications Research Laboratories

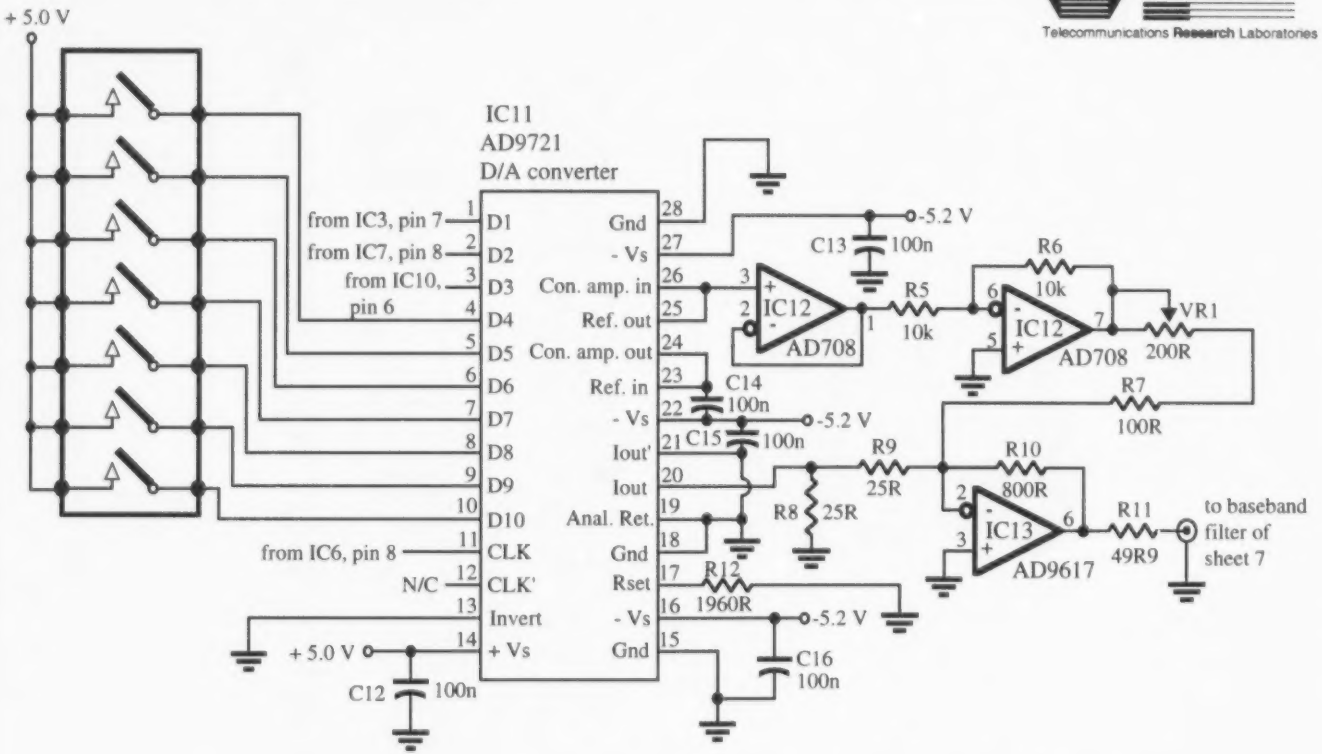

Note: For IC12, supply +5 V to pin 8 and -5 V to pin 4
For IC13, supply + 5 V to pins 7 and 8 and - 5 V to pins 4 and 5
Decouple IC13 with 100 nF and 3.3 uF tantalum (see data sheets)

Drawn By: Dave Moore	Title: 8-level ASK Encoder (Sheet 5 of 5)	Dwg. No:
		Rev: A Date: July 15 / 95

TRLabs
Telecommunications Research Laboratories

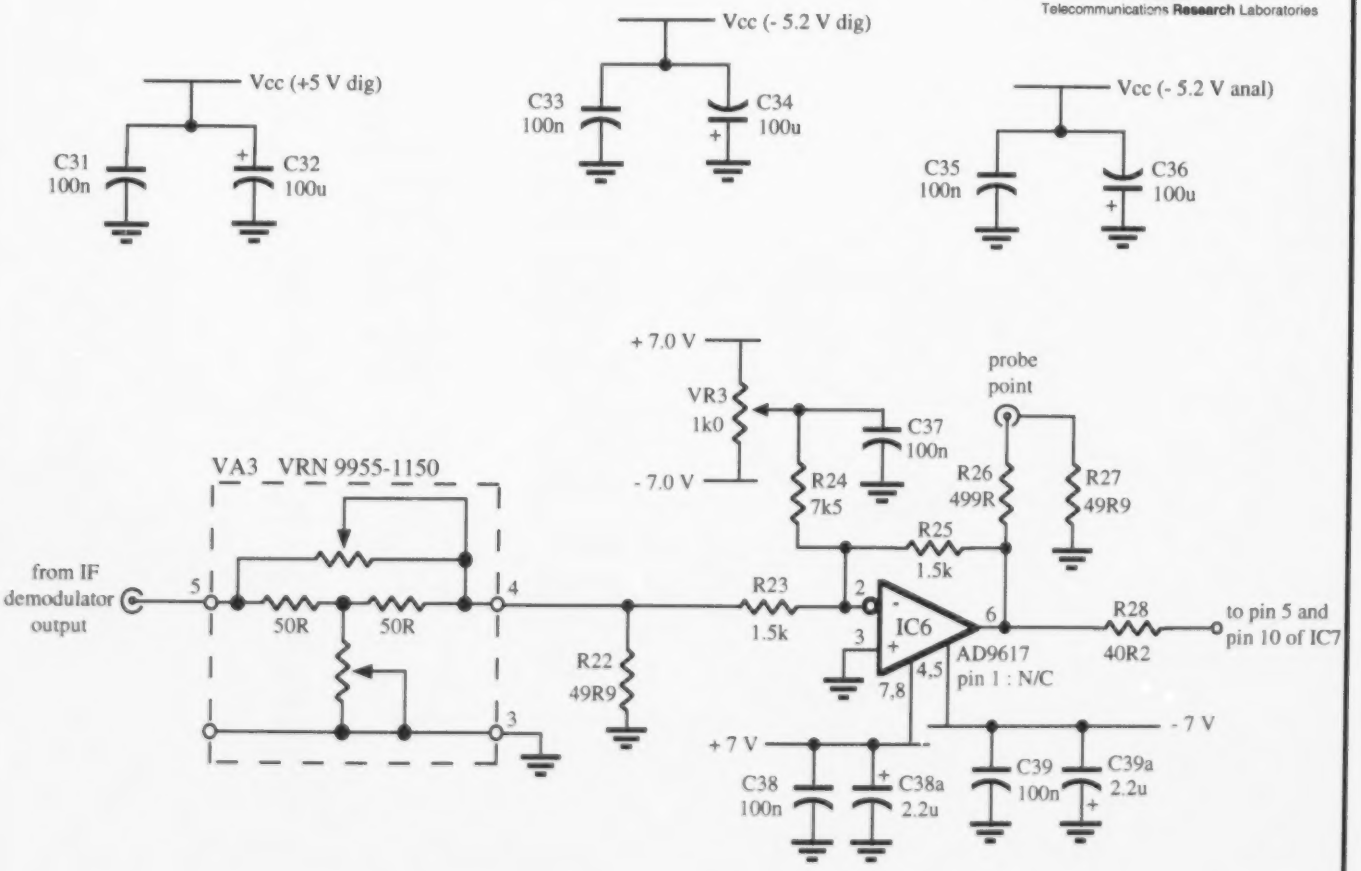

Drawn By: Dave Moore	Title: 8-level ASK Decoder (Sheet 1 of 6)	Dwg. No:	
		Rev: A	Date: Oct.4 / 95

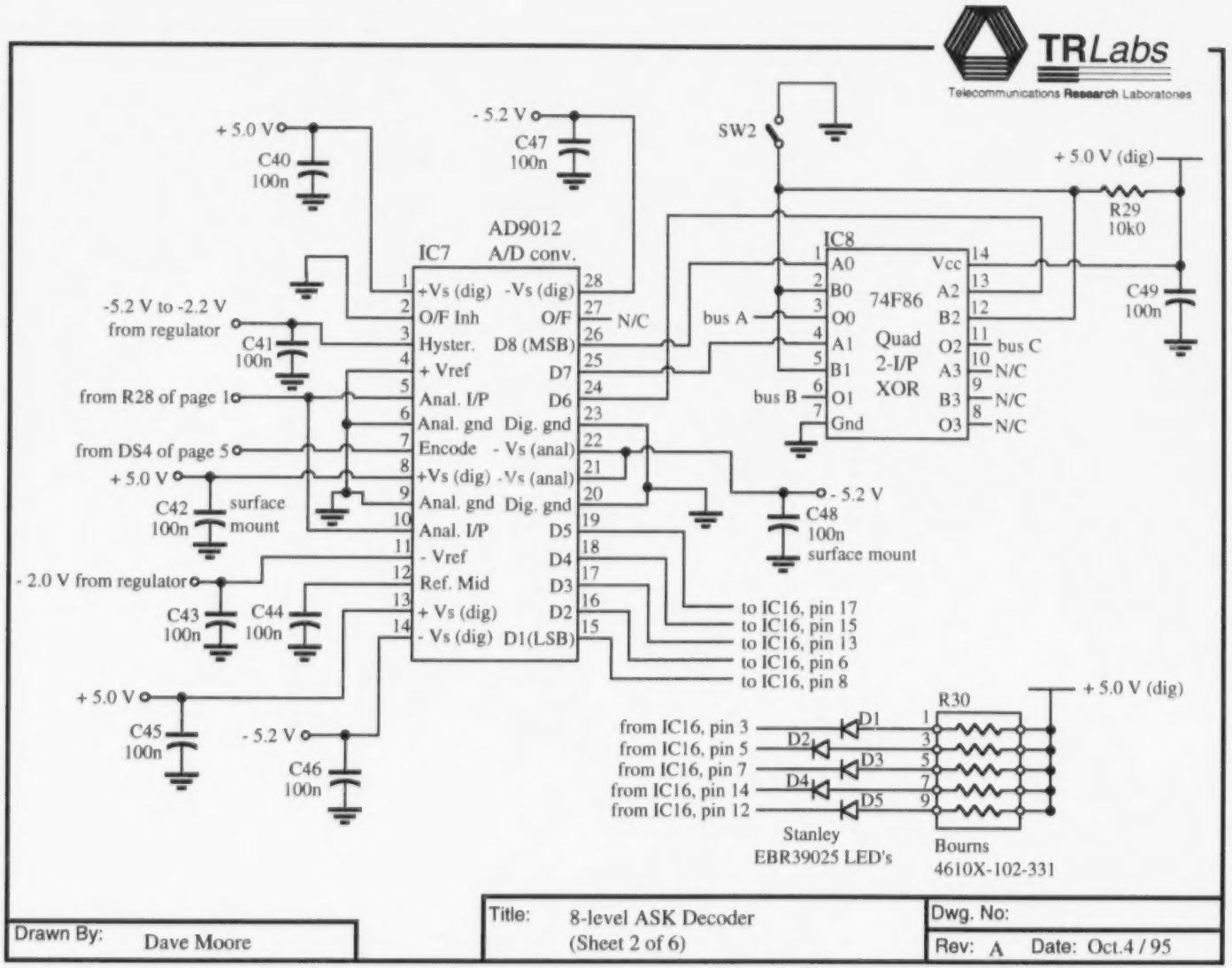
TRLabs
Telecommunications Research Laboratories
+ 5.0 V
C40
100n
- 5.2 V
C47
100n
SW2
+ 5.0 V (dig)
R29
10k0
AD9012
IC7 A/D conv.
IC8
74F86
Quad
2-I/P
XOR
-5.2 V to -2.2 V
from regulator
C41
100n
from R28 of page 1
from DS4 of page 5
+ 5.0 V
C42
100n
surface
mount
- 2.0 V from regulator
C43
100n
C44
100n
+ 5.0 V
C45
100n
- 5.2 V
C46
100n
bus A
bus B
bus C
N/C
C49
100n
C48
100n
surface mount
- 5.2 V
to IC16, pin 17
to IC16, pin 15
to IC16, pin 13
to IC16, pin 6
to IC16, pin 8
from IC16, pin 3
from IC16, pin 5
from IC16, pin 7
from IC16, pin 14
from IC16, pin 12
D1
D2
D3
D4
D5
R30
+ 5.0 V (dig)
Stanley
EBR39025 LED's
Bourns
4610X-102-331
Drawn By: Dave Moore
Title: 8-level ASK Decoder
(Sheet 2 of 6)
Dwg. No:
Rev: A Date: Oct.4 / 95

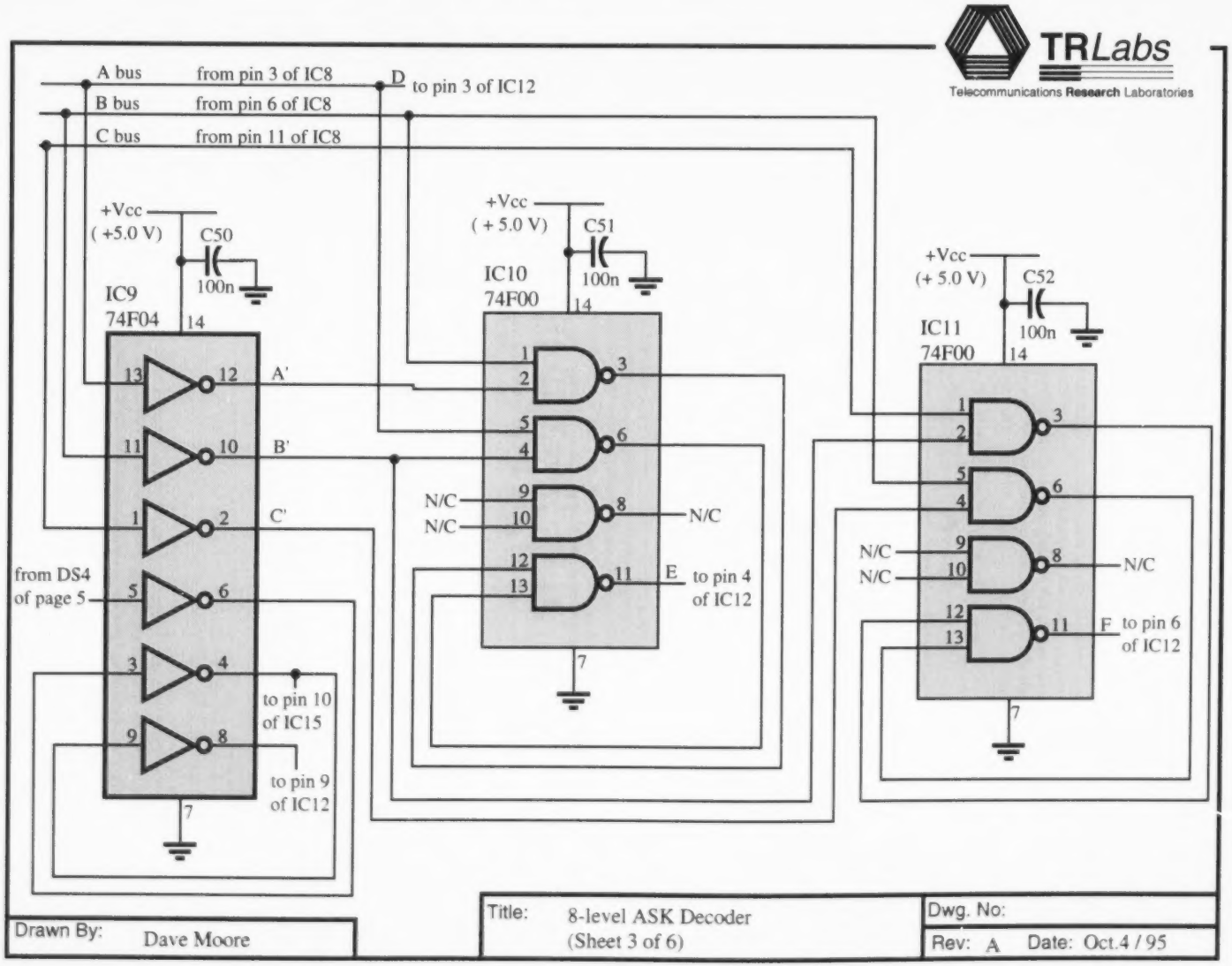
TRLabs
Telecommunications Research Laboratories
A bus from pin 3 of IC8
B bus from pin 6 of IC8
C bus from pin 11 of IC8
D to pin 3 of IC12
+Vcc (+5.0 V)
C50
100n
IC9
74F04
14
13
12
A'
11
10
B'
1
2
C'
from DS4 of page 5
5
6
3
4
to pin 10 of IC15
9
8
to pin 9 of IC12
7
+Vcc (+ 5.0 V)
C51
100n
IC10
74F00
14
1
2
3
5
4
6
N/C
9
N/C
10
8
N/C
12
13
11
E
to pin 4 of IC12
7
+Vcc (+ 5.0 V)
C52
100n
IC11
74F00
14
1
2
3
5
4
6
N/C
9
N/C
10
8
N/C
12
13
11
F
to pin 6 of IC12
7
Drawn By: Dave Moore
Title: 8-level ASK Decoder (Sheet 3 of 6)
Dwg. No:
Rev: A Date: Oct.4 / 95

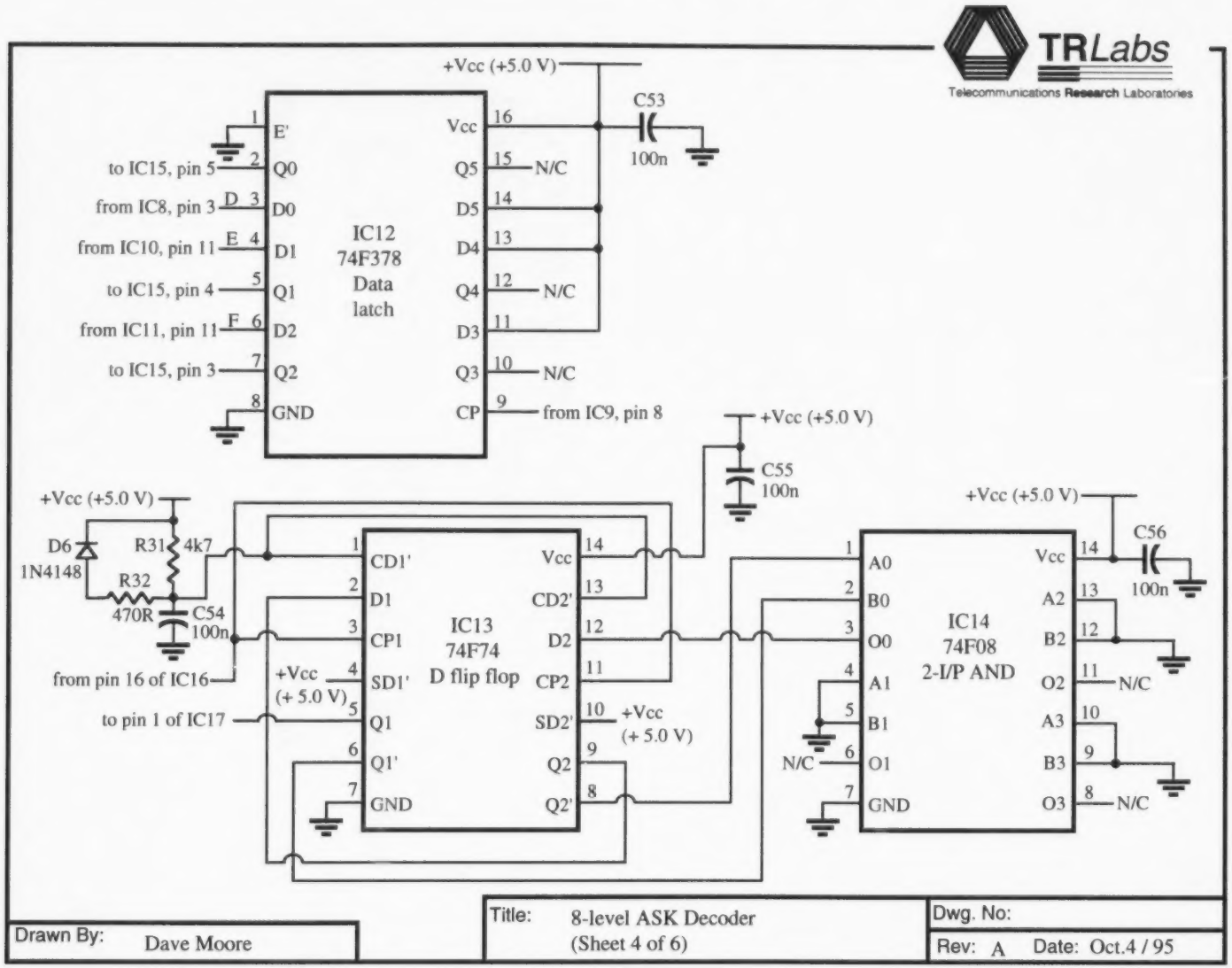
TRLabs
Telecommunications Research Laboratories
+Vcc (+5.0 V)
C53
100n
IC12
74F378
Data
latch
E'
Q0
D0
D1
Q1
D2
Q2
GND
Vcc
Q5
D5
D4
Q4
D3
Q3
CP
to IC15, pin 5
from IC8, pin 3
from IC10, pin 11
to IC15, pin 4
from IC11, pin 11
to IC15, pin 3
N/C
from IC9, pin 8
+Vcc (+5.0 V)
C55
100n
D6
1N4148
R31
4k7
R32
470R
C54
100n
from pin 16 of IC16
to pin 1 of IC17
+Vcc
(+ 5.0 V)
IC13
74F74
D flip flop
CD1'
D1
CP1
SD1'
Q1
Q1'
GND
Vcc
CD2'
D2
CP2
SD2'
Q2
Q2'
IC14
74F08
2-I/P AND
A0
B0
O0
A1
B1
O1
GND
Vcc
A2
B2
O2
A3
B3
O3
C56
100n
N/C
Drawn By: Dave Moore
Title: 8-level ASK Decoder
(Sheet 4 of 6)
Dwg. No:
Rev: A Date: Oct.4 / 95

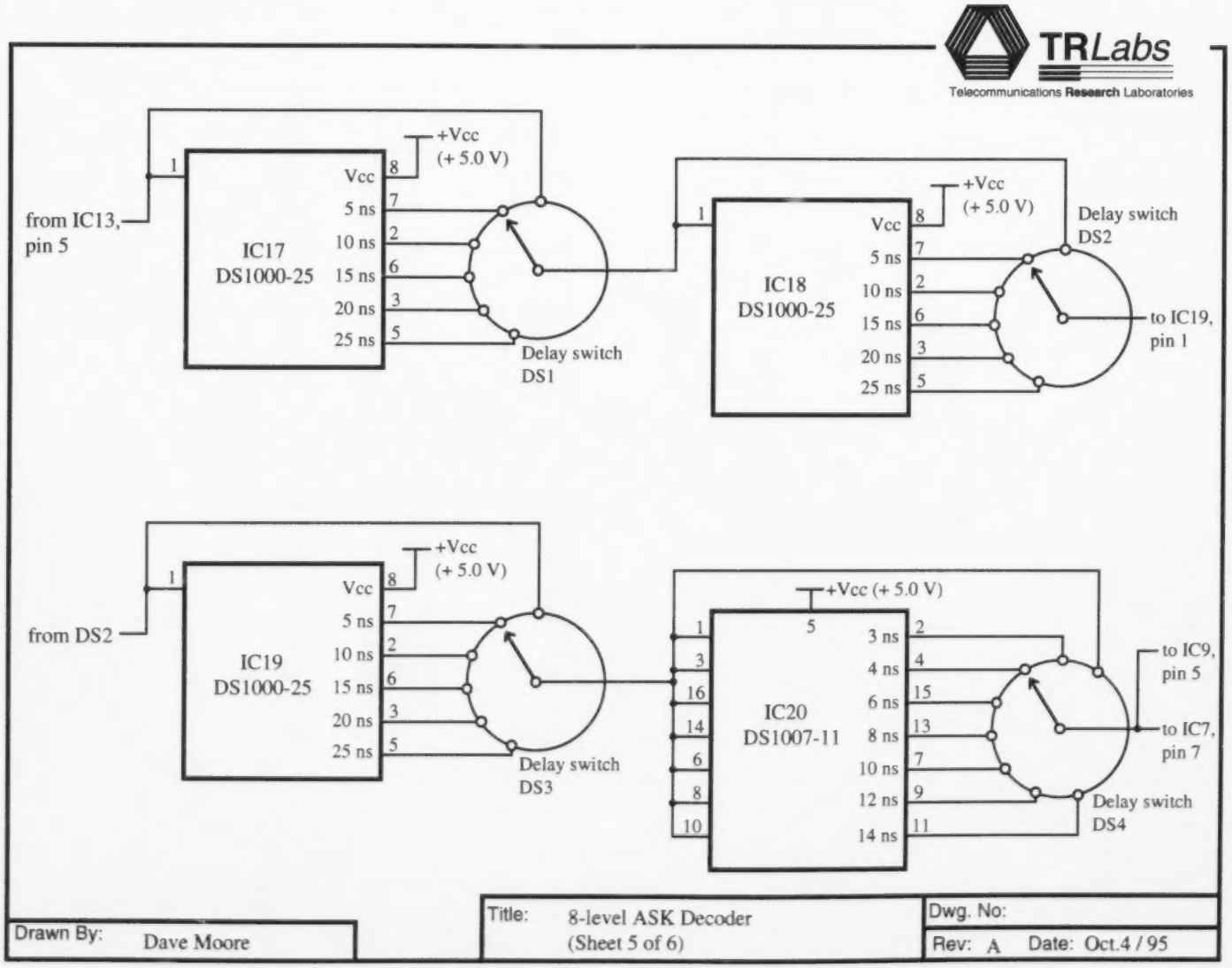
TRLabs
Telecommunications Research Laboratories
from IC13, pin 5
IC17 DS1000-25
+Vcc (+ 5.0 V)
Vcc
5 ns
10 ns
15 ns
20 ns
25 ns
Delay switch DS1
IC18 DS1000-25
Delay switch DS2
to IC19, pin 1
from DS2
IC19 DS1000-25
Delay switch DS3
IC20 DS1007-11
3 ns
4 ns
6 ns
8 ns
10 ns
12 ns
14 ns
to IC9, pin 5
to IC7, pin 7
Delay switch DS4
Drawn By: Dave Moore
Title: 8-level ASK Decoder (Sheet 5 of 6)
Dwg. No:
Rev: A Date: Oct.4 / 95

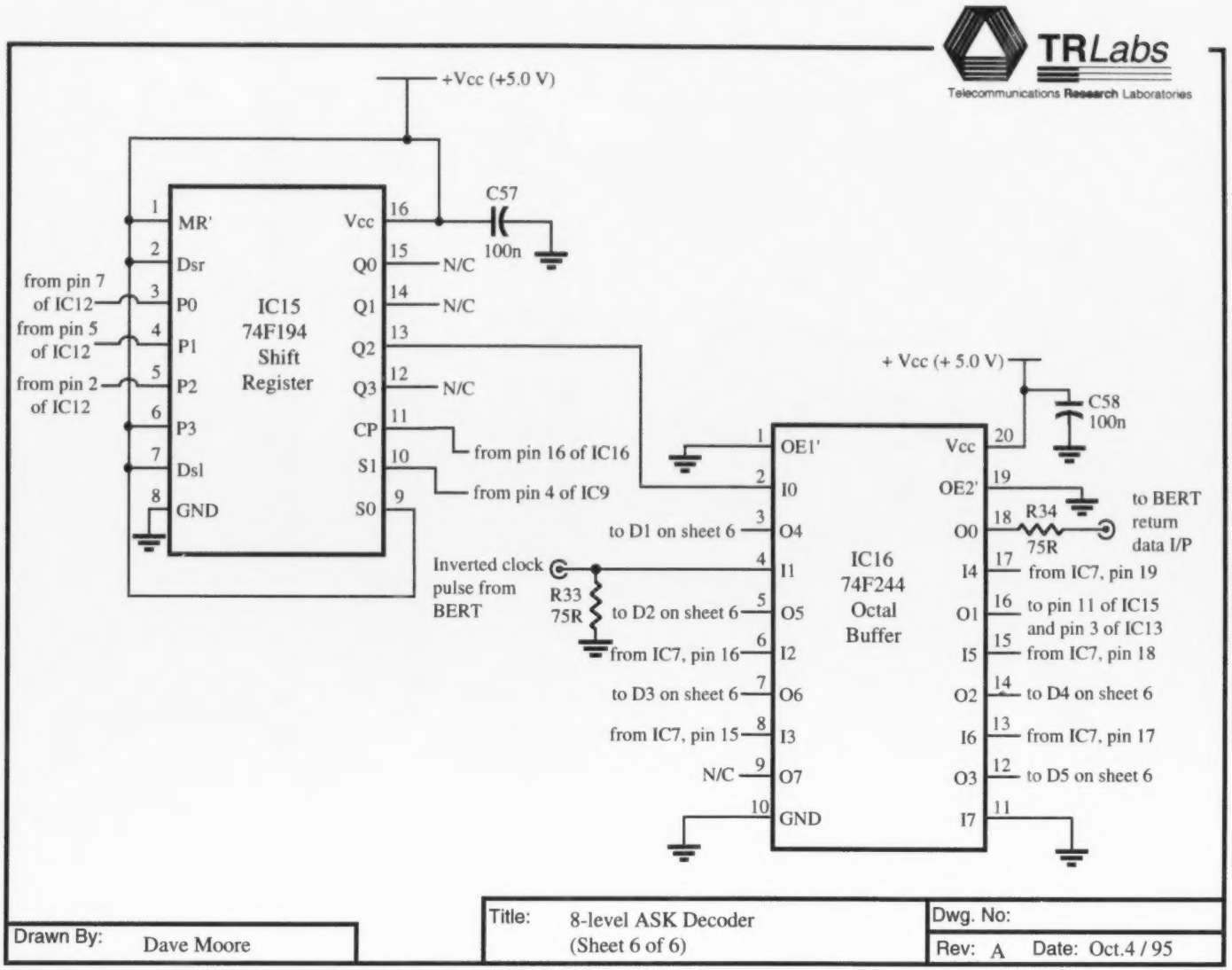
TRLabs
Telecommunications Research Laboratories
+Vcc (+5.0 V)
C57
100n
IC15
74F194
Shift
Register
MR'
Dsr
P0
P1
P2
P3
Dsl
GND
Vcc
Q0
Q1
Q2
Q3
CP
S1
S0
N/C
N/C
N/C
from pin 7 of IC12
from pin 5 of IC12
from pin 2 of IC12
from pin 16 of IC16
from pin 4 of IC9
+ Vcc (+ 5.0 V)
C58
100n
IC16
74F244
Octal
Buffer
OE1'
I0
O4
I1
O5
I2
O6
I3
O7
GND
Vcc
OE2'
O0
I4
O1
I5
O2
I6
O3
I7
R34
75R
to BERT return data I/P
from IC7, pin 19
to pin 11 of IC15 and pin 3 of IC13
from IC7, pin 18
to D4 on sheet 6
from IC7, pin 17
to D5 on sheet 6
to D1 on sheet 6
Inverted clock pulse from BERT
R33
75R
to D2 on sheet 6
from IC7, pin 16
to D3 on sheet 6
from IC7, pin 15
N/C
Drawn By: Dave Moore
Title: 8-level ASK Decoder
(Sheet 6 of 6)
Dwg. No:
Rev: A
Date: Oct.4 / 95